MULTI-MESH MODELLING AND APPLICATIONS TO TWO-PHASE FLOW AND CHEMICAL FLOODING PROBLEMS

BY

ADEDIMEJI ABDULSALAM ADEYEMI

A Dissertation Presented to the

FACULTY OF THE COLLEGE OF GRADUATE STUDIES

KING FAHD UNIVERSITY OF PETROLEUM & MINERALS

DHAHRAN, SAUDI ARABIA

In Partial Fulfillment of the
Requirements for the Degree of

DOCTOR OF PHILOSOPHY

In

PETROLEUM ENGINEERING

MARCH 2022

KING FAHD UNIVERSITY OF PETROLEUM & MINERALS

DHAHRAN- 31261, SAUDI ARABIA

DEANSHIP OF GRADUATE STUDIES

This thesis, written by Adedimeji Abdulsalam Adeyemi under the direction of his thesis advisor and approved by his thesis committee, has been presented and accepted by the Dean of Graduate Studies, in partial fulfilment of the requirements for the degree of DOCTOR OF PHILOSOPHY IN PETROLEUM ENGINEERING.

Dr. Abeeb Awotunde
(Advisor)

Dr Dhafer Al Shehri
Department Chairman

Dr. Shirish Patil
(Member)

Prof. Suliman Saleh Al-Homidan
Dean of Graduate Studies

Dr. Mohamed Mahmoud
(Member)

Date

Dr. Abdullah Sultan
(Member)

Dr. Kishore Mohanty
(Member)

To Bolatito and Ademola

ACKNOWLEDGMENTS

This work would not have been possible without the support of my advisor Dr. Awotunde, thank you very much for your guidance and tutelage. I also appreciate the immense support of my dissertation committee members Dr. Patil, Dr. Mahmoud, Dr. Sultan and Dr. Mohanty, thank you sirs for always making out time out of your very busy schedules. My sincere gratitude also goes to the chair of the department, Dr. Dhafer for his support always. I appreciate the contributions and support of the entire faculty and staff of the College of Petroleum Engineering and Geosciences as well as the entire university community. I will like to thank my many friends and CPG colleagues too numerous to mention for their moral support, encouragement and comradery. Thanks to my brothers Tunji and Doyin and my sisters Bimpe and Yinka, I could not have wished for a better support system. To my loving wife Semirah, thank you for your support, understanding, selflessness and patience. It really hasn't gone unnoticed. And finally, to my parents, I say thank you for all the sacrifices you have made over the years to get me here. This really is for you.

CONTENTS

LIST OF FIGURES

ABSTRACT

Full Name : Adedimeji Abdulsalam Adeyemi

Thesis Title : [Multi-Mesh Modelling and Applications to Two-Phase Flow and Chemical Flooding Problems]

Major Field : [Petroleum Engineering]

Date of Degree : [March 2022]

Modelling of flow and transport in porous media is essential to oil and gas production. Accurate modelling requires characterization of both fine scale and macro scale features of the reservoir. Geomodels are therefore typically too large for flow simulation and require upscaling. And while upscaling reduces cost, it is at the expense of accuracy. Different multi-mesh methods including Dual Mesh Method have been proposed over the years to battle this problem. In this work, first, we present a novel two mesh method, the extended dual mesh method EDMM which applies the novel approach of 'directional oversampling' to improve the downscaling and ultimately improve results. Then we developed two more novel approaches utilizing three mesh grid sizes. The extended triple mesh method ETMM and triple mesh method TMM leverage on the cost improvement from adding a third mesh grid size at the intermediate level. All three novel methods were tested on different challenging two-phase flow problems and the results consistently show the triple mesh methods outperforming their two-mesh equivalent. Finally, all the methods were applied to modelling enhanced oil recovery problems. Results show that the gains in performance from the proposed methods are consistent even in EOR processes.

ملخص الرسالة

تعد نمذجة التدفق والنقل في الوسائط المسامية أمرًا ضروريًا لإنتاج النفط والغاز. تتطلب النمذجة الدقيقة توصيف كل من المقياس الدقيق و المقياس الكلي للخزان. لذلك ، عادةً ما تكون النماذج الجيولوجية كبيرة جدًا لمحاكاة التدفق وتتطلب ترقية (وبينما تقلل الترقية من التكلفة ، فهي على حساب الدقة). تم اقتراح طرق مختلفة متعددة الشبكات بما في ذلك طريقة الشبكة المزدوجة على مر السنين لحل هذه المشكلة. في هذا العمل ، نقدم أولاً طريقة شبكتين جديدة ؛ وهي طريقة الشبكة المزدوجة الممتدة والتي تطبق نهجًا جديدًا لـ "زيادة العينات الاتجاهية" لتحسين تصغير الحجم وتحسين النتائج في نهاية بتطوير طريقتين جديدتين باستخدام ثلاثة أحجام للشبكات الشبكية. تعمل طريقة الشبكة الثلاثية وطريقة المطاف. ثم قمنا الشبكة الثلاثية الممتدة على تحسين التكلفة بإضافة حجم شبكة شبكي ثالث على المستوى المتوسط. تم اختبار جميع الطرق الجديدة الثلاثة على مشكلة تدفق مختلفة على مرحلتين مختلفة ، والنتيجة تظهر باستمرار تفوق طرق الشبكة الثلاثية على نظيرتها الثنائية. أخيرًا ، تم تطبيق جميع الطرق لنمذجة مشاكل الاستخراج المحسن للنفط. تظهر النتائج أن المكاسب في الأداء من الأساليب المقترحة متسقة حتى في عمليات الاستخلاص المعزز للنفط

1 INTRODUCTION

Petroleum reservoirs and subterranean aquifers are usually complexly heterogeneous. The complicated sedimentary processes that are involved in the rock formation are responsible for this heterogeneity. Transportation, deposition, and diagenetic processes, as well as hydrocarbon migration and trapping activities, are all examples of such processes. As a result, reservoir rocks are heterogeneous spatially and across multiple scales. As computational power and geo-statistical modelling have improved over the years, geo-modellers typically utilize a variety of sophisticated methods to capture extremely fine scale heterogeneities in geo-models. Such High resolution models (HRMs) are very fine models typically with a cell counts of 10^6 to 10^9. Even with the complexity of today's computers, reservoir modelling on such a precise scale is usually impractical. This is because simulating at this scale may be prohibitively expensive, especially when it comes to uncertainty quantification and optimization challenges, which may need thousands of runs on many realizations of the same model. This therefore suggests the need for upscaling. However, in order to effectively and accurately model flow in heterogeneous porous media, precise and extensive characterisation of petrophysical parameters is required (Bachu and Cuthiell, 1990).

In order to construct a low resolution model (LRM) of the order 10^5-10^6 cells suitable for executing flow simulations, it is necessary to always scale down the number of cells by scaling up the size of the cells in HRM. To achieve this, upscaling of properties that impact flow and transport in porous material is required. Upscaling is therefore a process of averaging fine scale petrophysical features of an HRM into equivalent coarse scale values. Depending on the problem at hand, different parameters require upscaling. Porosity and permeability (or transmissibility) are the two parameters that are often upscaled for single phase flow problems. More parameters, including capillary pressure and relative permeability curves, may require

upscaling in multiphase flow and more complex flow and transport problems (Jones, 1995; Durlofsky et al., 1995). Upscaling of flow is another term used for single phase upscaling since the elements upscaled affect the flow equation while multiphase upscaling is referred to as upscale of transport. The goal of upscaling is to obtain the effective coarse scale values of these properties without losing the most important and dominant flow and transport effects.

Multiscale and Multimesh methods on the other hand have been developed over the years in response to the accuracy loss from simulating on upscaled grids. The upscaling process itself introduces homogenization error by virtue of the fact that assigned upscaled properties are only an approximation of the fine scale properties. Also running flow simulation on a coarse scale introduces numerical dispersion error by virtue of the fact that the coarse scale discretization of the problem is only an approximation of the fine scale. The combination of numerical dispersion and homogenization error means that coarse scale solutions can be significantly less accurate than fine scale. This is what Multiscale and Multimesh methods attempt to solve. These methods attempt to obtain approximate fine scale solution (which are more accurate than coarse scale) at significantly less cost than the cost of fine scale simulation.

Modelling Enhanced oil recovery EOR processes can be even more costly owing to the higher complexities in the physical processes involved and consequently larger numerical problems per grid-cell. Given the higher complexity of EOR processes (i.e. more components mean more equations to solve), the cost of simulation can be significantly higher than two phase water flooding problems. Reducing cost of simulation is therefore imperative.

In this work, we have developed different Multimesh methods with the goal of improving on both the efficiency and the effectiveness of available methods. In Chapter 2, available literature is reviewed on the different methods used in modelling two phase flow as well as EOR

processes. These form the bases from which the new proposed methods were developed. In Chapter 3, the problem statement as well as the objectives of the research are enumerated.

In Chapter 4, the novel Extended Dual Mesh Method, EDMM, is introduced. This was developed for and tested on different water flooding problems. In Chapter 5, two Triple-Mesh Methods were introduced and tested also on water flooding problems as well as compared to EDMM.

In Chapter 6, all the novel methods developed so far for water flooding problems are then extended to and adapted for chemical EOR problems. Finally, in Chapter 7, the research is concluded and recommendations are made.

2 LITERATURE REVIEW

2.1 Production and Recovery

Production of oil and gas, and by extension recovery, is achieved by a variety of physical and sometimes chemical processes and phenomena. The applicable and effective recovery strategy depends on the kind of reservoir, the kind of fluids, the resources available, the target recovery factors as well as the economics of the alternatives. In general, recovery mechanisms are categorised as primary, secondary and tertiary (or enhanced) oil recovery mechanisms depending on the source of the mobilization and recovery energy Primary recovery mechanisms are mechanisms that involved mobilization and recovery of oil by only the natural energy in the reservoir. The primary mechanisms are therefore driven by expansion and compression forces of the reservoir fluids, the reservoir rock and as well as other natural forces including gravity and hydrodynamic forces. Secondary mechanisms utilize external energy for pressure maintenance. This basically involved injection of water or immiscible gas. The goal of secondary recovery is therefore to prevent or reduce pressure decline as well as drive hydrocarbon towards producers. Tertiary or enhanced oil recovery EOR techniques involves the injection of none native energy and or chemicals in order to improve recovery beyond secondary recovery levels. This is done by mobilizing otherwise unrecoverable oil by introducing energies or chemicals that alter the properties of the rock fluid system.

The goal of EOR techniques is therefore mobilization of oil. Mobilization of oil is controlled principally by two forces namely viscous and capillary forces. Viscous forces generally control flow while capillary forces control trapping. Two parameters consequently control mobilization namely Capillary number $N_c = \frac{\mu u}{\sigma}$ and Mobility Ratio *M*. Capillary number characterizes the ratio of viscous forces to capillary forces and therefore control residual oil saturation. EOR is therefore based on adjusting the mobility and or the interfacial (and thus

capillary) properties of the rock-fluid system. Capillary number is most effectively increased by reducing the interfacial tension between the fluid phases. As shown in Figure 1, a sufficient increase in N_c, usually by multiple orders of magnitudes, could significantly reduce the residual oil saturation of swept zones. This is usually done by the use of surfactants or the application of heat in EOR processes. Mobility Ratio *M* is the ratio of the mobility of the displacing fluid, usually water or gas, to the displaced fluid. While the effect of M on the microscopic displacement efficiently may not be significant in some cases, its effect is usually more significant in both the areal sweep and vertical sweep efficiencies, especially in heterogeneous or layered reservoirs. Mobility ratio, *M*, less than 1 is considered essential for a stable displacement. When *M* is greater than 1, displacement is unstable and which leads to the viscous fingering and channelling of displacing fluids. This bypass leads to reduction in sweep and thus recovery. To arrest this, suitable EOR methods are designed to alter the mobility ratio either by increasing the viscosity of the displacing fluid (polymer) or altering the relative permeability (mobility) through permeability alteration.

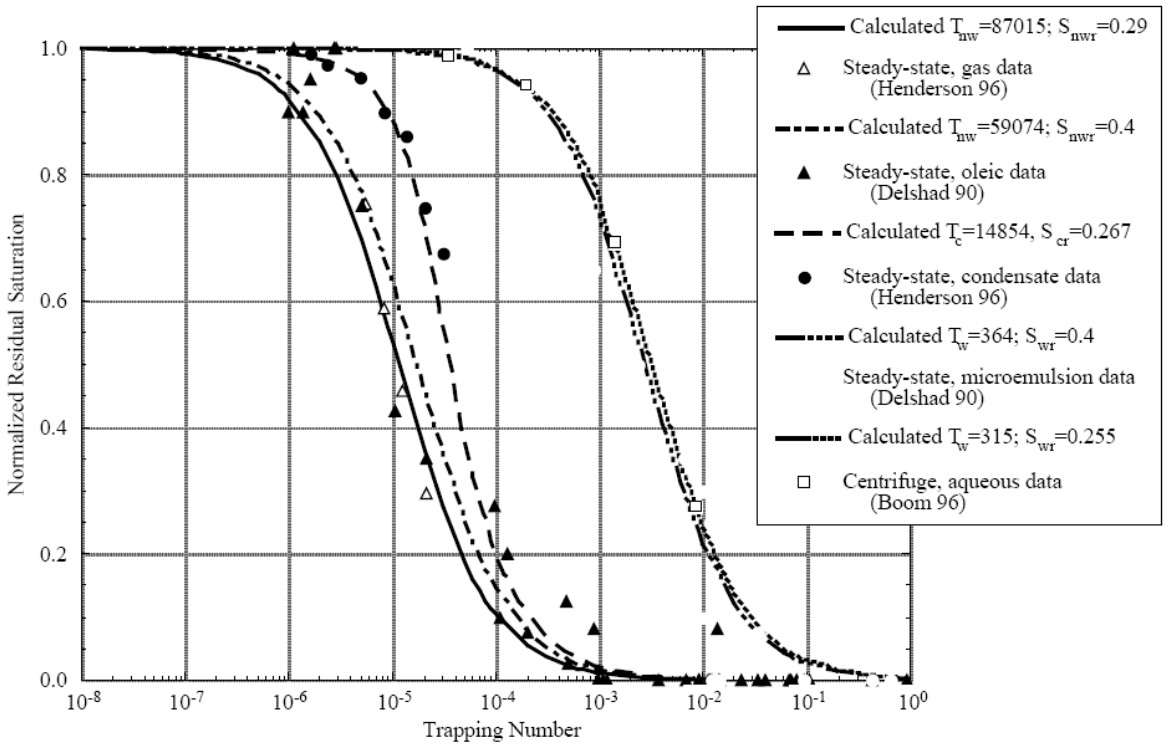

Figure 1: Capillary desaturation curves of different fluids in Berea sandstone (Pope et al 2000)

2.2 EOR Methods

Many EOR methods have been tested or proposed in literature. The choice of EOR method depends on the type of reservoir fluid system in question. Some of the parameters necessary for determining the suitability for, and the choice of, EOR processes include the hydrocarbon viscosity and density, hydrocarbon and rock chemistry, formation and injection water viscosity and salinity, reservoir temperature, reservoir depth, reservoir permeability, hydrocarbon remaining in place etc. For example, heavy oil reservoirs mostly require the thermal EOR methods while high temperature may affect effectiveness of chemical methods. EOR methods classification is shown in Figure 2 below

2.2.1 Thermal methods

Thermal EOR methods involved introducing thermal energy into the reservoir to improve recovery. They are best suited for heavy oil reservoirs and increase recovery mainly by

viscosity reduction but also by vaporization. Other mechanisms include rock and fluid expansion and steam distillation may further account for recovery improvements. Thermal methods account for more production worldwide than any other EOR method (Thomas, 2007). This is because heavy oil reservoirs generally achieve little to no recovery without EOR and thus require EOR to be producible economically. This is unlike non-heavy oil reservoirs which generally are producible commercially without EOR processes and only require EOR to increase recovery and or extend field life. They are significantly successfully used in heavy oil provinces such as in USA, Canada, and Venezuela. These most common thermal methods include Cyclic Steam Stimulation CSS, Steam-flooding, Steam Assisted Gravity Drainage SAGD and In Situ Combustion. These methods all involve the use of steam, or downhole combustion of fuel in the case of in situ combustion, to introduce heat and thus improve the mobility of heavy oil leading to recovery improvement.

2.2.2 Non-Thermal methods

These methods are used mostly in moderate to light oil reservoirs. They generally involve lowering interfacial tension or improving mobility ratio and can be generally classified into Miscible Injection, Chemical Methods and Immiscible Gas Injection EOR methods. Miscible Flooding involves injecting fluid that is miscible with reservoir oil at reservoir condition. This miscibility could be at first contact with the reservoir oil or multiple contacts in which case there is an exchange of components between injected fluid and reservoir oil until miscibility is achieved. Miscibility means that there is no interfacial tension between the phases. This leads to a smooth transition and almost 100 percent displacement in the swept zone. Injected fluids in miscible flooding includes miscible slug, enriched or vaporizing gas as well as miscible CO_2 or N_2. In Miscible Slug injection, a slug of miscible solvent (propane or pentane) is injected and driven by an immiscible less expensive fluid like lean gas or water. Depending on the reservoir pressure and reservoir oil composition, miscibility with natural gas may be achievable

at reservoir condition (vaporizing gas drive) or may require enrichment of gas with C2-C4 fractions (enriched gas drive). Non-hydrocarbon gases such as CO2 and N2 are also used. N2 required a very high pressure to achieve miscibility and so applicability is usually limited to very deep high pressure light hydrocarbon. Some of the limitation of miscible flooding include high, sometime uneconomic, cost as well as poor mobility issues such as viscous fingering (Romero-Zerón, 2012).

Chemical Flooding involves the injection of non-reservoir-native chemicals to improve recovery. Depending on the kind of reservoir, chemical EOR methods involves the injection of one or a combination of Polymers, Surfactants, Alkaline or Micellar. In Polymer Flooding, polymers such as polyacrylamides and polysaccharides are used to increase viscosity and thus reduce mobility of injected fluid. This usually reduces the mobility ratio, stabilizes the displacement front and lead to better vertical and areal sweep thereby increasing recovery. Polymers are widely used either alone or with other EOR chemical. Polymer flooding usually suffers from loss to the porous media, polymer degradation, and permeability (and injectivity) reduction and usually requires highly permeable formations to be practical. Alkaline flooding involves the injection of aqueous alkaline solution slugs. This improves recovery through 3 mechanisms namely wettability alteration (Froning, 1967), in situ surfactant generation as well as spontaneous emulsification. Alkali are rarely used alone and are usually combine with Surfactant and Polymers such as in Alkaline-Surfactant Polymer ASP flooding.

In Micellar flooding (Gogarty and Tosch, 1968), Micellar (microemulsion) slug is injected followed by polymer or brine or both. The micro-emulsions are usually stabilized by surfactants and generally miscible with both oil and water. This reduces the miscibility and thus increases displacement efficiency.

While many chemical EOR methods have been proven to be effective at recovery enhancement in the lab as well as in the field, they are not commonly used, especially compared to thermal methods. This is mostly because of the cost. Economics is a major consideration when making oil and gas investment decisions and chemical EOR methods don't always justify the investments economically.

Other EOR techniques, VAPEX (Das and Butler, 1995) which involves the use of solvents in Heavy Oil Extraction. Microbial EOR (Hitzman, 1994) involves use of microbes to produce in situ surfactants, polymers, biomass, solvents and gases which in turn increase recovery through wettability alteration, IFT reduction, emulsification etc. Foam injection is another method that has been considered in literature as a method or mobility control or as a blocking agent however, this has not led to anything significant in terms of field implementation.

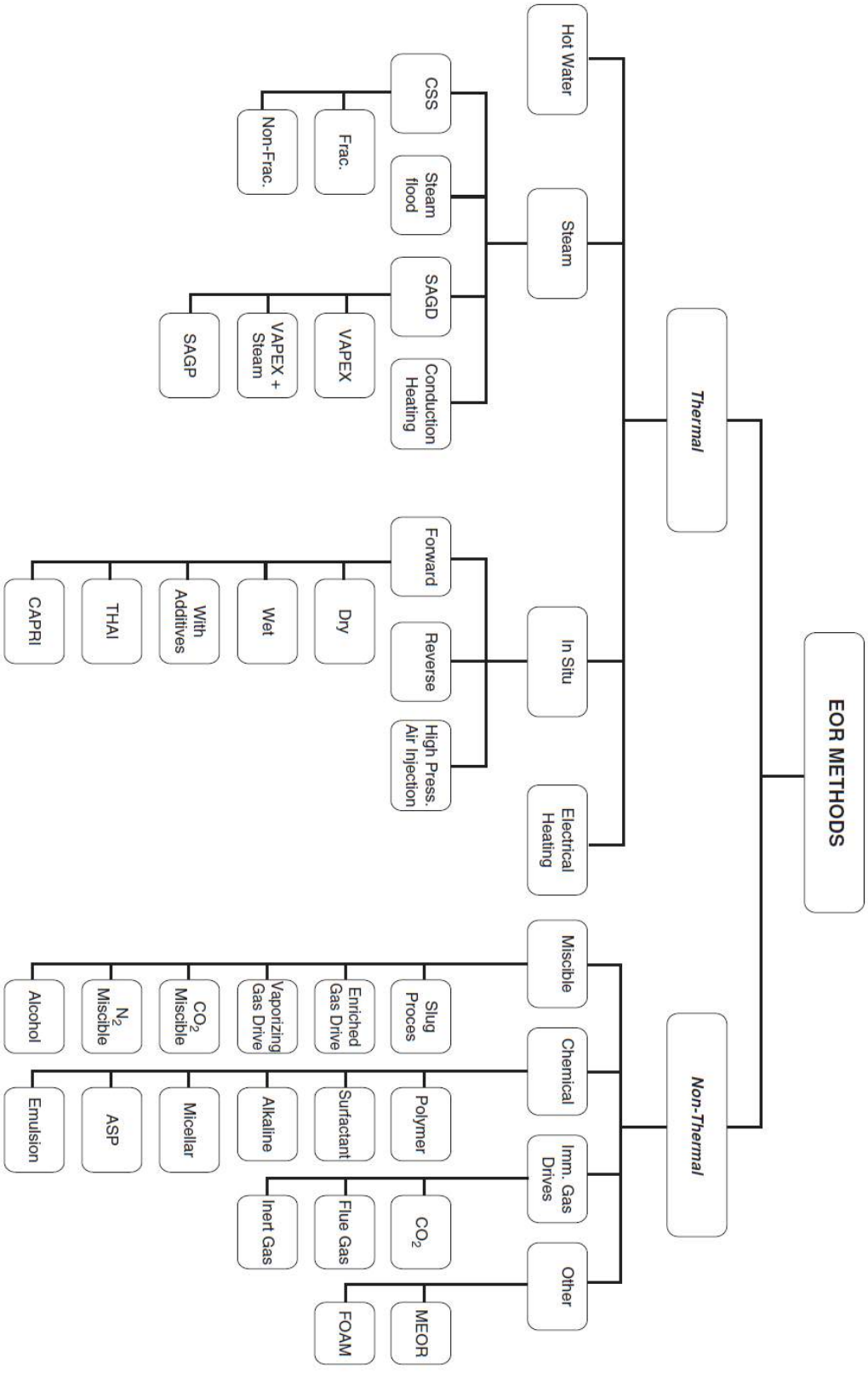

Figure 2: Classification of EOR techniques (adapted from Thomas 2007)

2.3 Reservoir Modelling

Petroleum reservoirs being porous rocks are controlled by the equations governing fluid flow in porous media. These equations are generally complex non-linear Partial Differential Equations PDEs. Depending on the complexity of the reservoir and the fluids, phenomena such as gravity, capillary pressure, wettability, compressibility, and adsorption have to be incorporated. This makes the PDEs generally difficult, and in most cases impossible to solve analytically. In order to therefore model the behaviour of reservoirs in recovery operations, numerically solutions are used. The process of numerically solving reservoir fluid flow and recovery problems is called reservoir simulation. It is an important tool in modern reservoir management. Reservoir simulation is major in decision making since it predicts outcome of available alternatives. It is therefore important in field development planning, production optimization, recovery optimization and enhanced oil recovery problems. Production figures from reservoir simulation are also important inputs for economic analysis as well as reserves estimation.

Computer programs specialized in modelling reservoirs are called reservoir simulators. There are different kinds of simulators the choice of which depends on the kind of problems to be solved. They include ‘black oil’ for simple multiphase flow problems where the composition of each phase is considered unchanged. These are most suited for primary and secondary recovery processes such as water flooding.

Compositional simulators are more complex than black oil and are used to simulate processes where there are changes in physical and chemical properties of the phases present in the reservoir such as miscible processes. For processes involving injection of none native chemicals into the reservoir such as in chemical EOR processes, chemical simulators are required. And for reservoirs where thermal energy is introduced into the reservoir for recovery,

thermal simulators may be required. Some processes may require an hybrid of these simulators to model multiple processes.

2.4 Upscaling and Multiscale Methods

Oil and gas reservoirs are typically heterogeneous. This is displayed spatially along dimensions and across scales. Heterogeneity is inherent in the reservoir rock and a product of the complex sedimentary processes involved in the deposition, burial, and diagenesis of the rock. Consequently, the petrophysical properties of reservoir rock are neither uniform nor isotropic since they are not only affected by the processes involved in the rock creation but also by the fluid saturation history of the pores spaces within the rock. To capture and model these complexities, geo-modellers combine static and dynamic characterization data with sophisticated geo-statistical methods to resolve these heterogeneities with as much fine details as possible. This means that the grid cells count in geo-models may be in the billions. Flow simulation however may be impractical to run at this scale. The computational requirement, coupled with the fact that thousands of simulation runs may be required (e.g. in uncertainty quantification or optimization problems), may mean that the simulation will be too expensive to the practical. A balance therefore has to be reached between the desirable accuracy of fine scale detail (Bachu and Cuthiell, 1990) and the huge cost of simulation at such scale.

The most widely employed method of simulation computational cost reduction is upscaling. This involves aggregating fine-scale grid cells into equivalent coarse-scale cells with approximately equivalent grid properties. Based on the method used to obtain the equivalent fine scale properties, upscaling methods can be classified as numerical or analytic methods. The generally more accurate methods are the numerical methods and they involve flow simulation on the fine scale grids to obtain the effective coarse-scale flow properties. Single phase methods (Chen et al., 2003; E. Pickup et al., 1992; Nielsen and Tveito, 1998; Chen and Durlofsky, 2006; Wen et al., 2003; Begg et al., 1989; Holden and Lia, 1992; Zijl and Trykozko,

2001) are the more commonly used methods and have been shown to be adequate in multiphase flow applications. On the other hand, multiphase methods (Hui and Durlofsky, 2005; Chang and Mohanty, 1997; Jones et al., 1995; Stone, 1991; Kyte and Berry, 1975) may be required for more complex problems including those with multiple lithologies and saturation tables. Upscaling techniques have been extensively reviewed (Barker and Thibeau, 1997; Christie and Blunt, 2001; Chen, 2005; J. Durlofsky, 2014; Farmer, 2002; Wen and Gómez-Hernández, 1996; Renard and De Marsily, 1997).

Flow based upscaling techniques can be classified based on the size and the manner in which the fine-scale problem is solved to obtain coarse-scale properties as well as the boundary and well conditions employed. Based on the size of the fine scale problem solved, we have global, local, quasi-global as well as extended local methods. Global methods (White and Horne, 1987; Holden and Nielsen, 2000) are those where the fine-scale problem is solved globally to obtain coarse-scale properties. While relatively accurate, the method can be very expensive or even impossible to solve depending on the size of the fine-scale problem. Also, to achieve good accuracy, the boundary conditions and flow scenario employed in the upscaling must be similar to that of the simulated scenarios. This means that global methods are expensive and may not be very robust in application to different flow scenarios (i.e. boundary conditions and well distribution). An alternative to global methods are the quasi-global or local-global methods (Chen and Durlofsky, 2006; Chen et al., 2003). These methods involve solving the global coarse scale problem to obtain global information that is then used as boundary condition to solve the local upscaling problems. This is a cheaper alternative to global upscaling.

Local methods on the other hand involve solving the upscaling problems locally in the domain of each coarse cell. This method requires the application of boundary conditions BC around the local domain the choice of which differentiates the different local methods (Durlofsky, 1991; King and Mansfield, 1999). Since global information is not used in choosing the

boundary condition, the BC may not be representative of the global problem and this may affect the accuracy of the upscaling. To reduce influence of the choice of boundary condition on accuracy, extended local methods were introduced (Holden and Lia, 1992; Gomez-Hernandez and Journel, 1994). In these methods, extended local, rather than purely local problems are solved. This method is also called oversampling and helps to minimize resonant errors typically associated with local methods (Wu et al., 2002). They therefore combine economic savings of local methods with reduction in error.

While dispersion and homogenization errors can be reduced by the application of good upscaling methods, they can be completely eliminated. Nothing can replicate fine scale resolution at the coarse scale. Therefore, upscaled solutions will by definition contain dispersion and homogenization errors. Consequently, multiscale methods were introduced as an improvement on upscaling. Multiscale Finite Element Method (MsFEM) (Hou and Wu, 1997) was introduced as a pioneer multiscale method. Over the following years, multiscale simulation as an area of research has been improved significantly leading to the development of different methods capable of handling complex problems (Chen and Hou, 2002; Jenny et al., 2003; Aarnes, 2004; Kippe et al., 2008; Hajibeygi and Tchelepi, 2014; Cusini et al., 2015; Efendiev et al., 2015; Yang et al., 2018; Fu and Chung, 2019; Shah et al., n.d.; Zhang et al., 2019, 2017). The basic idea of these methods is to lower the computational cost by mapping coarse solution on to the fine scale using local basis functions. This avoids the solution of the global fine scale problem thus lowering computational cost.

An alternate to multiscale methods is Dual Mesh method. As first proposed (Guérillot and Verdiere, 1995), the method involves solving the flow equation on the coarse scale and distributing the coarse flux as boundary conditions for locally solving the flow equation at the fine scale. This yields a conservative fine scale flux field without having to solve the global fine scale problem. The saturation equation is typically then solved on the fine scale. DMM

solutions converge to the exact solution (Verdière and Vignal, 1998) and the method has been developed widely for application in two phase flow (Gautier et al., 1999; Chen et al., 2003; Audigane and Blunt, 2004). Firoozabadi et al. (2009) combined DMM with vorticity based aggregation. Khoozan et al. (2011) proposed a cheaper analytical alternative for the local fine scale solution reconstruction. Babaei and King (2012) further improved results applying a local-global upscaling method and using the flux distribution obtained from the upscaling as boundary condition in the downscaling step. Apart from two-phase flow problems, the method has be applied to enhanced oil recovery EOR (Babaei and King, 2013; Li et al., 2016) and CO2 storage (Guérillot and Bruyelle, 2017). While much better than coarse scale solution, DMM may still be significantly inaccurate especially when compared with some multiscale methods (Kippe et al., 2008).

EOR processes may require a high resolution modelling to accurately capture the complexities in the associated fluid displacement fronts (Babaei and King, 2013; Haajizadeh et al., 1999; Van Batenburg et al., 2011). Also, accurate simulation of EOR processes are of particular importance as they are used to show the improvements in recovery and thus justify the typically huge investments that EOR processes require. Despite this, the high computation cost typically means that EOR processes are simulated at the coarse scale which significantly impacts accuracy.

EOR modelling needs multiscale-multimesh methods. However, only a limited number of these methods have been presented, bespoke for, or adapted to EOR modelling compared to water-flooding (Babaei and King, 2013; Kumar et al., 2014; Li et al., 2016; Muggeridge and Hongtong, 2014).

2.5 Dual Mesh Method

The traditional dual mesh approach is a two-mesh method that requires an HRM grid and an LRM grid. As a result, a suitable upscaling procedure must be used to convert the HRM into

an LRM. Geometric averaging GA and PSM are two upscaling approaches that have been employed with dual mesh in the literature (Begg et al., 1989). The dual mesh approach may be summarized in six steps (Audigane and Blunt, 2004).

1. HRM (fine scale) parameters such as saturation, permeability, and porosity are specified at each time step, and source terms are specified as well
2. Depending on the upscaling approach, LRM (coarse scale) saturation, as well as permeability or transmissibility, are computed.
3. The coarse scale pressure equations are solved and the coarse scale fluxes are computed.
4. The coarse fluxes are then used to compute the local fine scale boundary fluxes. This is done by transmissibility weighted distribution of the coarse scale fluxes into fine fluxes using the equation:

$$Q_x^{fine} = \frac{T^{fine}_{x_{i+(1/2)}}}{\sum_f T^{fine}_{x_{i+(1/2)}}} Q_x^{coarse} \qquad (1)$$

where Q_x^{fine} represent fine scale flux in the x direction in the cell *i* which is attached to the coarse cell face f.

5. Using the computed local boundary fluxes, the local fine scale flow problems are solved and the fine scale fluxes computed
6. Lastly, the fine scale saturations equation is solved.

The main sources of error in this method compared to solving conventionally on the fine scale can be classified broadly as homogenization and numerical dispersion. The method reduces numerical dispersion effects in the saturation computation significantly but doesn't completely eliminate it since the coarse fluxes employed are affected by this error. Also the homogenization error due to upscaling can be reduced using relatively accurate upscaling

techniques but cannot be totally eliminated since there is no perfect upscaling technique. Another drawback is the weak coupling between the coarse and fine scale problems. Asides from the inherent error in the coarse fluxes employed, the method of distributing the coarse fluxes as fine scale boundary conditions (transmissibility weighting) is an approximate and not an exact method. As such, the fine boundary conditions imposed are inherently erroneous as well. Because of these, the accuracy of DMM may suffer. The accuracy therefore depends not only on the upscaling method employed but also on the type of problem. Accuracy has been shown to sometimes degenerate in highly heterogeneous problems (Audigane and Blunt, 2004).

3 PROBLEM STATEMENT

As is clear from the literature review, there is a lot of room for improvement in the accuracy as well as the application of two-mesh solution methods before they can be considered mature enough to be included in commercial simulators. The methods available for downscaling are inherently inaccurate and need to be improved. There is also a need to extend these methods beyond simple two phase flow problems such that they can be employed in more complex problems. More complex problems like Chemical EOR problems are great candidates for these methods as they are even more computationally costly than two phase flow problems.

Some of the questions that will be explored in the work include whether current approaches to numerical modelling of Chemical EOR processes are efficient enough and if they can be improved. Whether or not the existing two phase flow two mesh methods can be adapted to Chemical EOR processes and if they are effective and efficient. Whether or not new Multimesh methods be developed. Also, how the performances of the Multimesh methods for Chemical EOR processes compare to simulation on fine scale and coarse (upscaled) scale in terms of cost and accuracy. And how the performances of these methods for Chemical EOR processes compare to Multimesh methods for simple 2 phase flow in terms of cost and accuracy

3.1 Research Objectives

This research aims at achieving the following objectives

1. Development and evaluation of a new efficient two phase flow two-mesh method for simulating water flooding problems
2. Development and evaluation of a new efficient two-mesh method for simulating Chemical Flooding Problems

3 Development and evaluation of a new efficient multimesh (3 levels) method for simulating water flooding problems

4 Development and evaluation of a new efficient multimesh (3 levels) method for simulating Chemical Flooding Problems

4 EXTENDED DUAL MESH METHOD

4.1 Introduction

While dual mesh method may be effective in simulation cost reduction, it is not the most accurate method especially when compared to multiscale methods (Kippe et al. 2008). This is because the DMM's fine scale solutions are directly dependent on coarse scale solutions, which, as previously stated, have intrinsic flaws. Despite the fact that fine scale reconstruction may improve dispersion error, because the coarse solution is applied directly as local BC, it doesn't reduce the homogenization error present in the coarse scale solution. This makes the accuracy of DMM highly dependent on the accuracy of the upscaling method, choice of boundary condition and complexity of problem.

This chapter introduces a novel approach which improves on the drawbacks of DMM. First, the governing equations for two phase flow are described. Then the Extended Dual Mesh Method EDMM as well as Directional Oversample DO approach is introduced. Following that, the technique's performance is evaluated using a set of test cases and examples. Finally, several of the approaches' peculiarities are explored, followed by findings and suggestions.

4.2 Governing Equations

Given an incompressible immiscible heterogeneous two-phase (water and oil) reservoir system, each phase's conservation equation is

$$\phi \frac{\partial S_w}{\partial t} + \nabla \cdot \vec{u}_w = -q_w ,$$

$$\phi \frac{\partial S_o}{\partial t} + \nabla \cdot \vec{u}_o = -q_o \quad \text{.....(2)}$$

where ϕ represents porosity, and $\vec{u_i}$, q_i and S_i represent the velocity vector, sink/source term, and saturation of phase *i* respectively, while the subscripts w and o respectively indicate water

and oil phases. Capillary and gravity effects are assumed to be negligible. The Darcy velocities can be expressed as

$\vec{u}_w = -\lambda_w \bar{\bar{k}} \cdot \nabla p$,

$\vec{u}_o = -\lambda_o \bar{\bar{k}} \cdot \nabla p$ .....(3)

where p denotes pressure, λ_w and λ_o denote the water and oil mobilities, respectively, and $\bar{\bar{k}}$ denotes porous medium's diagonal permeability tensor. Mobilities can be expressed as follows:

$\lambda_w = \frac{k_{r_w}(S_w)}{\mu_w}$,

$\lambda_o = \frac{k_{r_o}(S_w)}{\mu_o}$ .....(4)

where k_{r_i} and μ_i .denote the relative permeability and viscosity, respectively.

Because $S_w + S_o = 1$, if $\dot{u} = \dot{u}_w + \dot{u}_o$, the Eq. (2) can be written in the following way:

$\nabla \cdot \vec{u} = -q$ .....(5)

$\phi \frac{\partial S_w}{\partial t} + \nabla \cdot (f_w \vec{u}) = -q_w$ .....(6)

where $q = q_w + q_o$ and f_w denotes the fractional flow of water and that $\vec{u}_w = f_w \vec{u}$

This yields the total velocity equation:

$\lambda_t \bar{\bar{k}} \cdot \nabla p = \vec{u}.$ .....(7)

where $\lambda_t = \lambda_w + \lambda_o$. Substituting the velocity Eq. (7) in Eq. (5) yields the pressure equation as:

$\nabla \cdot \left(\lambda_t \bar{\bar{k}} \cdot \nabla p \right) = q$ .....(8)

Eq. (6) is the transport (or saturation) equation. This along with the flow (pressure) equation represents the two equations that require solutions in order to solve this problem. These non-linear equations can be solved using a number of numeric approaches. In this work, the IMPES

scheme is used in which the flow equation is solved implicitly while the saturation equation is explicitly solved.

4.3 **IMPES Finite Volume Method**

4.3.1 Flow equation discretization.

The flow equation can be discretized as followed using the finite volume scheme:

$$\int_{V_i} \nabla \cdot \left(\lambda_t \bar{\bar{k}} \cdot \nabla p \right) dV = \int_{V_i} q dV \quad \text{.....(9)}$$

where V_i denotes volume of cell *i*. Eq. (9) can be approximated to the discrete equation :

$$\sum_{j \in N(i)} T_{ij} (p_j^{n+1} - p_i^{n+1}) = q_i^{n+1} \quad \text{.....10}$$

where *j* denotes cells interfacing cell *i*, p_i^{n+1} denotes pressure in cell *i* at time-step *n*+1 while q_i^{n+1} represents the sink/source term in volumes per unit volume of cell *i*. Transmissibility T_{ij} can be expressed as:

$$T_{ij} = \frac{\lambda_{t_{ij}} k_{ij} A_{ij}}{\left\| d_{i\Gamma j} \right\| + \left\| d_{j\Gamma i} \right\|} \quad \text{.....11}$$

where A_{ij} denotes the interface area, while $d_{i\Gamma j}$ represents the vector joining the centre of cell *i* to the interface.

$$k_{ij} = \left(\frac{1}{k_i} + \frac{1}{k_j} \right)^{-1} \quad \text{.....12}$$

and $\lambda_{t_{ij}}$ represents the total upstream weighted interface mobility i.e.

$$\lambda_{t_{ij}} = \begin{cases} \lambda_{t_i} \text{ if } p_i^n > p_j^n \\ \lambda_{t_j} \text{ if } p_j^n > p_i^n \end{cases} \quad \text{.....13}$$

Eq. (10) yields the system of equations:

$$\bar{\bar{T}} \vec{P}^{n+1} = \vec{q} \quad \text{.....14}$$

where $\bar{\bar{T}}$ denotes the inter-block transmissibility matrix, $\vec{P}^{n+1}$ denotes the unknown pressure vector while $\vec{q}$ is the sink/source term vector. The coefficients of the matrix $\bar{\bar{T}}$ are:

$\bar{\bar{T}}[i,i] = \sum_{j \in N(i)} T_{ij}$ and

$\bar{\bar{T}}[i,j] = T_{ij}$ .....

(15)

Equation 14 is evaluated implicitly and is stable unconditionally.

4.3.2 Transport equation discretization.

The transport equation can be discretized as follows:

$$\phi \int_{V_i} \frac{\partial S_w}{\partial t} dV + \int_{V_i} \nabla \cdot (f_w \vec{u}) dV = \int_{V_i} q_w dV \quad \text{.....16}$$

$$\frac{V_i \phi}{\Delta t}(S_{w_i}^{n+1} - S_{w_i}^{n}) + \sum_{j \in N(i)} T_{ij} f_{w_{ij}} (P_j^{n+1} - P_i^{n+1}) = q_{w_i}^{n+1} \quad \text{.....17}$$

$f_{w_{ij}}$ is the interface fractional flow of water and is also evaluated using upstream-weighting.

Since Equation 17 is solved explicitly after pressures have been evaluated, $S_{w_i}^{n+1}$ can be evaluated directly since they are the only unknowns.

4.4 Extended Dual-Mesh Method

The majority of DMM research have so far concentrated on either enhancing coarse scale solutions by employing better upscaling methods (Firoozabadi et al., 2009;) or improving the approach for distributing boundary conditions(fluxes), or both (Babaei and King, 2012; Khoozan et al., 2011). However, because of the very nature of upscaling, considerable inaccuracy is inherent in the coarse scale solution, the improvements can only go so far. As a result, enhancing the distribution accuracy of an erroneous (coarse) solution may not always result in significant error reduction. In contrast to DMM (Table 1), EDMM is the first approach that attempts to increase accuracy by minimizing the impact of the coarse scale solution on the accuracy of the fine scale reconstruction. Oversampling (extending the local problem borders outside the region of interest such that boundary conditions are applied at a distance from this domain) has been proven to lessen the influence of, and error caused by, boundary conditions

(Hou and Wu 1997; Wen et al. 2003). This is the foundation for MsFEM's oversampling and extended local upscaling. Oversampling therefore forms part of the bases upon which the Extended-Dual Mesh Method (EDMM) was developed.

Table 1 Comparing the techniques employed in accuracy improvement in DMM and EDMM

DMM	EDMM
Both methods improve simulation results by downscaling the pressure equation and solving the saturation equation on the fine scale	
The approximate BC used in the coarse flow solution passes the error down to the fine flow solution.	This error is further reduced by using the newly added directional oversampling DO.
The coarse scale problem and the fine scale problems are poorly coupled	Better coupling between coarse and fine scale problems e.g. fine scale saturation (at the interphase) is utilized to compute coarse scale transmissibility.
DMM improvements so far have focused on the upscaling methods and downscaling BC	EDMM focuses on lowering the influence of the upscaling method and choice of BC on the accuracy

EDMM utilizes two distinct mesh sizes of grids, an HRM grid and an LRM grid with upscaled HRM properties. Any upscaling method can be used, but the accuracy of the upscaling has an impact on the accuracy of the final output. However, one of EDMM's goals and strengths is to limit the effect of the upscaling method. First, the flow problem is implicitly solved on the

coarse scale using the standard IMPES scheme. After that, the coarse scale fluxes are computed. Along the coarse grid cell boundaries, the global fine-scale grid is divided into several partitions. Each fine-scale partition might be as little as one coarse block or as large as a few coarse blocks. To obtain fine-scale velocity field, extended local flow problems are solved for each partition with boundary conditions similar to DMM. This is then used to explicitly solve for fine-scale saturation. As a result, this approach only employs oversampling (directional oversampling) in the downscaling stage, and should not be mistaken with other methods that use oversampling in the upscaling step.

4.4.1 Directional Oversampling

Because adjacent local solutions may not share the same boundary conditions, extended local solutions to the flow problem (pressure equation) may produce non-conservative global velocity fields. But the flow solution cannot be utilized to solve for transport without conservation. EDMM solves this challenge by ensuring that fine-scale velocity fields are conserved globally. To do so, we introduced a technique known as Directional Oversampling (DO). DO is a novel extended local approach that ensures a conservative global fine-scale velocity field by ensuring that oversampling is done only once per boundary.

Figure 3 describes directional oversampling. To begin, the HRM is partitioned along the LRM cell borders (numbered 1-9 in Figure 3, the partitions are shown in thick red lines). The extended local flow problems are then solved in order (from 1 to 9 or 9 to 1), with the imposed Neumann BCs being either the already calculated fine-scale flux (from contiguous partitions that have already been solved) or transmissibility weighted coarse flux identical to that used in DMM.

1. Type-1 partition boundaries are those that correspond to the global outer border.
2. Type-2 partition boundaries are shared with preceding partitions.

3. Type-3 partition boundaries are shared with succeeding partitions.

Because the extended local downscaling is done sequentially, it is important to note that the order of the preceding and succeeding partitions is determined by the solution direction chosen. When solving from partition 1 to partition 9, partition 1 has two succeeding partitions (partitions 1 and 4), no preceding partitions, and two global boundary (see Figure 3). As a result, partition 1 has two Type-3 and two Type-1 boundaries. Conversely, partition 5 has two Type-2 and two Type-3 borders due to its two preceding (partitions 2 and 4) and two succeeding (partitions 6 and 8) partitions. Therefore for each partition to be solved, the preceding partitions have already been solved for fine-scale fluxes, whereas the succeeding partitions only have coarse-scale fluxes.

In DO, the global BC is applied to Type-1 boundaries for each fine-scale partition solved, whereas fine-scale fluxes from already solved preceding partitions are applied to Type-2 boundaries Oversampling and transmissibility weighted coarse-scale flux are used for Type-3 boundaries. The continuity of fine-scale fluxes across partition boundaries assures global conservation of the velocity field obtained from DO solution method. This therefore can be subsequently utilized to solve the fine-scale saturation transport equation.

4.4.2 Steps in EDMM Implementation

The steps in the implementation of EDMM can be broken down as follows.

1. Definition of fine-scale properties: The fine-scale grid parameter, such as permeability, porosity, saturation, and sink/source terms, are defined.
2. Upscaling: This stage entails defining the coarse grid properties and upscaling fine-scale properties for the coarse grid. Any accurate transmissibility or permeability upscaling approach can be used although transmissibility upscaling methods have been found to be more accurate and less costly over time since permeability upscaling still requires

transmissibility computation. Three upscaling approaches are employed in this study. These are the following:

a) Upscaling transmissibility using the Pressure Solve Method (PSM). To obtain coarse interblock diagonal transmissibilities, a local, single phase flow based approach similar to that utilized by Gautier et al. (1999) was adopted. In all test models, this approach was employed as the base upscaling method.
b) Global Well Drive (WDU) method: This flow-based global upscaling method, similar to Zhang et al. (2005), was utilized in model 2 and the results were compared to the PSM's.
c) Geometric Average (GA): Model 2 also employed the method of permeability upscaling, and the results were compared to the PSM results.

As a result, a coarse grid with upscaled permeability or transmissibility, as well as saturation and porosity, which are straightforward volumetric averages of fine-scale saturation and porosity, is produced, preserving both total pore volume and volume of each saturating fluid between the fine-scale and coarse grids.

The coarse mobility $\lambda_{t_{ij}}$ used for transmissibility computation in this technique differs from that used in conventional Dual Mesh or Standard IMPES: the average fine-scale grid mobility at the coarse interface applying upstream weighting is specified in Eq.(18)

$$\lambda_{t_{ij}} = \begin{cases} \lambda_{t_i} \text{ if } p_i^n > p_j^n \\ \lambda_{t_j} \text{ if } p_j^n > p_i^n \end{cases} \tag{18}$$

where,

$$\lambda_{t_i} = \frac{\sum_f \lambda_{t_i}^{fine}}{n_f} \tag{19}$$

where λ_{t_i} represents average mobility at the coarse interface f and $\lambda_{t_i}^{fine}$ represents the mobility in the fine-scale grid blocks on the coarse interface *f*. n_f is the number of smaller (fine-scale) grid blocks in coarse grid block *i* that share interface *f*. The coarse scale inter-block mobilities are therefore controlled by the fluid saturation at the boundary, not the average saturation of the coarse block, which improves the coupling between the fine and coarse-scale problems.

3. Solving the coarse scale pressure equation: This entails solving the flow equation for coarse grid pressure, and then the coarse grid velocity field is computed.
4. Solving the Extended Local Flow Equation on the Fine Scale: This entails partitioning the HRM grid and application of DO to solve extended local fine-scale flow problems for fine-scale pressure. This is then used to compute the fine-scale velocity field, as discussed earlier and depicted in Figure 3.
5. Solving the Saturation Equation: A conservative fine-scale velocity field is generated after step 4, this is then utilized to solve Eq. (6) explicitly for fine-scale saturation.

Figure 4 depicts the EDMM flow chart, which summarizes the above steps.

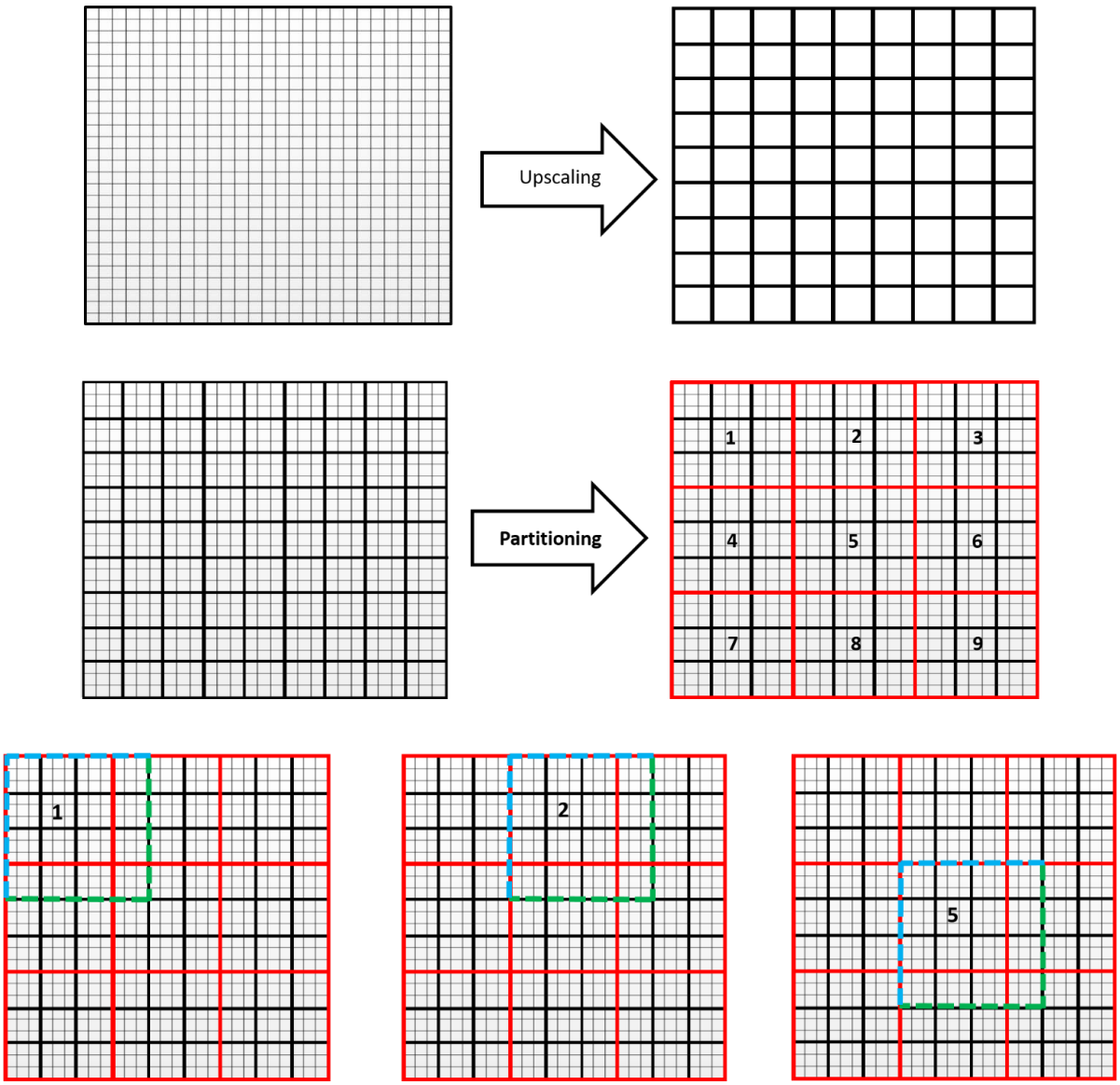

Figure 3: An illustration of some major EDMM procedures. ***Up:*** *Step 2 of the EDMM implementation is depicted by an HRM 27 by 27 (thin black lines) and an upscaled LRM 9 by 9 (thick black lines). The global coarse flow problem is solved on the LRM.* ***Middle:*** *Shows the meshing into 9 partitions (3 by 3) numbered from 1 to 9. Each partitioned domain's flow problem is solved in the downscaling step.* ***Down****: Shows the borders of the directional oversampling DO-solved local flow problems. Due to the sequential nature of DO, the local flow problem for partition 1 must be solved before moving on to partition 2 and so on. The global-Type-1-boundaries (in dotted blue line) for partition 1 are the –x and –y borders, therefore an external boundary condition (typically no flow boundary) is applied. The Type-3 (+y and +x) borders are oversampled beyond the partition 1 boundary (in dotted green), and transmissibility weighted flux BC is employed here. The velocity field within partition 1 is then computed once the flow problem is solved while region that has been oversampled is discarded. For partition 2, the -x boundary (in blue dotted lines) is shared with partition 1 (Type-2) therefore the fluxes computed for partition 1 are used as Neumann BC, while the +x and +y*

boundaries (Type-3) are oversampled and transmissibility weighted fluxes are used as Neumann BC.

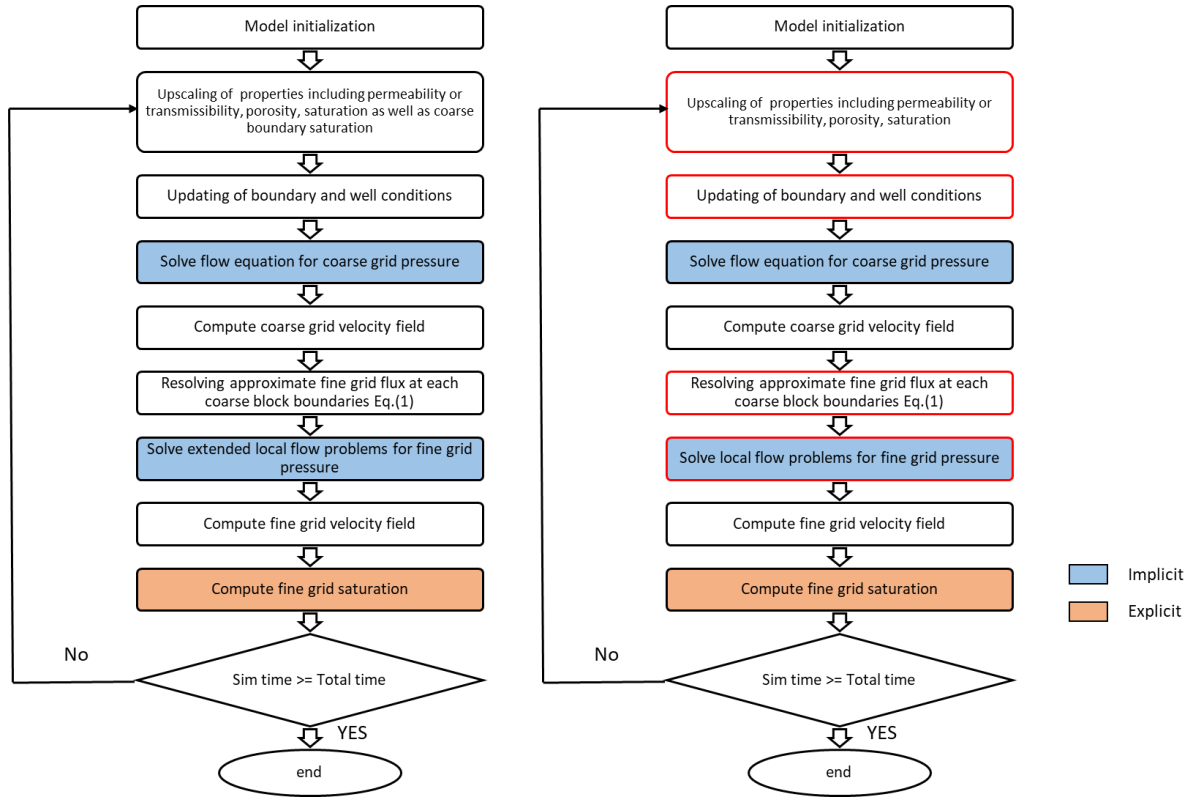

Figure 4 DMM (right) and EDMM (left) algorithms flowchats. In the EDMM flowchats, red borders show steps that are different from DMM.

4.5 Results and Implementation

Three separate water flooding test problems were used to evaluate the EDMM. In each case, grids with various permeability fields and well distributions were used. The problems were created to evaluate the method's accuracy, efficiency and robustness. The primary control for the producers is total rates, while the injectors are controlled by total voidage replacement. The performance of the various techniques was evaluated using two error indicators. The first indicator E_{fw} measures the error water cut and is expressed as

$$E_{fw} = \frac{1}{t_{total}} \sum_{i=1}^{nt} \left| \frac{\left[f_w^f(i) - f_w^c(i) \right] \Delta t_i}{f_w^f(i)} \right| \qquad (20)$$

Here, $t_{total} = \sum_{i=1}^{n_t} \Delta t_i$ represents the total simulation time, nt represents the total number of time steps, f_w^f represents the water cut of the fine-scale model, and f_w^c represents the water cut of the assessed model.

The second error indicator E_{bt} estimates error in water breakthrough time and is expressed as

$$E_{bt} = \frac{1}{n_w} \sum_{j=1}^{nw} \left| \frac{t_{bt}^f(j) - t_{bt}^c(j)}{t_{bt}^f(j)} \right| \qquad (21)$$

where n_w represents the total number of producer and t_{bt}^f represents the fine-scale model water breakthrough time, and t_{bt}^c is the evaluated model's breakthrough time. The two error estimated together help assess the accuracy of the modelling of the water front advance as well as the total saturation field.

4.5.1 Model 1: The Refinement Model

EDMM was first tested on this model. This is a synthetic 2D model with a log permeability field shown in Figure 5. The model's permeability field is heterogeneous, with values ranging from 1 mD to 1000 mD. The fine-scale model measures 1200 ft by 2200 ft, with regular Cartesian cells of 20 feet by 10 feet each. Because there is no dip in the model, no gravity effect is taken into account. The coarse grid is made up of regular cells, with each coarse grid being 100 feet by 50 feet i.e. containing 25(5 by 5) fine-scale grids. The fine-scale grid in this model is a refinement of the coarse grid, with all fine-scale grid blocks inside a coarse cell having the same permeability as the coarse grid. The fine-scale grid's global permeability field is thus heterogeneous, whereas the local permeability field inside each coarse grid domain of the fine scale grid is homogeneous. This eliminates the necessity for upscaling, making it the optimum test for the method's accuracy without the influence of the upscaling process. Table 2 lists the model's parameters. The model has five wells, one central injector, and four distributed

producers, as illustrated in Figure 5. The purpose of the example was to see how effectively the approach handled complicated well distributions. To evaluate the performance of EDMM as well as other methods, the following methods were used to solve the problem.

1. IMPES on the LRM grid
2. IMPES on the HRM grid
3. DMM Method
4. EDMM Method

Table 2 ***Model Inputs*** *used in models 1, 2, and 3(excluding where stated otherwise)*

Model Inputs			
Porosity		0.25	
Permeability		Specified heterogeneous distribution	
Oil Viscosity (cP)		0.3	
Water Viscosity (cP)		3	
Krw_{max}	0.6	Kro_{max}	1
Swc	0.1	Sor	0.18
Nw (Corey)	2	No (Corey	2
Well primary control		Total liquid rates (Producer(100 stb/day) Injectors(Total voidage replacement)	

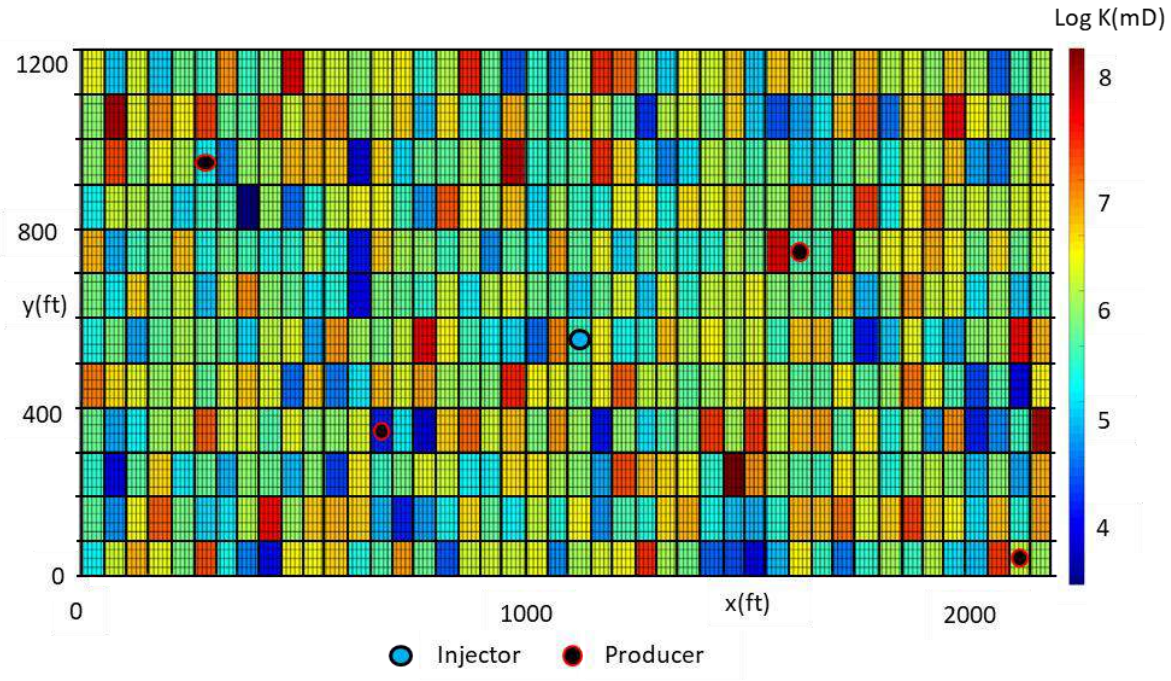

Figure 5: Model 1 permeability field with on well locations. The coarse cell boundaries are shown in thick lines, while the fine cell boundaries are represented by thin lines.

Figure 6 shows the water cut at the four producers over the course of 3500 days. The plots show that EDMM performs much better than DMM in all four producers in terms of predicting water breakthrough time and water cut during the 3500 days simulated. For example, the DMM water breakthrough time is off by more than 20 days in three of the four wells, more than 50 days in two of the wells, and more than 100 days in one well. EDMM, on the other hand, accurately forecasts the breakthrough in all four wells to within 10 days. Also, over the course of 3500 days, the water production from EDMM is more accurate in all four wells, and much more accurate in two of the four wells. The DMM approach is much more accurate than the coarse solution, but not nearly as much as the EDMM. Figure 17 shows the error indicators for each approach, which also supports this. DMM is 2.2 times more accurate (less error) than the coarse solution in forecasting water cut and 1.84 times more accurate in predicting water

breakthrough. In this case, EDMM is 4.7 times more accurate in predicting water cut and 27 times more accurate in predicting breakthrough than the coarse solution.

Given that upscaling was not done in this example because the fine-scale grid is a refinement of the coarse grid (and thus no homogenization errors are expected), this first example therefore clearly demonstrates that EDMM reduces numerical dispersion errors, outperforms DMM, and is a good approximation of the fine-scale model.

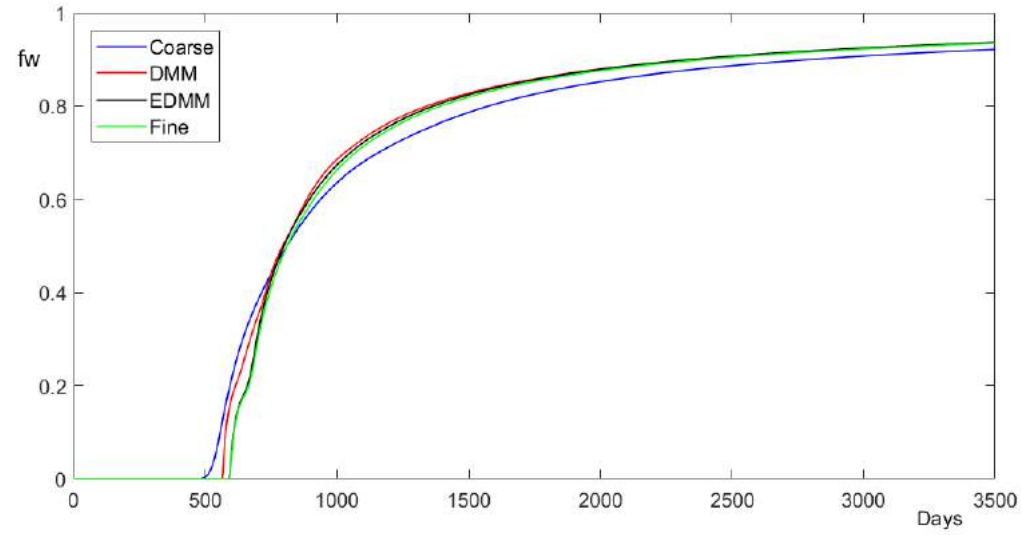

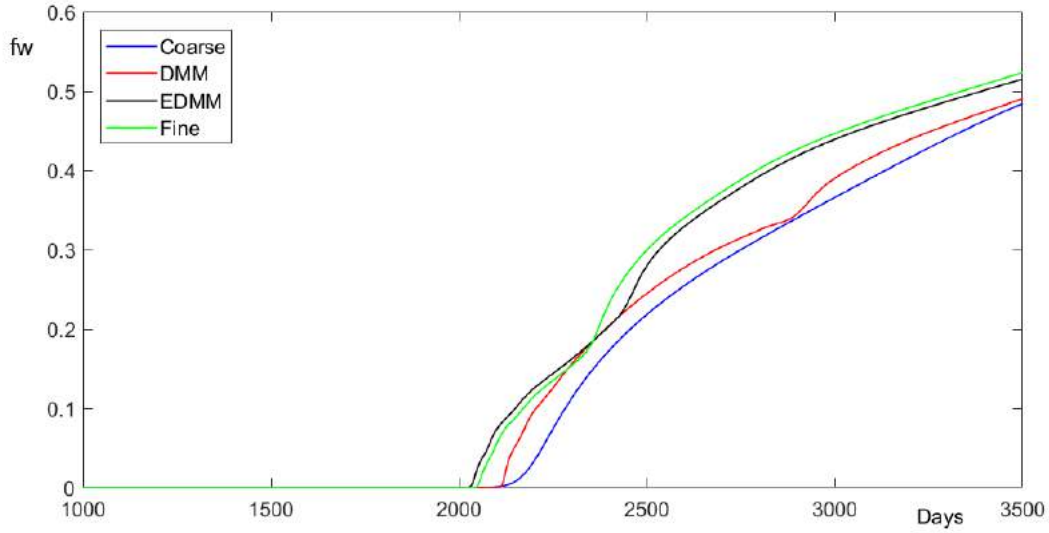

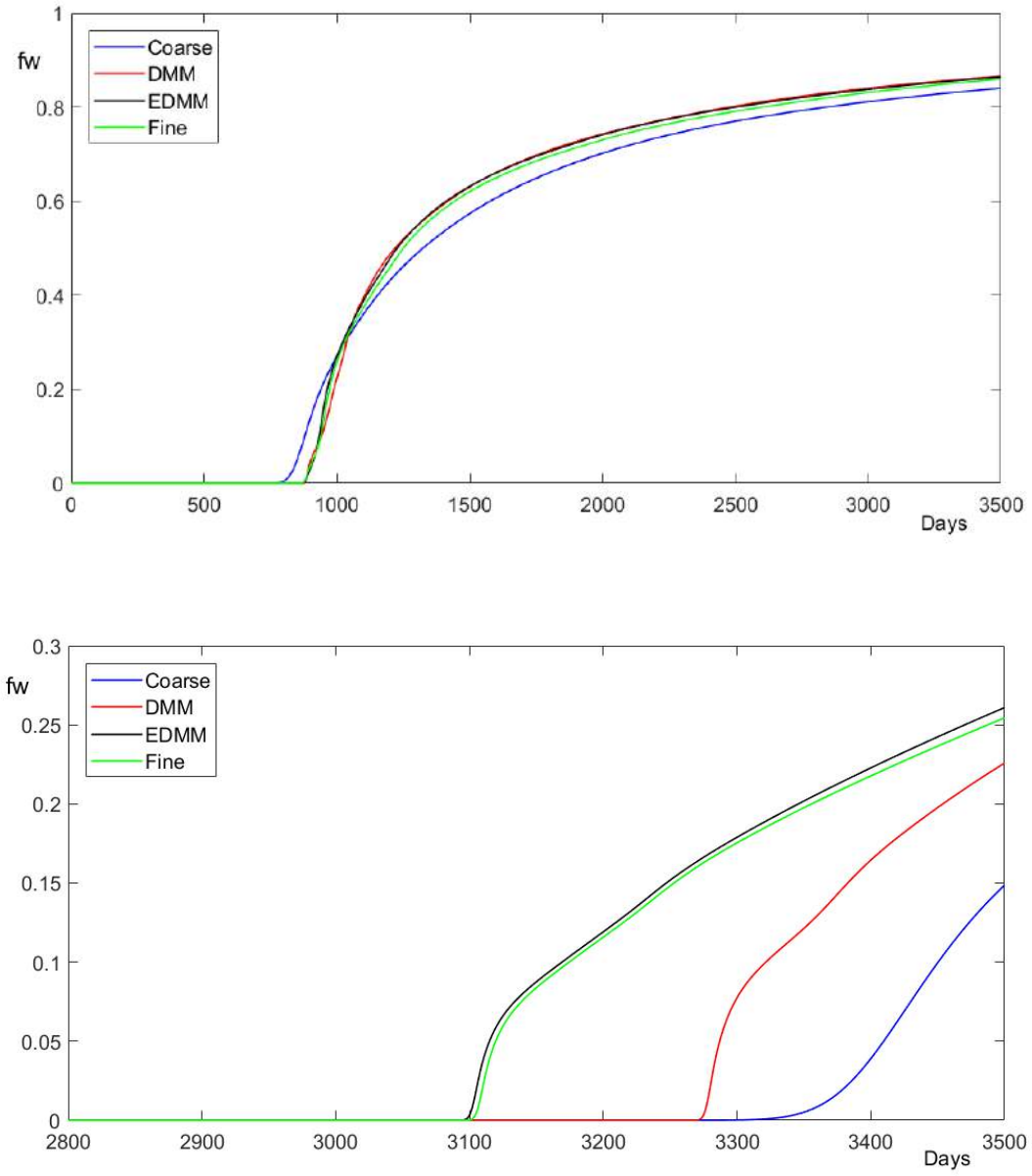

Figure 6: Plots of water cut (fw) vs. time (in days) of model 1 production wells using various solution approaches, i.e. Fine scale, EDMM, DMM, and coarse scale

4.5.2 Model 2: SPE 10 Layer 59

This is layer 59 of the 3D model of the 10th SPE Comparative Project model (Christie and Blunt, 2001), which is a 2D model with log permeability field as shown in Figure 7. The model is a channelized reservoir with a very heterogeneous permeability field that varies by seven orders of magnitude. The fine-scale model measures 1200 ft by 2200 ft, with regular Cartesian cells of 20 feet by 10 feet each. Like model 1, this model has no dip, therefore no gravity impact

is taken into account. The coarse grid has 12 by 44 regular cells, making each coarse grid cell 100 ft by 50 ft in size i.e. including 25 (5 by 5) fine grid cells. The coarse model is a scaled-up version of the fine model. PSM, WDU, and GA upscaling techniques were utilized in the EDMM implementation, while PSM was employed in both the DMM and Coarse Models implementations. This was done to compare the upscaling methods' accuracy and evaluate the impact of the upscaling method on the EDMM approach. The parameters for the base case are listed in Table 2. The model contains three wells distributed as shown in Figure 7 with two production wells and one water injection well. This case was created to see how well the method handles high permeability heterogeneity, as well as how well alternative upscaling strategies perform in water cut and recovery forecasts. Simulation runs were carried out using the following approaches to assess the method's performance.

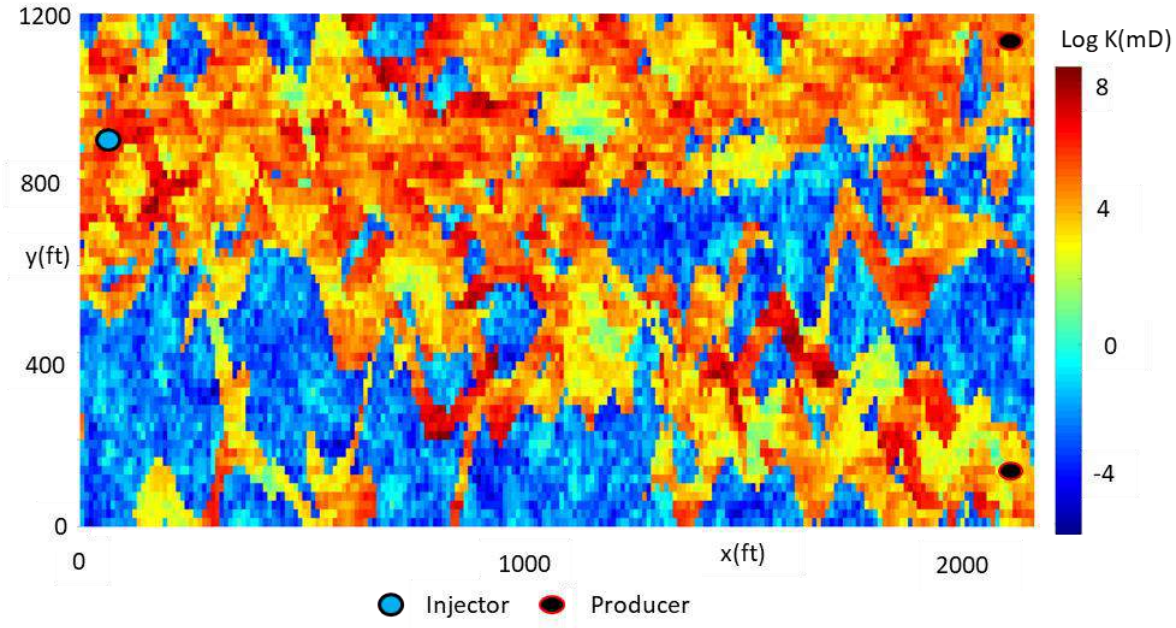

Figure 7 Model 2 permeability field and well locations

1. IMPES on the LRM grid (with PSM upscaling)
2. IMPES on the HRM grid
3. DMM Method (with PSM upscaling)

4. EDMM Method (with PSM, WDU and GA upscaling)

This example is also used to see how the mobility ratio M affects EDMM accuracy. M=1 was used for the favourable mobility scenario, while with M=10 was used for the unfavourable mobility case.

Figure 8 shows the velocity distribution error E_u of the different solution techniques after 1000 days in the M=10 scenario, where $E_{ux} = \left| u_x^f - u_x \right|$, u_x^f represents the reference fine scale velocity in the x direction and u_x represents the velocity using the solution method used. It is evident that the EDMM velocity solution outperforms the DMM solution in both the x and y axes. The saturation distributions of the various solution approaches are shown in Figures 9 to 11 after 600, 1000, and 2000 days respectively. They all demonstrate how EDMM is superior at resolving fine scale spatial saturation distribution. Figure 12 shows the water fractional flow curves at the two producers during the course of the 3000 days of simulation. Again, the curves demonstrate that EDMM outperforms DMM in both wells when it comes to predicting water breakthrough time and water cut throughout the simulation period. In one well, the DMM water breakthrough is off by over 40 days, while in the other, it is off by over 100 days. EDMM, on the other hand, accurately forecasts the breakthrough in both wells to within 5 days. EDMM's water cut is likewise more accurate in both wells over the course of 3000 days, and much more accurate in one of them. Figure 17 shows that DMM is 5.5 times more accurate than the coarse solution in forecasting water cut and 5.2 times more accurate in predicting water breakthrough. In this case, EDMM is 20 times more accurate in predicting water cut and 182 times more accurate in predicting breakthrough than the coarse solution. This example clearly demonstrates that EDMM excels in highly heterogenous systems, which was noted as one of DMM's flaws (Blunt and Audigane).

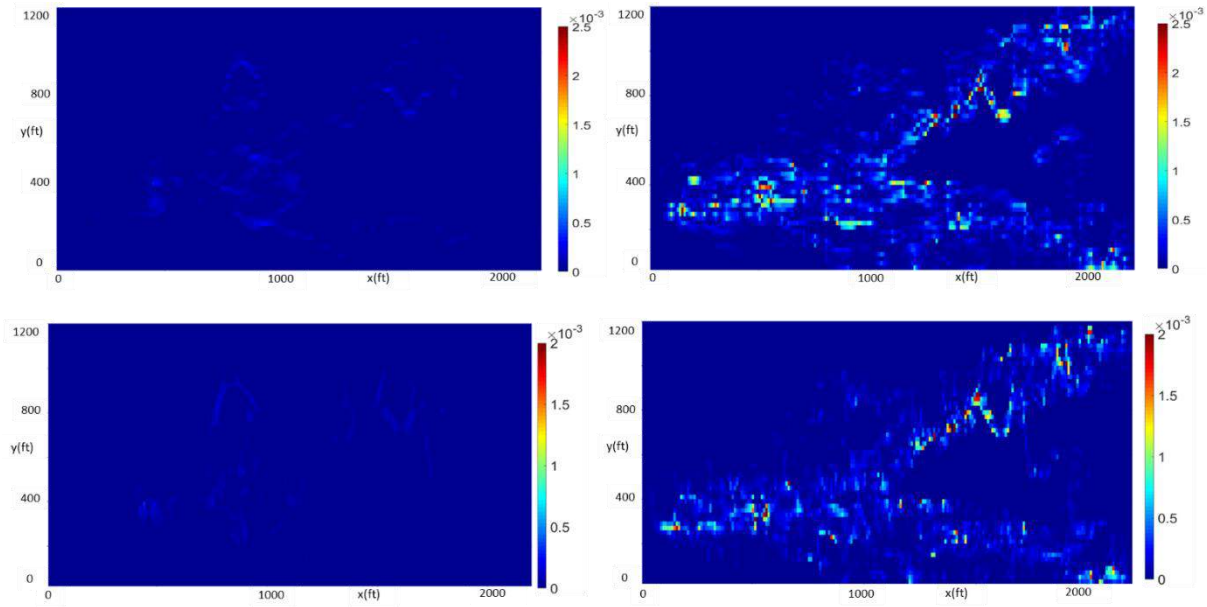

Figure 8: The Model 2 Velocity Error E_u *. Top left: EDMM* E_{uy} *, Top Right: DMM* E_{uy} *, Bottom left: EDMM* E_{ux} *,, Bottom Right: DMM* E_{ux} *,*

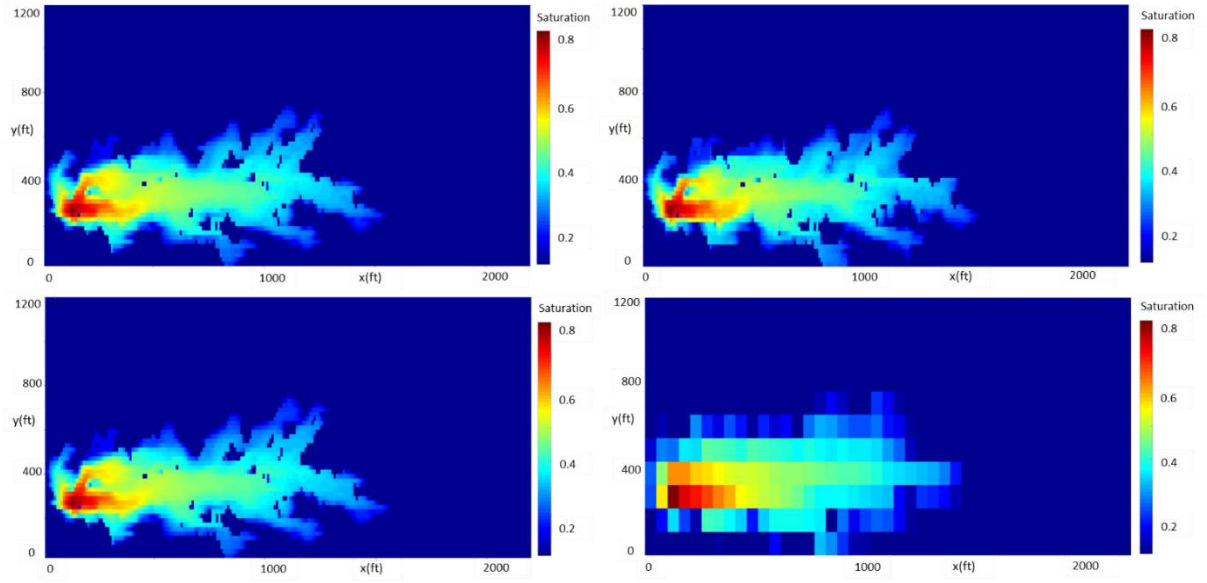

Figure 9: Saturation field of Model 2 after 600 days. Fine (top left), DMM (top right), EDMM (bottom left), and Coarse (bottom right).

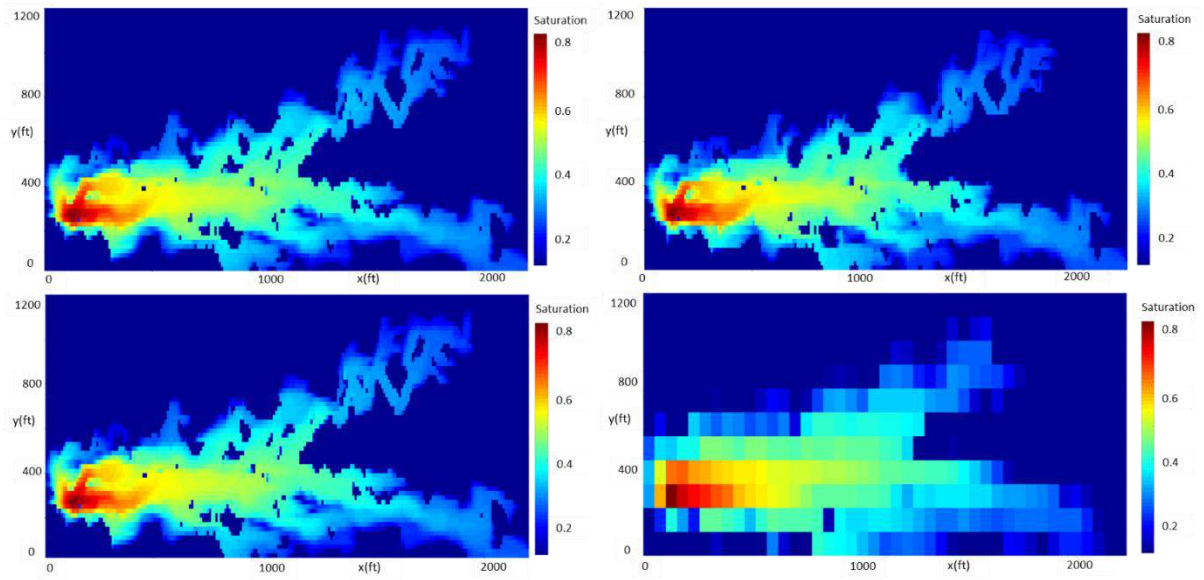

Figure 10: Saturation field after 1000 days. Fine (top left), DMM (top right), EDMM (bottom left), and Coarse (bottom right).

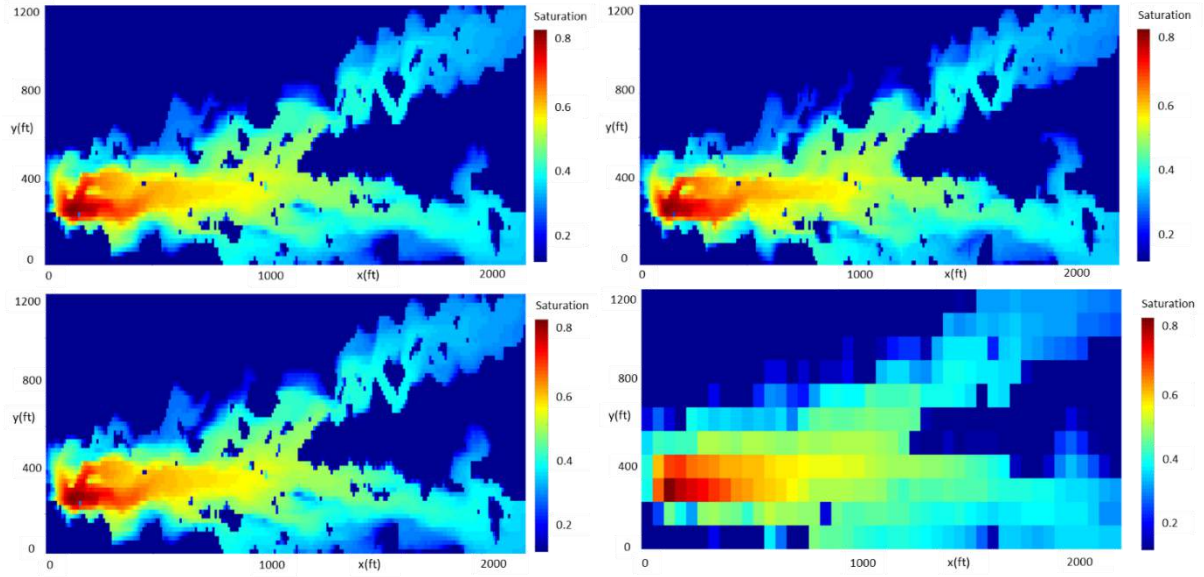

Figure 11: Saturation field for Model 2 after 2000 days. Fine (top left), DMM (top right), EDMM (bottom left), and Coarse (bottom right).

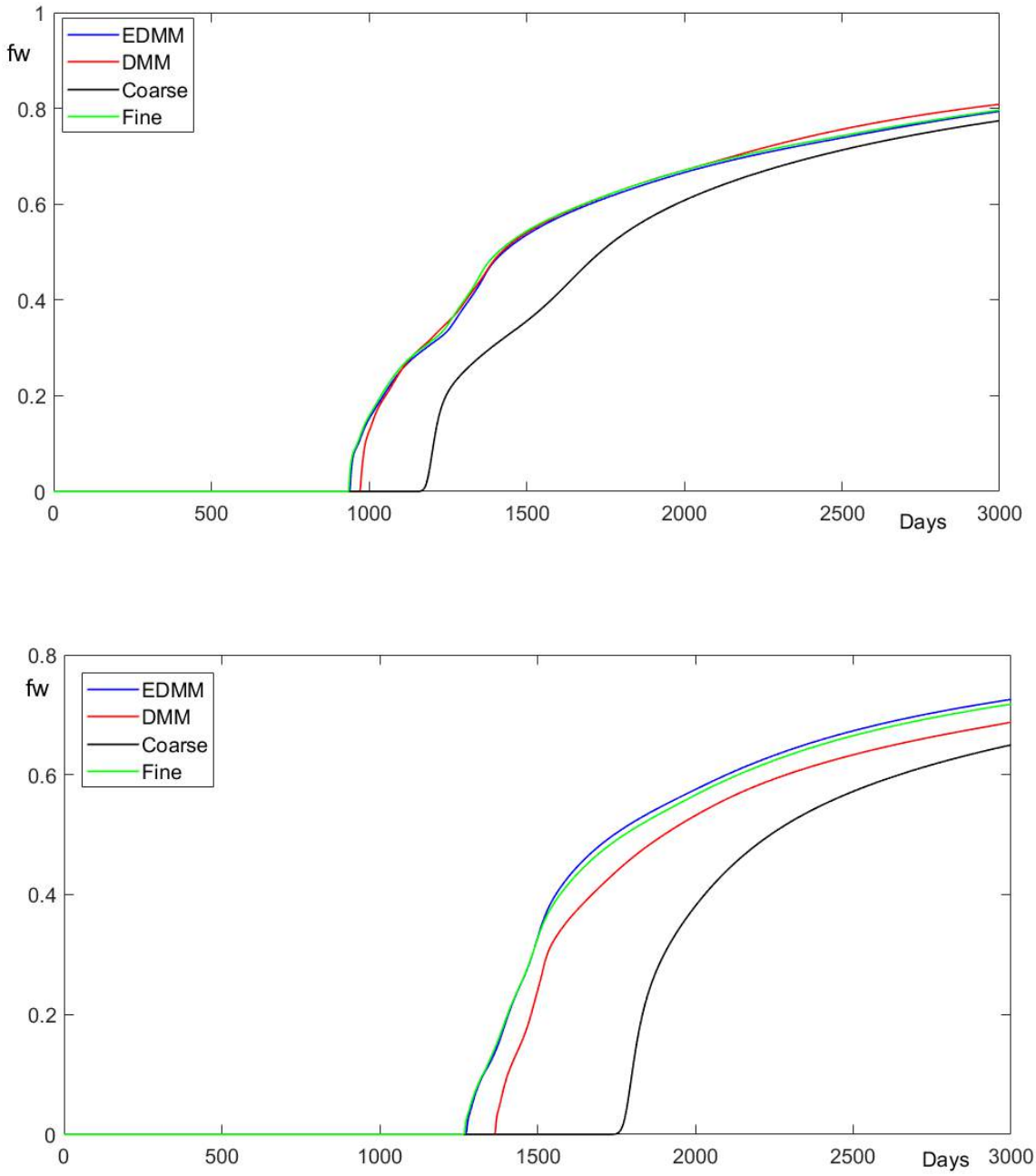

Figure 12: Plots of water cut (fw) vs. time (in days) for the two producers (top and bottom) in model 2 using PSM upscaling.

PSM upscaling was used to in all the examples discussed so far. The performance of the EDMM approach with different upscaling is shown in Figure 13. The plot shows that EDMM is accurate in all upscaling approaches. Even EDMM paired with GA, a far less accurate upscaling method than flow-based methods, produces results that are similar in accuracy to

Dual Mesh (with PSM). Given that GA has a substantially larger homogenization error, the fact that EDMM (with GA) results are similar in accuracy to DMM (with PSM) indicates that the EDMM helps in reducing homogenization error. Because Model 1 improves numerical dispersion alone, Model 1 and Model 2 together show that EDMM reduces both homogenization and numerical dispersion errors. Alternative EDMM implementations on model 2 were also investigated, with the results displayed in Figure 14 and explained in Section 4.7.

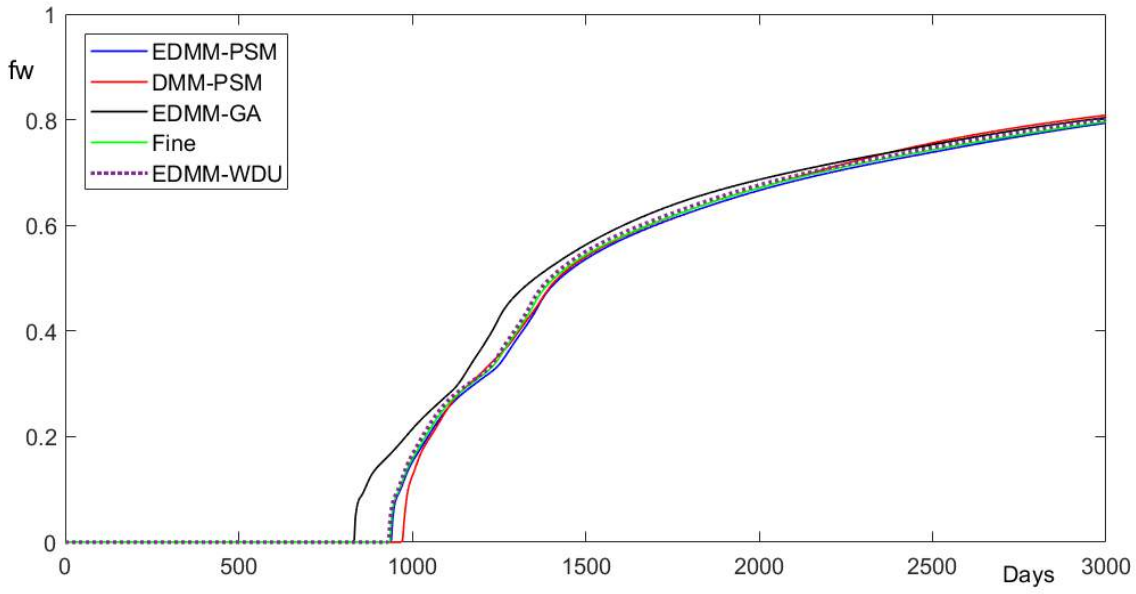

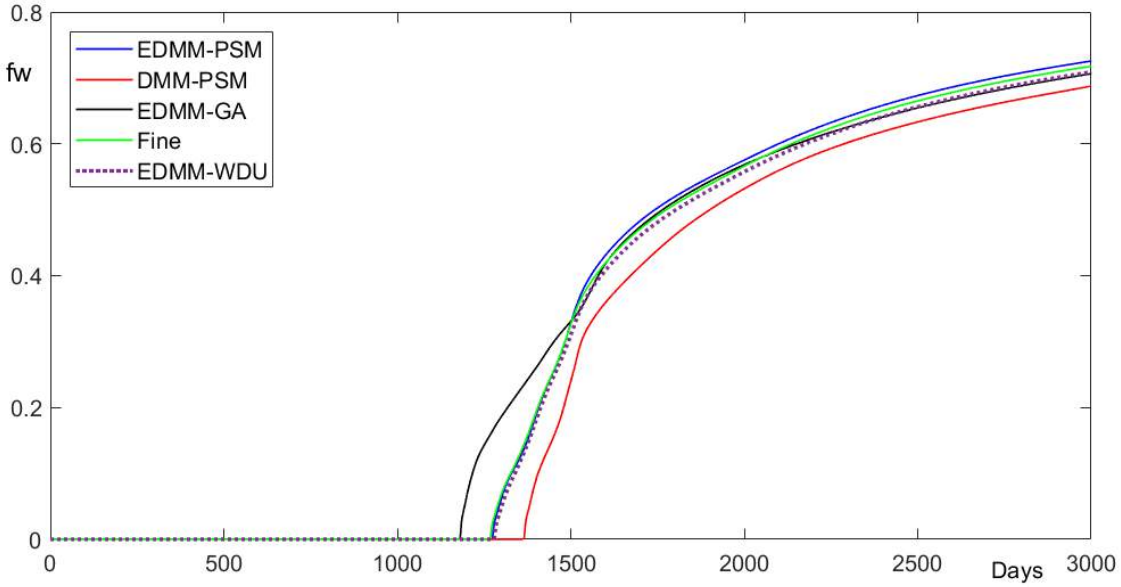

Figure 13: Plots of water cut (fw) vs. time (in days) for the two producers (top and bottom) in model 2 using different upscaling methods.

Figure 15 shows water cut at the producer in the case of M = 1. Again, the plots indicate that EDMM outperforms Dual Mesh in both wells when it comes to predicting water breakthrough time and water cut across the simulated timeframe and in both wells. This illustrates the robustness of EDMM with mobility and reveals that, at least throughout the range of mobilities studied, EDMM maintains its accuracy.

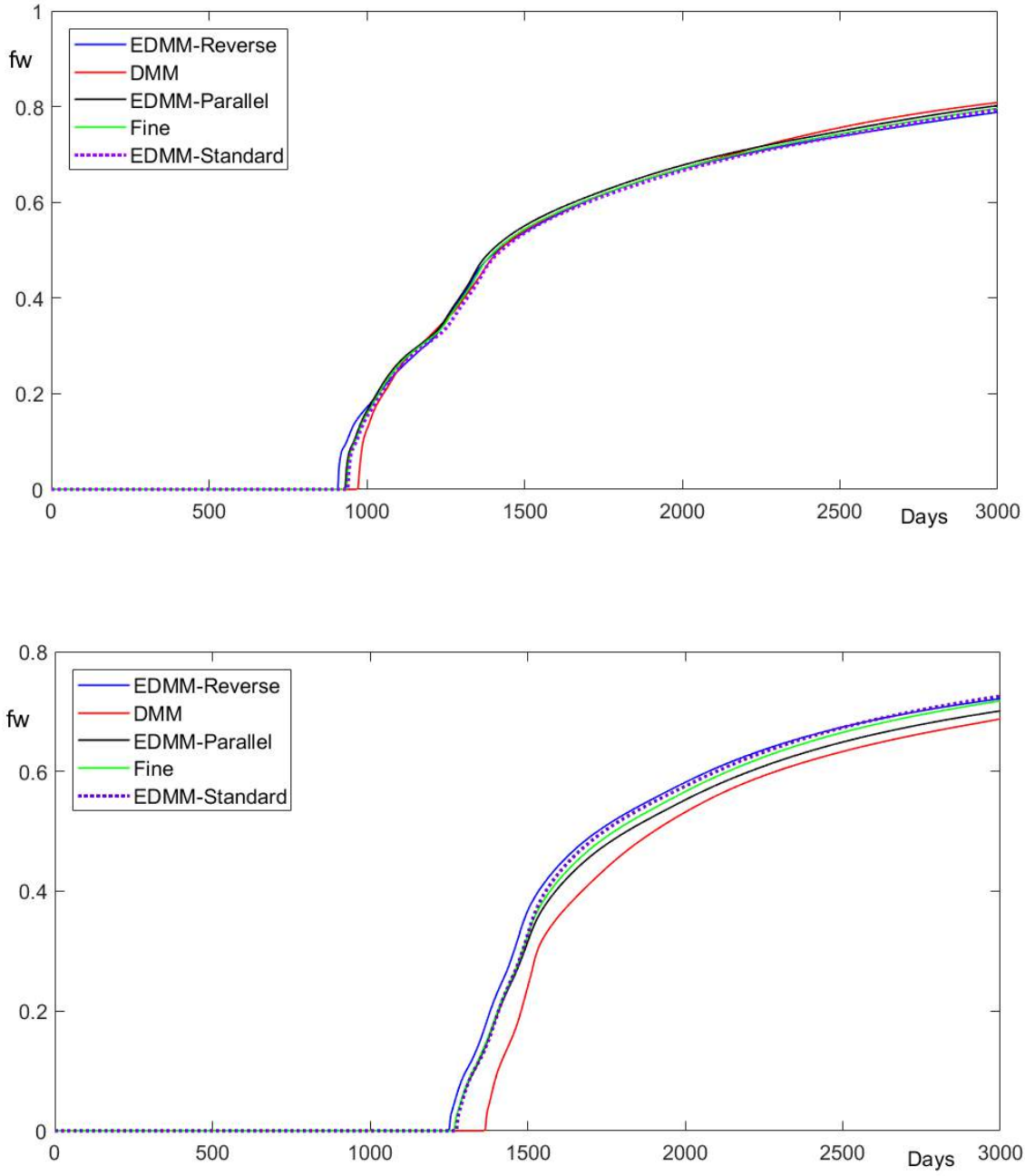

Figure 14: Plots of water cut (fw) vs. time (in days) for the two producers (top and bottom) in model 2 demonstrating the outcomes of different EDMM implementations

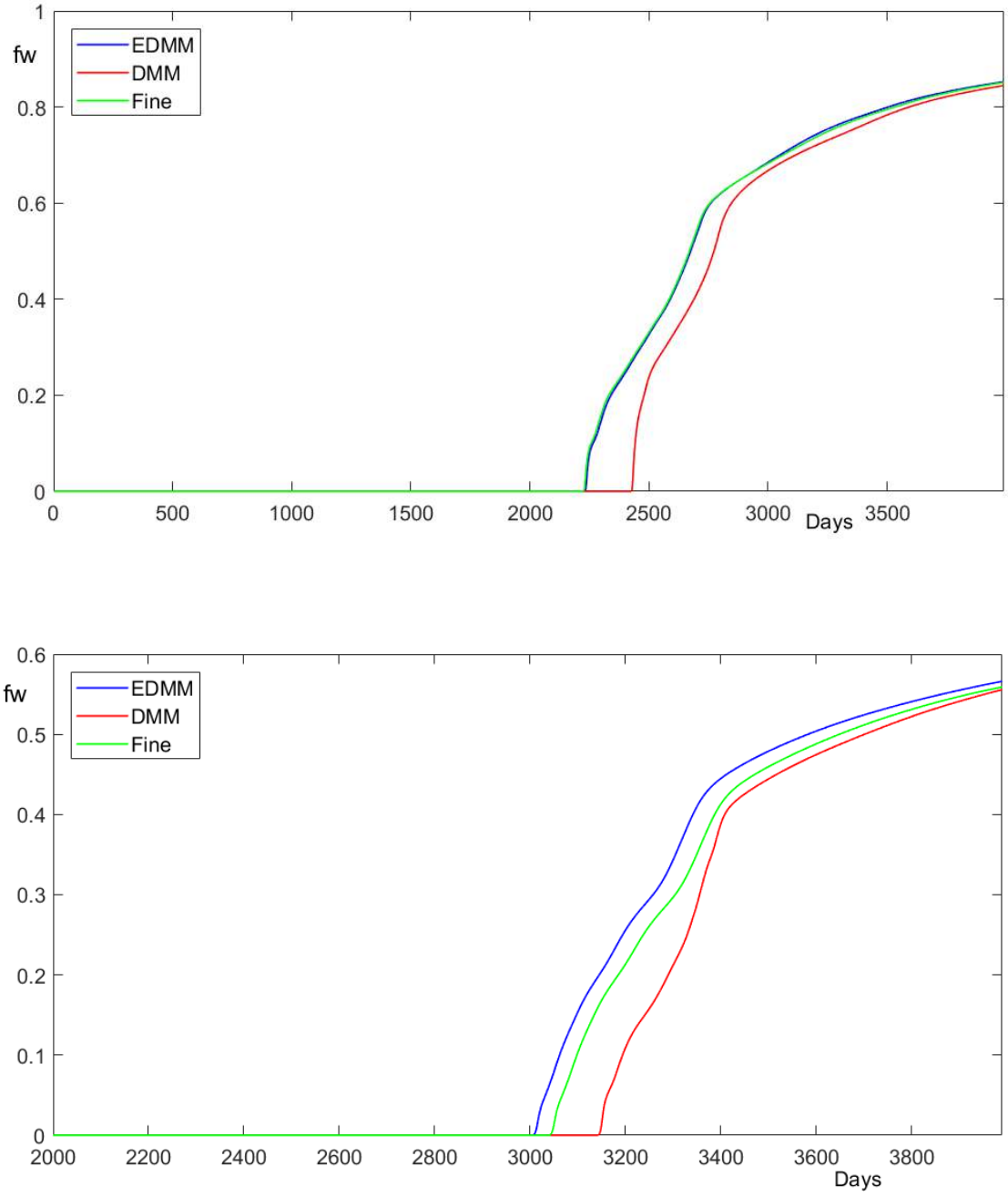

Figure 15: Plots of water cut (fw) vs. time (in days) for the two producers (top and bottom) in model 2 (M=1).

4.5.3 Model 3: 3D Case (SPE 10 Layers 59-68)

This is a 3D model that examines the speed up effect in a much bigger system as well as the accuracy of EDMM in a 3D example. Permeability field of Layers 59 to 68 of the 3D model of the 10th SPE Comparative Project model were used. The model is a channelized reservoir

system with a very heterogeneous permeability field that varies by seven orders of magnitude. The fine-scale model is 1200 ft by 2200 ft and 50 feet thick, with $60\times220\times10$ regular cells fine scale grid cells measuring 20 ft by 10 ft by 5 ft, while the upscaled coarse-scale model has $12\times44\times5$ cells. The upscaling method employed was PSM. The model has three wells, two producers, and one water injector, with the producers controlled by total rates and the injector set to replace total voidage of the producers, similar to model 2. The following methods were used to perform simulations:

1. IMPES on the LRM grid (with PSM upscaling)
2. IMPES on the HRM grid
3. DMM Method (with PSM upscaling)
4. EDMM Method (with PSM upscaling)

The fractional flow curves of water at the two producers are shown in Figure 16. Again, EDMM outperforms DMM in both wells in terms of predicting water breakthrough time and water cut throughout the simulation period, just as it does with 2D models. EDMM's water cut is likewise more accurate in both wells across the simulation time. Figure 17 shows that, while DMM is twice as accurate as the coarse solution in forecasting water cut and breakthrough time, EDMM is nearly 6 times as accurate. This only adds to what has already been demonstrated in the prior examples. It also indicates that, while EDMM and DMM are still much more accurate than the coarse solution in the 3D case, they are slightly less accurate than in the 2D models (model 1 and model 2).

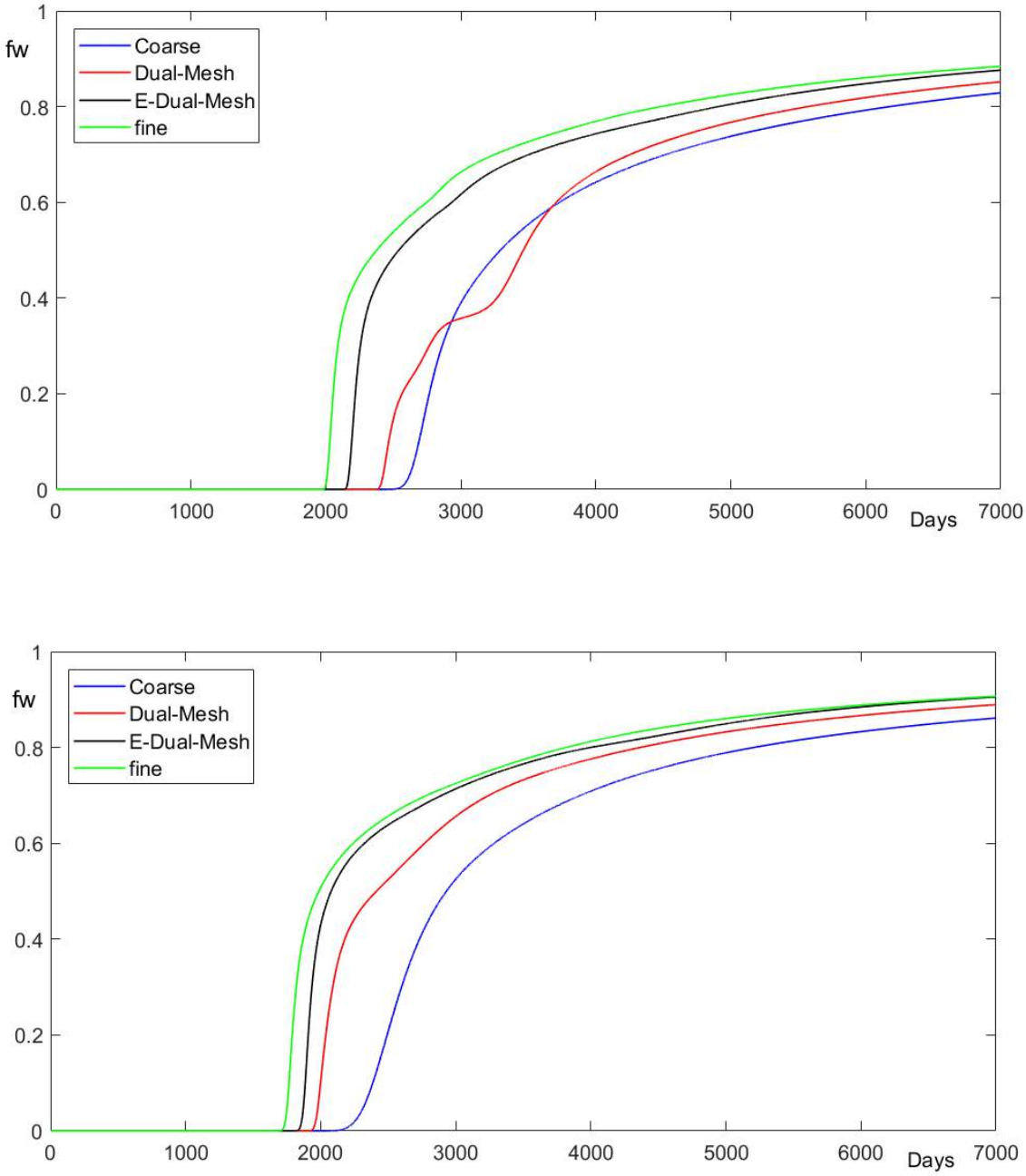

Figure 16: Plots of water cut vs. time (in days) for the two producers (top and bottom) in model 3.

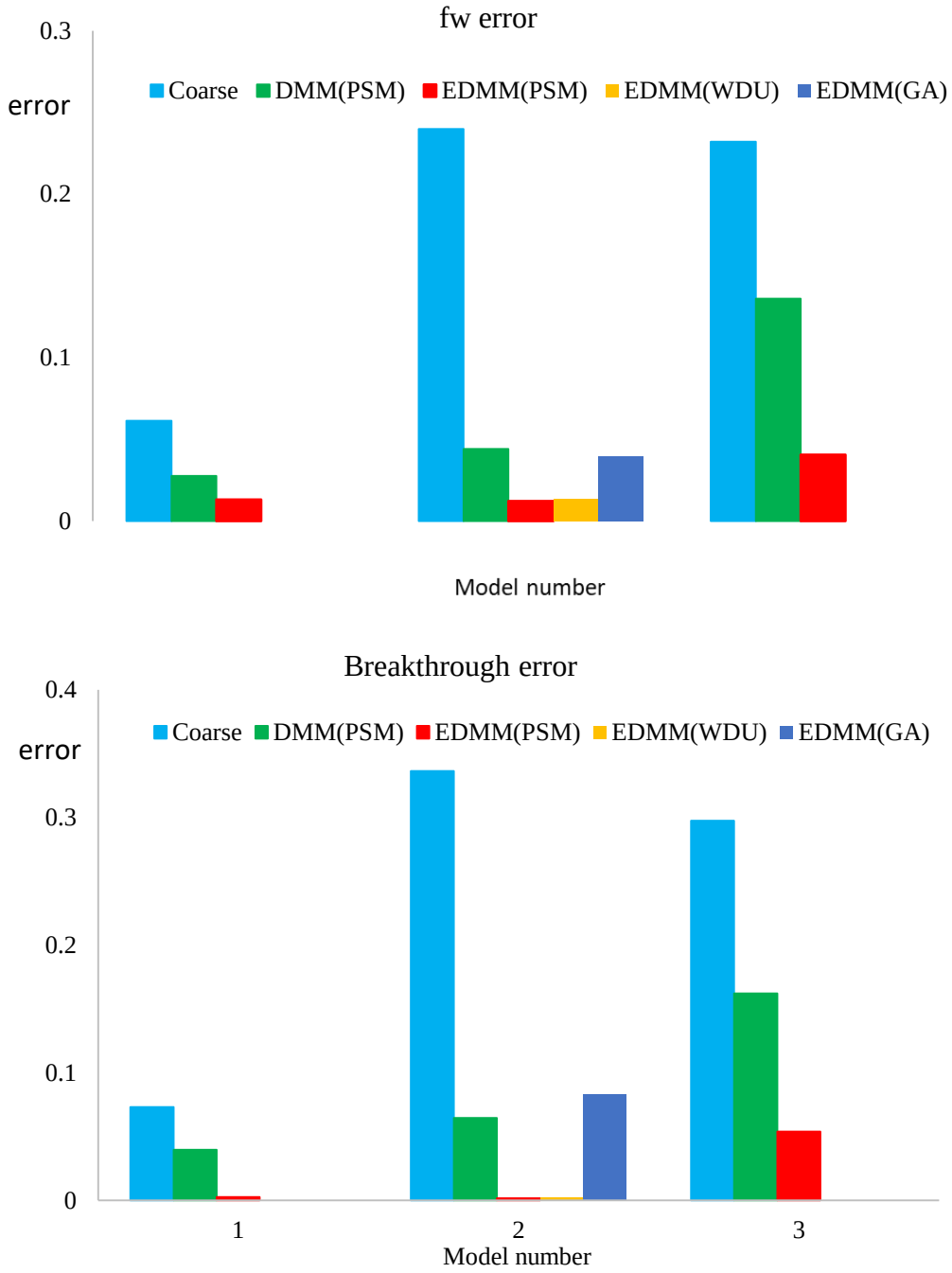

Figure 17: Errors for the three models (top) and (bottom).

4.6 Sequentiality.

The fine scale resolution to the EDMM's pressure equations (Step 4) is a sequential process. Because successive partitions need the fine-scale fluxes (current time index n+1) of the preceding boundary blocks (boundary conditions) to remain conservative, the directional oversampling of local fine-scale pressure downscaling specified in Step 4 is done sequentially.

As a result, the previous partitions must be solved first. This suggests that the solution's direction, i.e. the choice of start and end locations, has an impact on the results. Model 2 was also solved in the reverse direction to see what influence this had on the solution (i.e. the last coarse partition was solved first). Figure 14 shows these results. First, it demonstrates that the solution sequence has an influence and that the base case solution is not equal to the reverse solution. When their agreements with fine-scale solutions are evaluated, it also indicates that both solutions are extremely accurate and far superior to DMM solutions. These findings imply that, while the method's sequential nature influences the solution, the solution sequence has little impact on the method's accuracy. The direction from injector to producer looks to be the most accurate. As a result, in circumstances where a dominating flow direction can be determined, such as by looking at the distribution of producer injectors, the reconstruction from injectors to producers may be prioritized.

4.7 Speed Up

Because there are many elements that impact the cost of simulation runs, such as the efficiency of the code and the solver used, it is difficult to estimate the cost savings of a multiscale technique (Arbogast and Bryant, 2002). The speed up factor as used here is defined as the ratio of the simulation time spent on global fine-scale pressure solution to the time spent on pressure solution using the other approach (since saturation is solved similarly at the fine-scale; and in the DMM and EDMM methods). The average speed up ratios of the DMM and EDMM approaches in 2D and 3D implementations are shown in Figure 18. While DMM has a greater speed up factor, it is obvious that both DMM and EDMM greatly accelerate the pressure solution. As a result, it is reasonable to compare their accuracies. Given the similar speed (cost) of DMM and EDMM, the EDMM's substantially superior accuracy shows that it is an upgrade over DMM. An Intel Xeon CPU 3.5 GHz CPU with 16 GB of RAM was utilized for all of the runs presented.

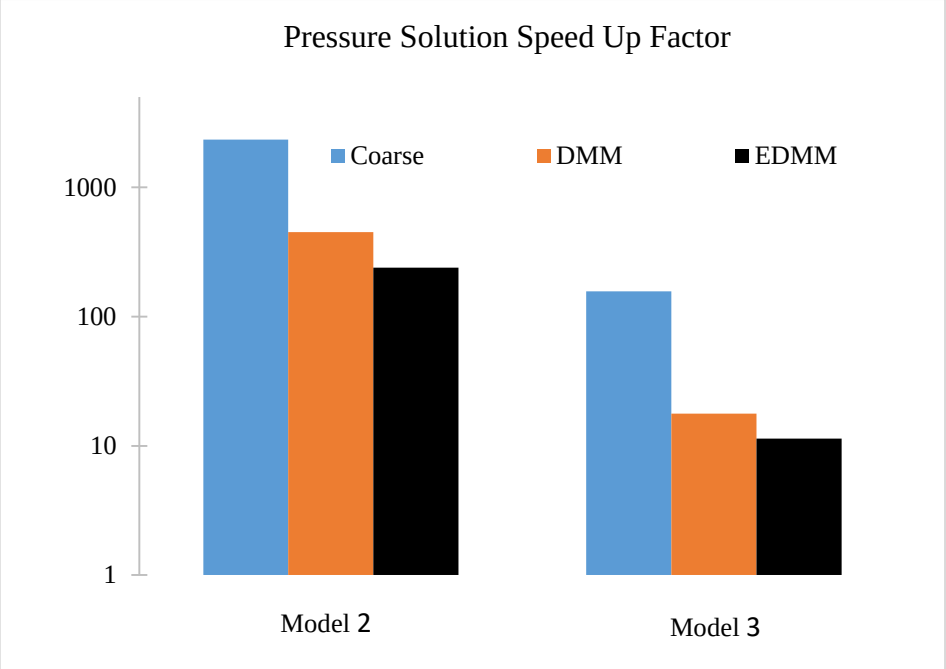

Figure 18: Average pressure solution speed up factors for the simulated cases using the Coarse, DMM, and EDMM techniques. The ratio of simulation time spent on fine-scale pressure solution to simulation time spent on the other method's pressure solution is known as the speed up factor.

4.8 Parallelization

Parallel computing is a method of further increasing the speed of a computation. However, because the fine-scale fluxes boundary condition (at current time index n+1) is required for the extended local calculation of fine-scale pressure (specified in Step 4), the technique as presented must be modified to allow for concurrent solutions to Step 4. This is due to the fact that fine-scale solutions to preceding partitions are needed as BC for succeeding partitions, which means they must be solved first and hence cannot be solved simultaneously. Explicit fine-scale border flux (i.e. flux at earlier time-index n) may be used to enable parallel processing. This is totally parallelizable, and it would speed up the EDMM approach even more in really big cases. Explicitly handling the boundary condition theoretically, on the other hand, should have an impact on the solution. This explicit parallel implementation of EDMM on

model 2 was done to investigate this impact. The explicit parallel EDMM implementations on model 2 are shown in Figure 14 along with the standard implementations of EDMM. It demonstrates that the parallel EDMM implementation is comparable to the normal EDMM in terms of accuracy and is an improvement over DMM. This demonstrates the EDMM's practicality and accuracy when used in parallel.

4.9 Discussions

So far, the standard approach (in literature) to improving accuracy in DMM-based approaches has been to focus on either improving the upscaling methods thus reducing the error in the coarse scale solution or the improving local fine scale distribution of coarse fluxes utilized as BC. EDMM is the first approach that we are aware of that enhances DMM accuracy without taking any of these two approaches. Here, the error passed down from the coarse scale was decreased by minimizing the effect of the coarse solution (BC) on the reconstruction through DO, resulting in improved results. EDMM, unlike other DMM advancements (Babaei and King, 2012; Firoozabadi et al., 2009; Firoozabadi and Ashjari, 2009), is a completely separate method from DMM; it is based on DMM but takes a completely new approach. As a result, the improvement is more substantial than iterative. DO is also a more generic method, thus it may be used with any upscaling methodology and any boundary condition, unlike some of the more recent advancements to DMM, which are tied to specific upscaling methods or BC distributions. However, this comes at a price. As may be seen in Figure 18. Because of the larger (oversampled) fine-scale reconstruction problems, the cost of EDMM is higher than DMM. When comparing the two techniques, this must be taken into account. Some of the drawbacks of DMM are also present in EDMM as proposed. One of these is that with sharper fronts, accuracy suffers. As explained by Babaei and King (2012), unstable fronts are simpler to rebuild than acute, stable fronts because saturation changes are more gradual.

4.10 Conclusion

A novel dual mesh technique has been successfully used to simulate two-phase flow problems with accuracy comparable to fine-scale solutions at a substantially lower cost than fine-scale solutions. EDMM is easy to use, works with any upscaling approach, and has been proven to be reliable in its use. It was also demonstrated that it may be parallelized. Three separate cases were used to evaluate the approach, and the results were compared against fine-scale, DMM, and coarse-scale solutions. The approach is a major improvement over the DMM, significantly better than coarse grid solutions and comparable in quality to fine-scale solutions, according to the results. It has been demonstrated to be accurate in not only forecasting water breakthrough at producer wells, but also water cut following breakthrough. Even in very heterogeneous grids, EDMM results are dependably good (models 2 and 3). It has been shown to improve accuracy by reducing both homogenization and numerical dispersion errors, independent of the upscaling approach used. This approach might be expanded to incorporate capillarity and, eventually, compressibility.

5 TRIPLE MESH METHODS

5.1 Introduction

In the previous chapter, EDMM was introduced as an improvement on the accuracy weaknesses of DMM. This approach is more expensive than the conventional DMM even though it has higher accuracy. Both DMM and EDMM are two-level systems that may be an upgrade on coarse-scale solutions, however, they are not necessarily optimized for speed or accuracy. While almost all available multiple mesh methods involve two mesh systems, two mesh systems are not necessarily optimal in terms of cost or accuracy. In this chapter, two novel multimesh methods are presented, the Extended Triple Mesh Method, ETMM and the Triple Mesh, Method TMM. As the names suggest, both methods involve three mesh sizes of grids. In this chapter, first the methods are described, then they are tested on different water-flooding examples. Comparison was then made between the performances of the two methods and the fine-scale and coarse-scale solutions as well as the two dual mesh methods, the EDMM and the DMM. The outline of the chapter is as follows: The governing flow equations are first introduced, followed by TMM and ETMM. Three problems of different complexities were then solved by the methods and comparisons were made between the performances. Finally, the results were discussed, conclusion was made and recommendations were presented.

5.2 Governing Equations

This section describes the governing equation on which the new methods are based on. Consider an incompressible, heterogeneous two-phase (oil and water) porous system. The conservation equations for the phases (oil and water) are given by:

$$\phi \frac{\partial S_w}{\partial t} + \nabla \cdot \vec{u}_w = -q_w \quad \text{..... 22}$$

$$\phi \frac{\partial S_o}{\partial t} + \nabla \cdot \vec{u}_o = -q_o \quad \text{..... 23}$$

where S_i, $\vec{u_i}$, q_i and are the saturation, the Darcy velocity vector, and the source term respectively, ϕ is the porosity and the subscripts 'o' and 'w' found throughout this paper represent oil and water respectively. Negligible capillary is assumed in this work. The Darcy velocities of the two phases are given by

$$\vec{u}_w = -\lambda_w \bar{\bar{k}} \cdot (\nabla p + \gamma_w i_z) \quad \text{..... 24}$$

$$\vec{u}_o = -\lambda_o \bar{\bar{k}} \cdot (\nabla p + \gamma_o i_z) \quad \text{..... 25}$$

where λ_o and λ_w are the oil and water mobilities respectively, p represents pressure, γ_o and γ_w are the oil and water gravities respectively and $\bar{\bar{k}}$ is the diagonal permeability tensor of the porous medium. The mobilities can be written as

$$\lambda_w = \frac{k_{r_w}(S_w)}{\mu_w} \quad \text{..... 26}$$

$$\lambda_o = \frac{k_{r_o}(S_w)}{\mu_o} \quad \text{..... 27}$$

where μ_i and k_{r_i} represent the viscosity and relative permeability of the phase I respectively. Since the sum $S_w + S_o = 1$, if $\dot{u} = \dot{u}_w + \dot{u}_o$, then the systems of Eq. (22-23) can be written as:

$$\nabla \cdot \vec{u} = -q \quad \text{..... 28}$$

$$\phi \frac{\partial S_w}{\partial t} + \nabla \cdot f_w \left(\vec{u} + \lambda_o (\gamma_w - \gamma_o) \overline{\overline{k}} \cdot i_z \right) = -q_w \quad \text{..... 29}$$

where $q = q_w + q_o$ and f_w is the fractional flow of water such that $\vec{u}_w = f_w \left(\vec{u} + \lambda_o (\gamma_w - \gamma_o) \overline{\overline{k}} \cdot i_z \right)$

The total Darcy velocity can be written as:

$$\vec{u} = \overline{\overline{k}} \cdot \left(\lambda_t \nabla p + (\lambda_w \gamma_w + \lambda_o \gamma_o) i_z \right) \quad \text{..... 30}$$

where, $\lambda_t = \lambda_w + \lambda_o$. Substituting for total velocity Eq. (30) in Eq. (28) give the flow (or pressure) equation given by:

$$\nabla \cdot \left(\overline{\overline{k}} \cdot \left(\lambda_t \nabla p + (\lambda_w \gamma_w + \lambda_o \gamma_o) i_z \right) \right) = q \quad \text{..... 31}$$

The flow equation together with Eq. (29), which is called the saturation (or transport) equation represent the two equations whose solution must be found in this problem. A variety of numerical schemes can be used to find a solution to these coupled set of non-linear equations. The scheme that is used in this chapter is IMPES where the transport equation is solved explicitly while the flow equation is solved implicitly.

5.3 Multilevel Modelling

There have been no researches that have been done that proves that two mesh levels are optimal for accuracy or cost. Despite that, almost every multimesh method available entails the use of two levels of upscaling-downscaling. As far as our knowledge goes, this attempt is the first one at three mesh-level downscaling as well as at comparison of the performances of one, two and three mesh levels. Here, we propose and evaluate the performances of two triple mesh methods: the Triple Mesh Method TMM and the Extended Triple Mesh Method ETMM described below.

5.4 Triple Mesh Method TMM

The TMM involves the use of 3 levels of successively coarser mesh sizes i.e. fine-scale grid, FSG, the intermediate-scale grid, ISG, and the coarse-scale grid, CSG. Two levels of upscaling is therefore needed. The compatibility of this method with any upscaling method affords the combination of the method with any accurate upscaling method. The transport equation is solved on the finest scale while the global pressure equation is solved on the coarsest scale. The TMM can be divided into these following steps

Step 1: Properties Definition. This step entails the definition of FSG properties including porosities, permeabilities, saturations as well as source term and boundary conditions.

Step 2: Upscaling. In this step, the FSG is upscaled into the ISG and the CSG. Whilst compatible with any method, a local flow-based upscaling method, the Pressure Solved Method (PSM) for transmissibility upscaling was used in this work similar to application by Begg et al. (1989).

Step 3: Solving the CSG Pressure Equation. Here, the flow equation on CGS is solved and the coarse-scale velocity field is computed.

Step 4: Successive Downscaling. In this step, the flow solution is successively downscaled to the fine-scale from the coarse-scale. It is a two-stage step. First, the local flow problems are solved with transmissibility weighted flux boundary in each coarse cell domain in the ISG in order to get the velocity field on the ISG. The boundary conditions are similar to DMM i.e. from CSG velocities distribute using EQ. (1). Then the ISG is downscaled to the FSG by repeating the process i.e. solution to local flow problems are found with transmissibility weighted flux boundary on the FSG with boundary fluxed obtained from ISG velocities distributed using Eq. (1). This gives a conservative flux field on both the intermediate and fine scale.

Step 5: Solving the Transport Equation. In this step, the already computed conservative fine-scale flux field is used to solve the transport equation on the finest scale.

These steps are illustrated in Figure 19 and summed up in the flow chart shown in Figure 20.

5.5 Extended Triple Mesh Method ETMM

One downside to local methods is that they can be quite inaccurate. The application of extended local methods i.e. oversampling is one of the ways that the inaccuracy has been addressed. Better results have been shown to be obtained using Extended local methods compared to purely local methods (Adeyemi et al., 2021; Babaei and King, 2013, 2012) in chapter 4. The ETMM, like the TMM needs 3 grids of successively coarser mesh sizes i.e. the FSG, the ISG and CSG. Two levels of upscaling is also needed by the ETMM and it is compatible with different upscaling methods. ETMM employs two downscaling steps and involves solving the global pressure equation on the CSG and the transport equation on the FSG. The ETMM downscaling entails applying 'direction oversampling method', DO to solve extended local problems, unlike the TMM. Solving extended local problems instead of the local problems in TMM is required in each of the downscaling steps involved. ETMM is divided into the following steps.

Step 1: Properties Definition. This step entails the definition of FSG properties including porosities, permeabilities, saturations as well as source term and boundary conditions.

Step 2: Upscaling. In this step, the FSG is upscaled into the ISG and the CSG. Whilst compatible with any method, a local flow-based upscaling method, the Pressure Solved Method (PSM) for transmissibility upscaling is used in this work similar to application by Begg et al. (1989).

Step 3: Solving the CSG Pressure Equation. Here, the solution of the flow equation on CGS is found and the coarse-scale velocity field is computed.

Step 4: Successive Downscaling. In this step, the flow solution is successively downscaled to the fine-scale from the coarse-scale. This is a two-stage step. Directionally oversampled extended local problems are solved with transmissibility weighted flux boundary conditions in order to get the velocity field on the ISG. To downscale from the ISG to the FSG, the process is then repeated i.e. directionally oversampled extended local flow problems are solved on the FSG with transmissibility weighted flux boundary condition. There is a conservative flux field on both the intermediate and fine scale by the end of this step.

Step 5: Solving the Transport Equation. In this step, the already computed conservative fine-scale flux field is used to solve the transport equation on the FSG.

These steps are illustrated in Figure 19 and summed up in the flow chart shown in Figure 20. The major difference between the methods TMM and ETMM are summed up in Table 3.

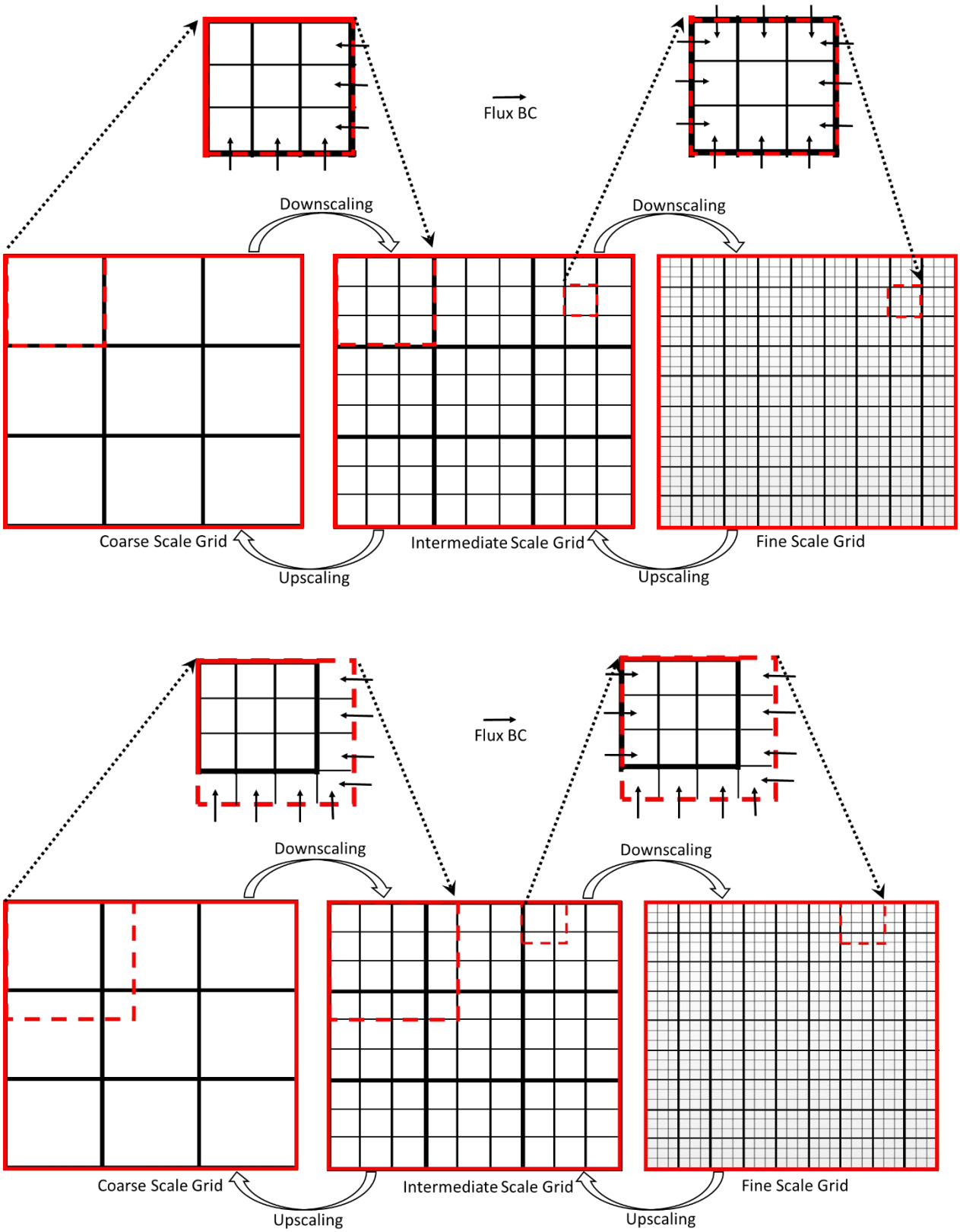

Figure 19: Illustration of successive downscaling of TMM (above) and ETMM (below)

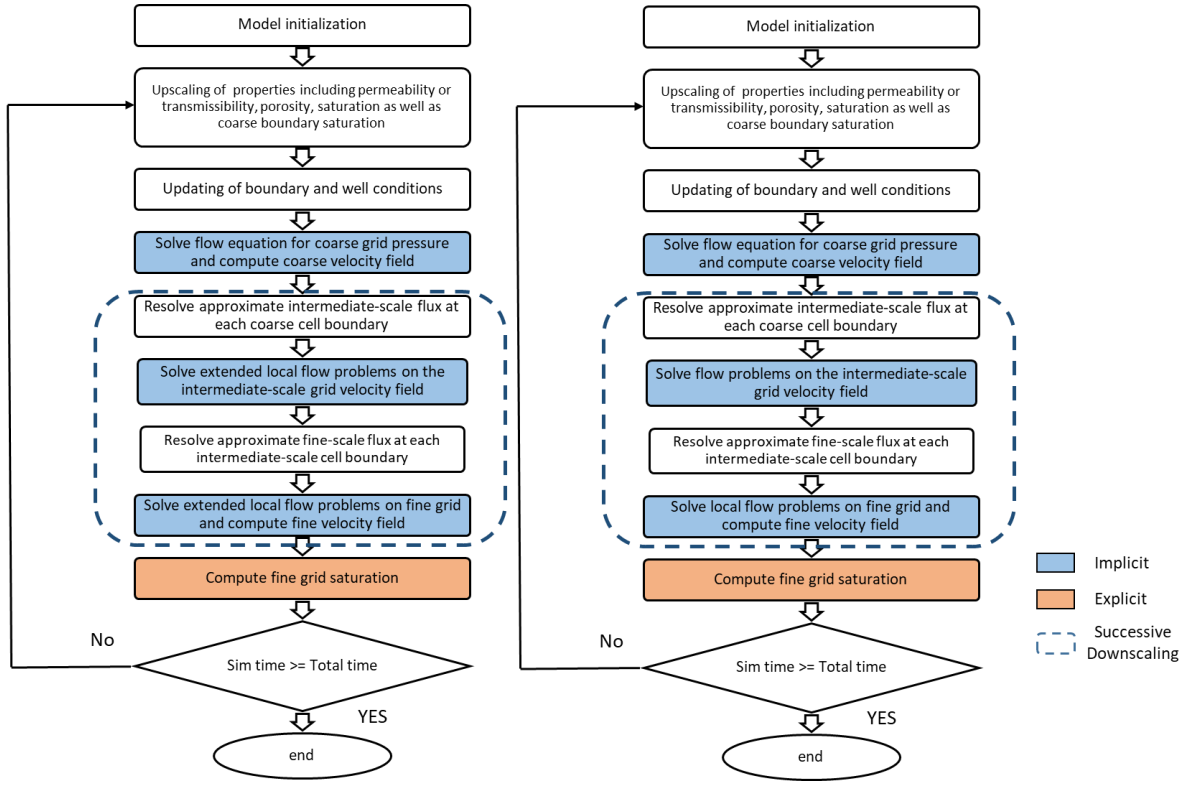

Figure 20: Flow chart for ETMM(left) and TMM(right) algorithms

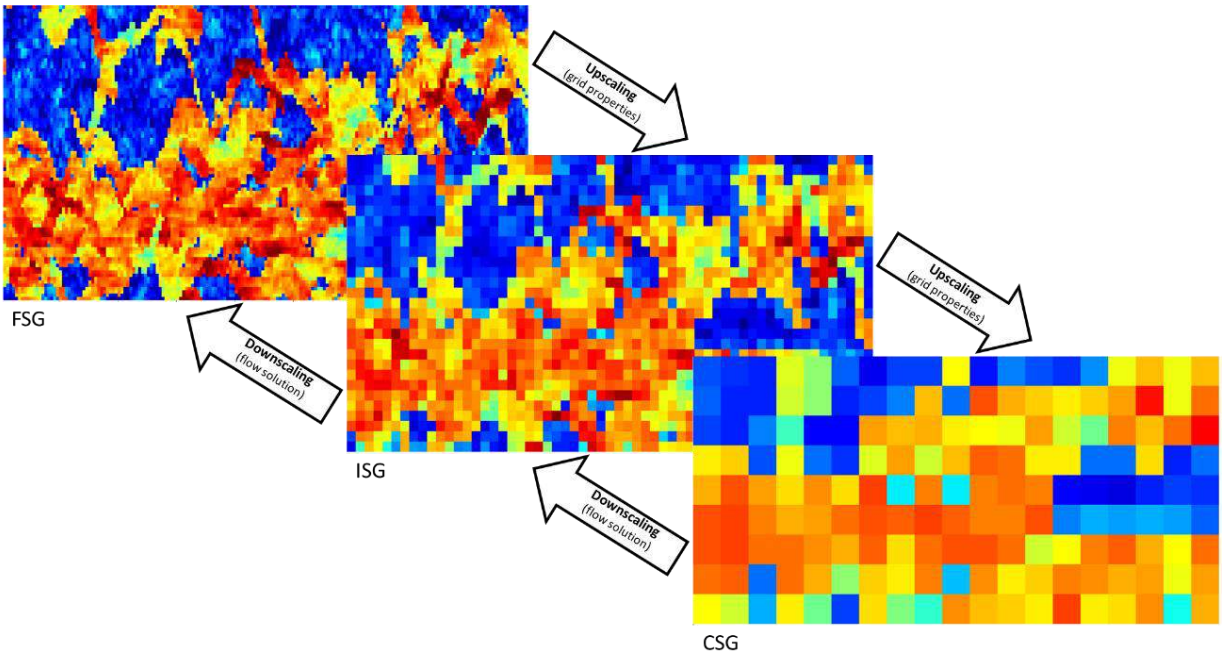

Figure 21: Successive upscaling-downscaling of Layer 59 of the 10th SPE Comparative Project model (Christie and Blunt, 2001) permeability field.

Table 3 – Comparison between the approaches to TMM and ETMM method

TMM	**ETMM**
Both involve two levels of downscaling of the flow solution and solves saturation at the fine scale	
Errors inherent in the coarse-scale and intermediate-scale solutions are passed down to the fine scale through the BC	Effects of the BC on the accuracy is reduced through the application of directional oversampling
Limited coupling between the fine-scale, intermediate-scale and coarse-scale models	Improved coupling between the three scales
Highly dependent on the accuracy of the upscaling method	ETMM focuses on reducing the impact of upscaling method and BC of choice on the accuracy

5.6 Implementation and Results

For the effectiveness and efficiency of the proposed methods to be evaluated, the methods were tested on three problems. There is a unique grid property distribution and well distribution for each problem. Some form of IMPES scheme is used in every solution option that was explored, in which the pressure equations are solved implicitly for pressure and fluxes computed while the saturation equation is solved explicitly. In the way these schemes, DMM, EDMM, TMM and the ETMM are implemented, the solution to saturation is done on the finest scale and the global pressure equation is solved on the coarse scale and downscaled. Two error indicators were used to evaluate how well the methods performed. The first one is the water cut error E_{fw} and it is expressed as

$$E_{fw} = \frac{1}{t_{total}} \sum_{i=1}^{nt} \left| \frac{\left[f_w^f(i) - f_w^c(i) \right] \Delta t_i}{f_w^f(i)} \right| \quad \text{.....} 32$$

where $t_{total} = \sum_{i=1}^{n_t} \Delta t_i$ represents the simulation duration, nt represents the number of time steps, f_w^f and f_w^c respectively represent the fine-scale model water cut and the water cut of the evaluated model.

Error in water breakthrough time E_{bt} is the second error indicator and it is expressed as

$$E_{bt} = \frac{1}{n_{wells}} \sum_{j=1}^{nw} \left| \frac{t_{bt}^f(j) - t_{bt}^c(j)}{t_{bt}^f(j)} \right| \quad \text{.....} 33$$

n_{wells} represents the number of producers, t_{bt}^f and t_{bt}^c is the time till water breakthrough in the fine-scale model and the evaluated model respectively. Residual oil saturation of 0.18 and initial water saturation, S_{wi} of 0.1 were used and the modelling of the relative permeability was done with Corey type function. An idea of the accuracy of the models, not only in predicting recovery but also in predicting the water breakthrough time which is probably the most significant and impactful event in the life of a production system is got from the two error indicators.

Table 4 *Input parameters for the three models (except where otherwise stated)*

Parameter	
Porosity	0.25
Permeability	Specified heterogeneous distribution
Oil Viscosity (cP)	0.3
Water Viscosity (cP)	3
Well primary control (Producers)	Total liquid rates
Well primary control (Injectors)	Injectors (Total voidage replacement)
Wellbore radius (ft)	0.3
Kro_{max}	1
Sor	0.18
No (Corey)	2
Krw_{max}	0.6
Swc	0.1
Nw (Corey)	2

5.6.1 The Refinement Model

This is a synthetic 2D model with log permeability distribution shown in Figure 22. The reservoir has a dimension of 1200ft by 2200ft with average thickness of 5ft. The FSG is 90 by 180 i.e. it contains 16200 cells, ISG is 30 by 60 i.e. contains 1800 cells while the CSG is 20 by 10 i.e. contains 200 cells. Every ISG cell therefore contains 9 FSG cells and every CSG cell contains 9 ISG cells i.e 3 by 3 or 81 FSG cells i.e. 9 by 9. The ISG and the FSG models do not require upscaling because they are refinements of the CSG model. This means that the local problems within each coarse cell domain are homogeneous while the global problem has a

heterogeneous permeability field. This first problem has the idea of eliminating as much homogenization error due to upscaling in the ISG and the CSG as possible so as to observe the effect that the proposed methods have on numerical dispersion. There are 5 wells, one central injector flanked by 4 producers distributed in the model as shown in Figure 22.

The residual oil saturation of 0.18 and initial water saturation of 0.1 was used. Table 4 was used to model the saturation functions. Upscaling was done using PSM. The following are the solution approaches tested.

1. Standard IMPES on the fine-scale (refinement) grid
2. Standard IMPES on the coarse-scale grid
3. Dual Mesh Method
4. Extended Dual Mesh Method
5. Triple Mesh Method
6. Extended Triple Mesh Method

Figure 31 highlights the errors that the different methods have relative to the fine-scale model while Figure 23 shows the 4000-day simulation water-cut at the four producers. The error indicators show that all the tested methods are great improvements on the coarse-scale solution. They all have better accuracy both in water-cut predictions and prediction of the breakthrough time. Another observation is that in general, the accuracies of the DMM and TMM are similar while that of the ETMM and EDMM are also similar. This despite the fact that TMM is a cheaper solution method than DMM and ETMM is also cheaper than EDMM. There is this consistency in all four producer wells.

Numerical dispersion error is expected to dominate (over homogenization) in this given that it is a refinement model. The effectiveness of ETMM and TMM in reducing numerical dispersion are therefore shown in this example. So the fact that ETMM is a cheaper solution than EDMM whilst displaying similar levels of error is impressive and so is the fact that TMM and the much

more expensive DMM have similar accuracy. Additionally, the fact that the EDMM and ETMM are more accurate compared to DMM and TMM shows how effective directional oversampling is at error reduction.

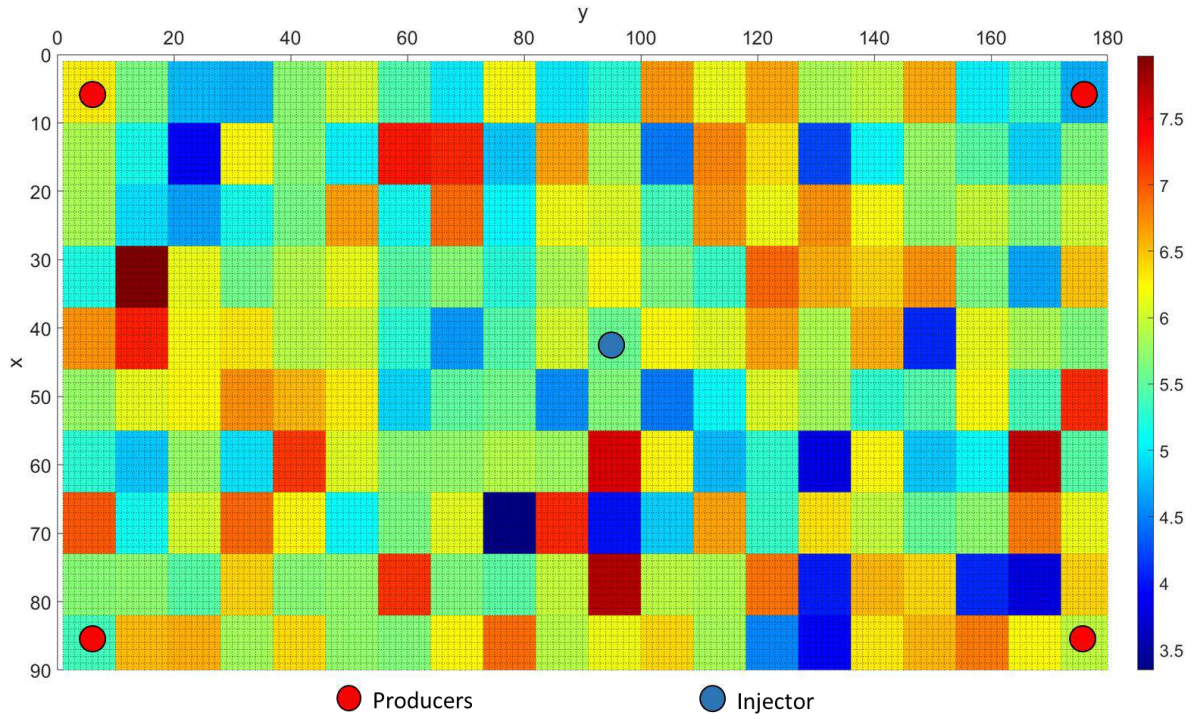

Figure 22: Model 1 permeability field with well locations superimposed

(a)

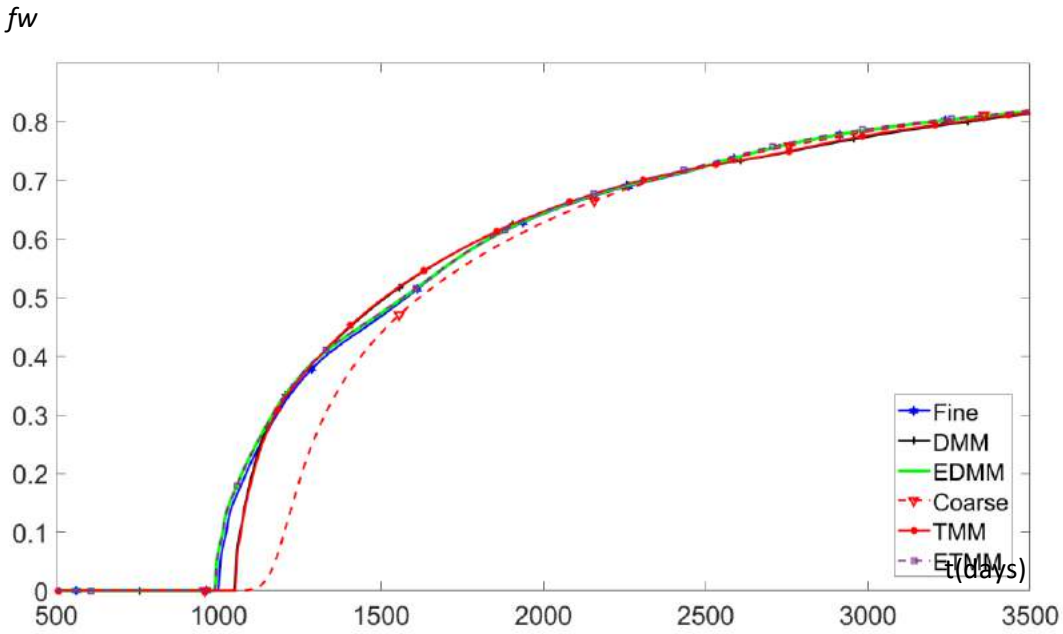

(b)

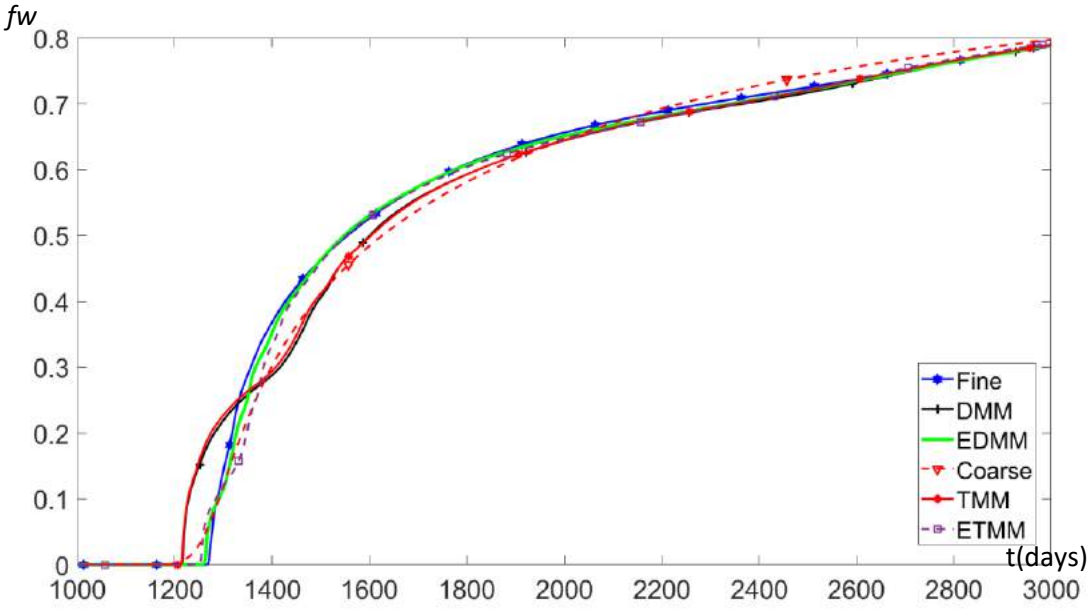
fw
0.8
0.7
0.6
0.5
0.4
0.3
0.2
0.1
0
1000
1200
1400
1600
1800
2000
2200
2400
2600
2800
3000
t(days)
Fine
DMM
EDMM
Coarse
TMM
ETMM

(c)

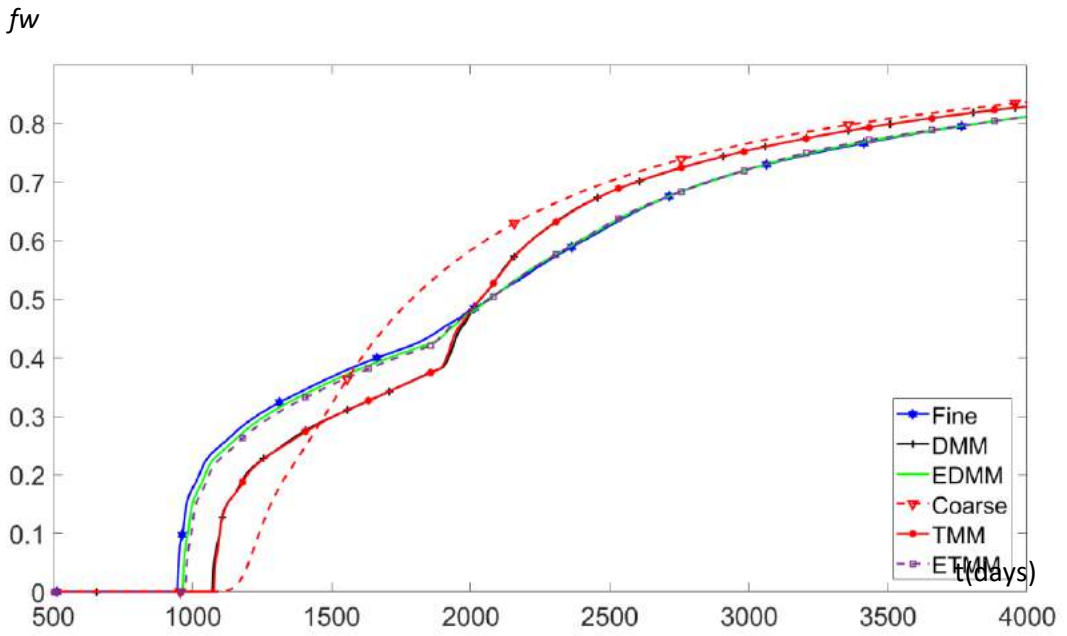
fw
0.8
0.7
0.6
0.5
0.4
0.3
0.2
0.1
0
500
1000
1500
2000
2500
3000
3500
4000
t(days)
Fine
DMM
EDMM
Coarse
TMM
ETMM

(d)

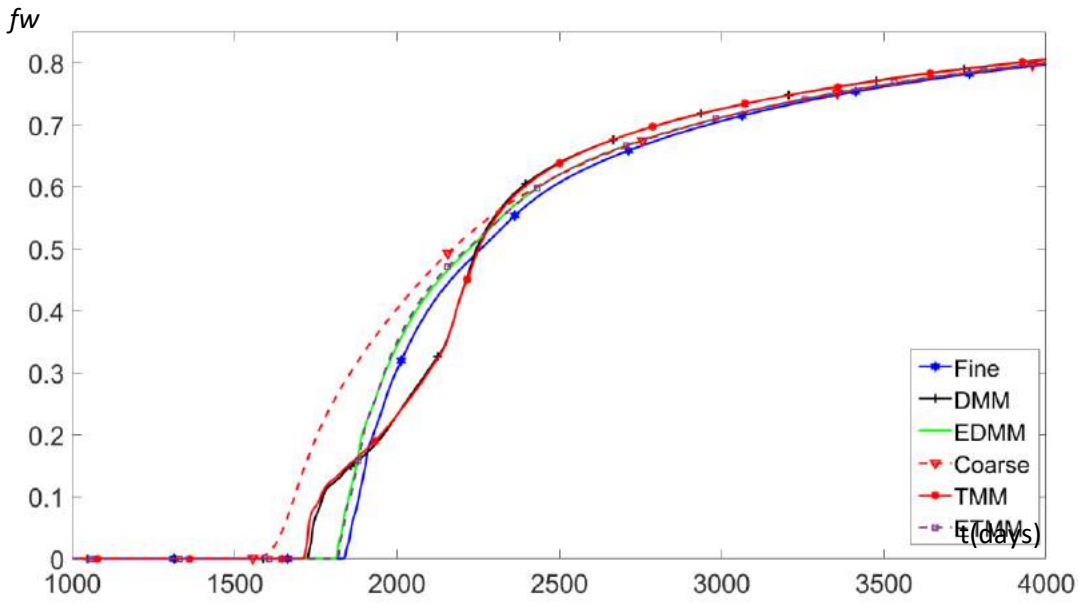

Figure 23: Water cut (fw) vs time (in days) plots for Model 1 four producers using the different solution methods

5.6.2 SPE 10 Model Layer 1

This is a 2D model with a log permeability field shown in Figure 24. It is a version of layer one of the 3D model of the 10th SPE Comparative Project model that has been slightly modified. It is a highly heterogeneous model with permeability field varying between six orders of magnitude. The reservoir has a dimension of 1200ft by 2200ft with thickness of 5ft. The FSG is 90 by 180 i.e. it contains 16200 cells, ISG is 30 by 60 i.e. contains 1800 cells while the CSG is 20 by 10 i.e. contains 200 cells. Every ISG cell therefore contains 9 FSG cells and every CSG cell contains 9 ISG cells i.e. 3 by 3 or 81 FSG cells i.e. 9 by 9. The CSG and ISG are upscaled versions of the FSG. The PSM method was used in the two upscaling steps. After Model 1 tested the effects of the methods in reducing dispersion error, this model tests their effectiveness in reducing combined homogenization and dispersion errors. There are 5 wells,

one central injector flanked by 4 producers distributed in the model as shown in Figure 24. The following are the solution approaches tested.

1. Standard IMPES on the fine-scale grid
2. Standard IMPES on the coarse-scale grid (with PSM upscaling)
3. Dual Mesh Method (with PSM upscaling)
4. Extended Dual Mesh Method (with PSM upscaling)
5. Triple Mesh Method (with PSM upscaling)
6. Extended Triple Mesh Method (with PSM upscaling)

Figure 31 highlights the errors that the different methods have relative to the fine-scale model while Figure 25 shows the 4000-day water-flooding water-cut at the four producers. The accuracy of all the tested schemes as shown in the plot are higher than the CSG in predicting breakthrough time as well as recovery. The DMM, EDMM, TMM, ETMM methods have significant higher accuracy compared to the CSG results and this is clearly shown by the error values (E_{fw} and E_{bt}). There is a consistent pattern with Model 1 when compared to these four schemes. The accuracies of EDMM and ETMM are similar and clearly more than that of the DMM and TMM also with their similar accuracies.

This example, like Model 1, shows how effective TMM and ETMM are at reducing cost by adding an intermediate layer without a significant decrease in accuracy. Like the previous example, it also shows how effective directional oversampling is when applied in ETMM and EDMM methods, to improve accuracy when compared to plain local downscaling method used in TMM and DMM. This example shows how that the methods are effective in handling real heterogeneous reservoirs. It also shows that even with the additional error (homogenization) in the coarse pressure introduced by the upscaling, the improvements in results are consistent.

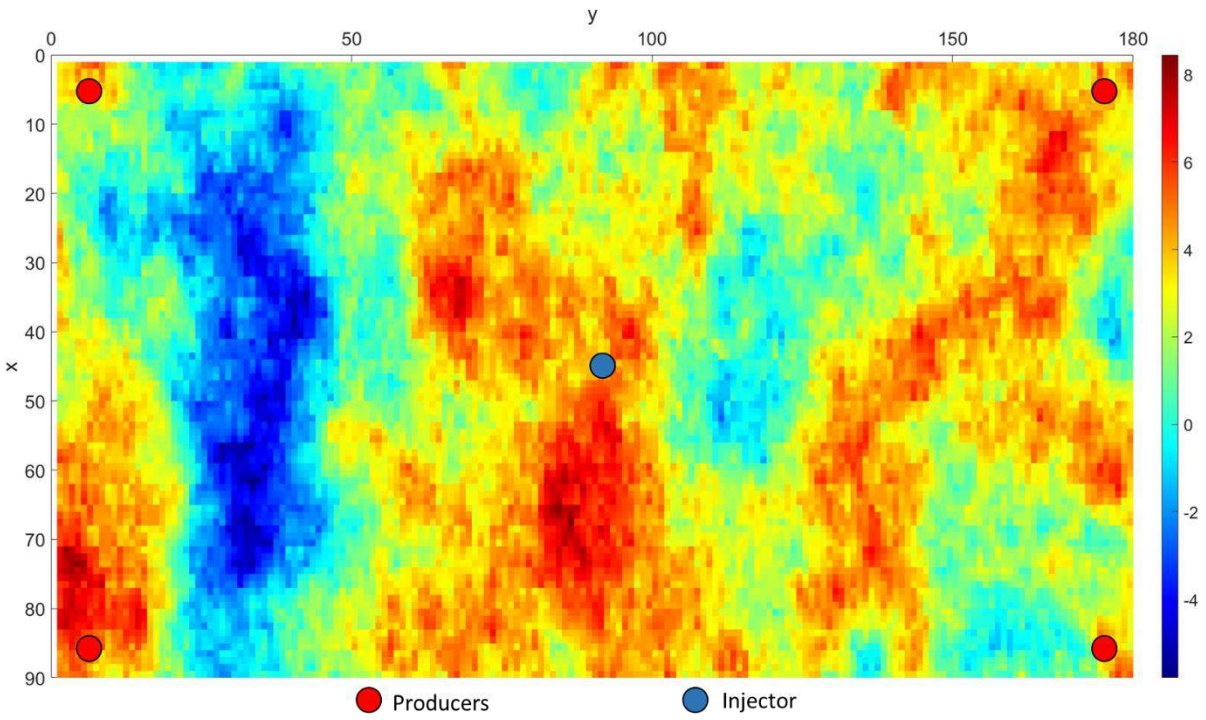

Figure 24: Model 2 permeability field and well distribution

(a)

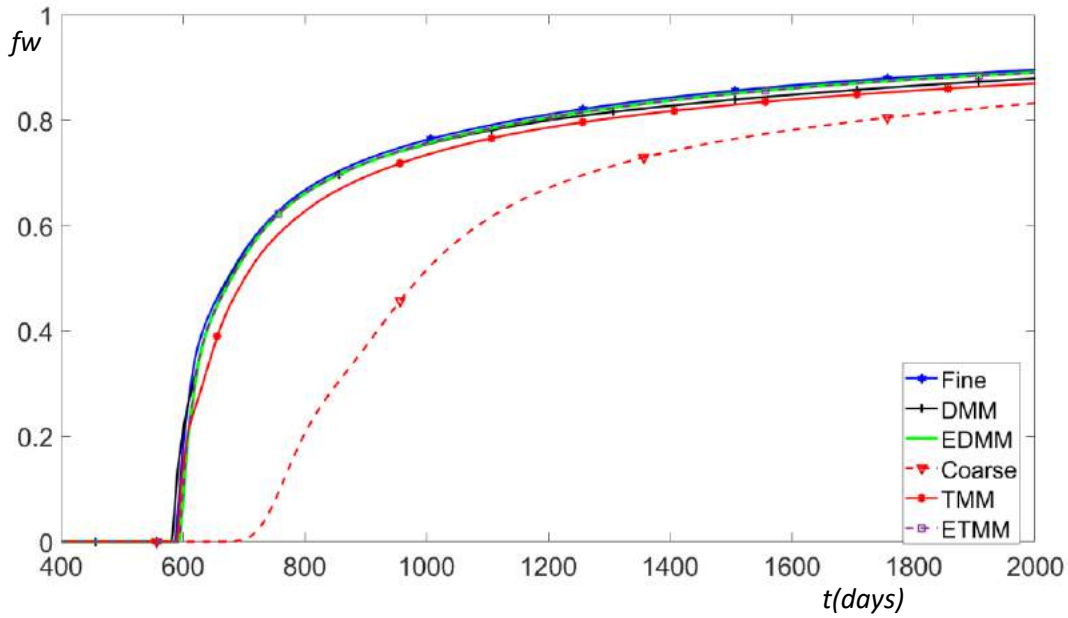

(b)

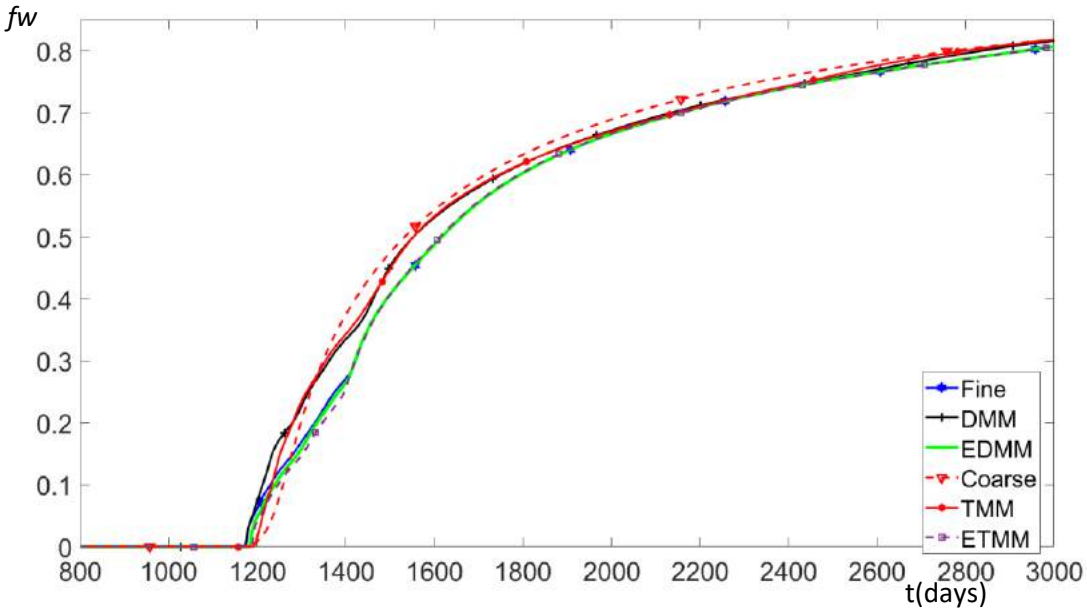
fw
0.8
0.7
0.6
0.5
0.4
0.3
0.2
0.1
0
800
1000
1200
1400
1600
1800
2000
2200
2400
2600
2800
3000
t(days)
Fine
DMM
EDMM
Coarse
TMM
ETMM

(c)

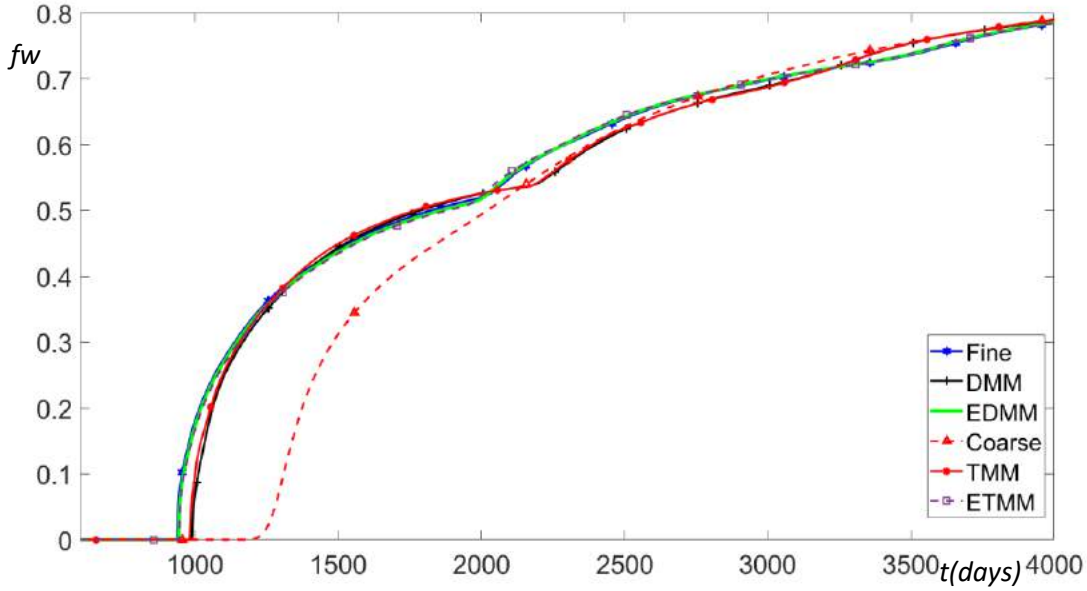
fw
0.8
0.7
0.6
0.5
0.4
0.3
0.2
0.1
0
1000
1500
2000
2500
3000
3500
4000
t(days)
Fine
DMM
EDMM
Coarse
TMM
ETMM

(d)

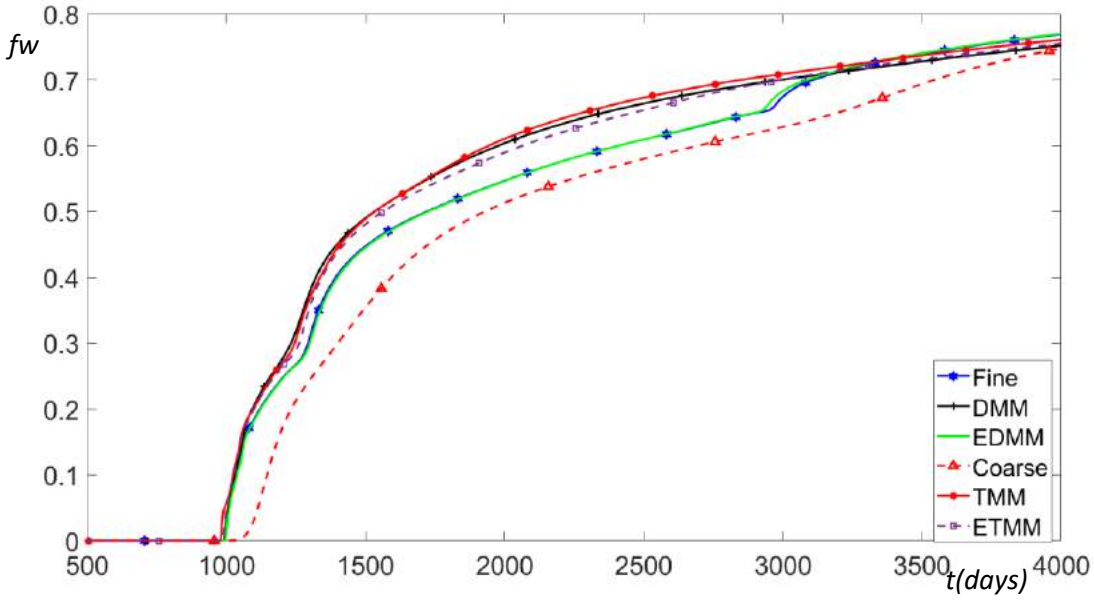

Figure 25: Water cut (fw) vs time (in days) plots for Model 2 four producers using the different solution methods i.e. Coarse scale, EDMM, DMM, ETMM, TMM and Fine scale

5.6.3 SPE 10 Model Layer 59

This is a 2D model with a log permeability field shown in Figure 26. It is a version of layer 59 of the 3D model of the 10th SPE Comparative Project model that has been slightly modified. The model represents a highly heterogeneous channel sand with permeability field varying between seven orders of magnitude. The reservoir has a dimension of 1200ft by 2200ft with thickness of 5ft. The FSG is 90 by 180 i.e. it contains 16200 cells, ISG is 30 by 60 i.e. contains 1800 cells while the CSG is 20 by 10 i.e. contains 200 cells. Every ISG cell therefore contains 9 FSG cells and every CSG cell contains 9 ISG cells i.e. 3 by 3 or 81 FSG cells i.e. 9 by 9. The CSG and ISG are upscaled versions of the FSG. The PSM method was used in the two upscaling steps. This model tests the effectiveness of the method in extremely heterogeneous systems. The model contains a water injector and two producers as shown in Figure 26.

Figure 31 highlights the errors in the different solution methods relative to the fine-scale model solution. Figure 27 shows the 3500-day water-flooding water-cut in the two producers. All the four methods tested are more accurate than the CSG solutions in terms of prediction of water-cut as well as breakthrough time and this is clearly shown in both the error values and the figures. The results show that proposed ETMM and TMM methods have a similar accuracy level to their EDMM and DMM respectively which is also consistent with that of previous examples. The CSG solution shows the most error of the three tested examples owing to the fact that this example has the most heterogeneous permeability field. Thus, the significant improvement in results therefore shows the effectiveness of the proposed method in highly heterogeneous systems.

Figure 28 shows the saturation distribution after 1000 days. Whereas all the downscaling methods utilized made the saturation distribution resolution better, the more accurate extended methods EDMM and ETMM clearly display local boundary artefact significantly less obviously than the DMM and TMM solutions. The fact that EDMM and ETMM are less affected by the imposed local boundary conditions makes them do a better job resolving the saturation near the local boundaries and therefore not display straight line artefacts around the local boundaries as obviously as DMM and TMM.

The saturation distribution error E_{SD} of all the solution methods after 1000 and 3000 days is shown in Figure 29 and Figure 30 respectively. $E_{SD} = \left| Sw_x^f - Sw_x \right|$ where Sw_x is the water saturation using the solution method employed and Sw_x^f is the water saturation of the reference fine-scale. There is a consistency between these figures and the water breakthrough and water-cut errors in showing similarities in the error levels between the ETMM and EDMM methods and also between the TMM and DMM methods. They therefore also show that the purely local methods are less accurate than the extended methods.

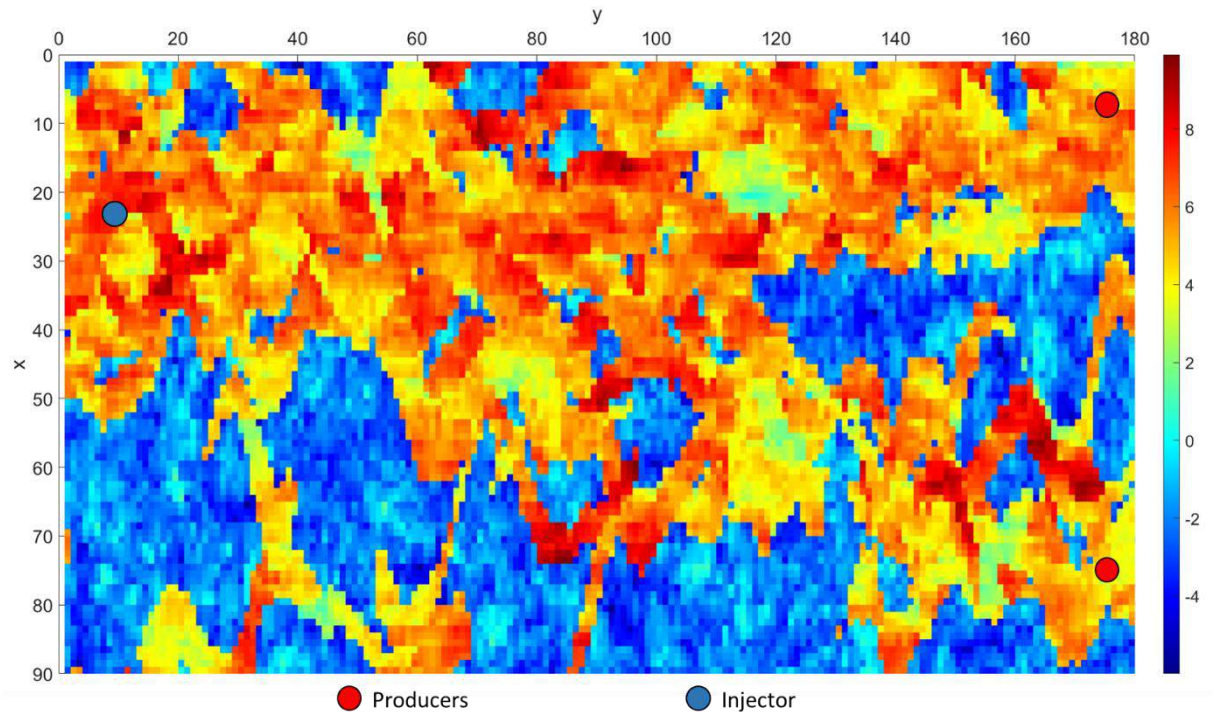

Figure 26: Model 3 permeability field with well locations superimposed

(a)

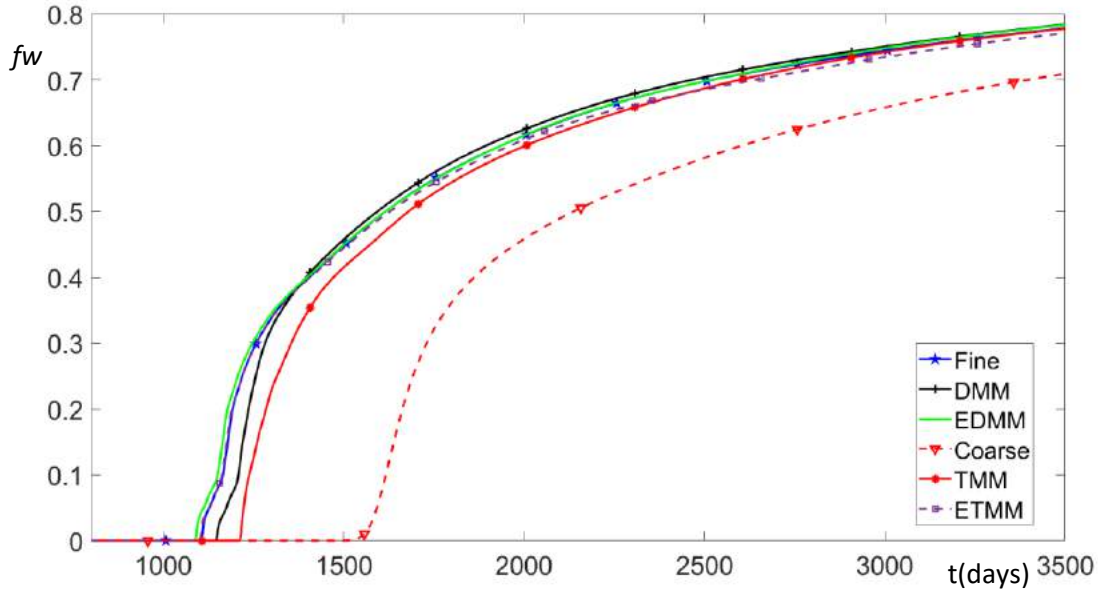

(b)

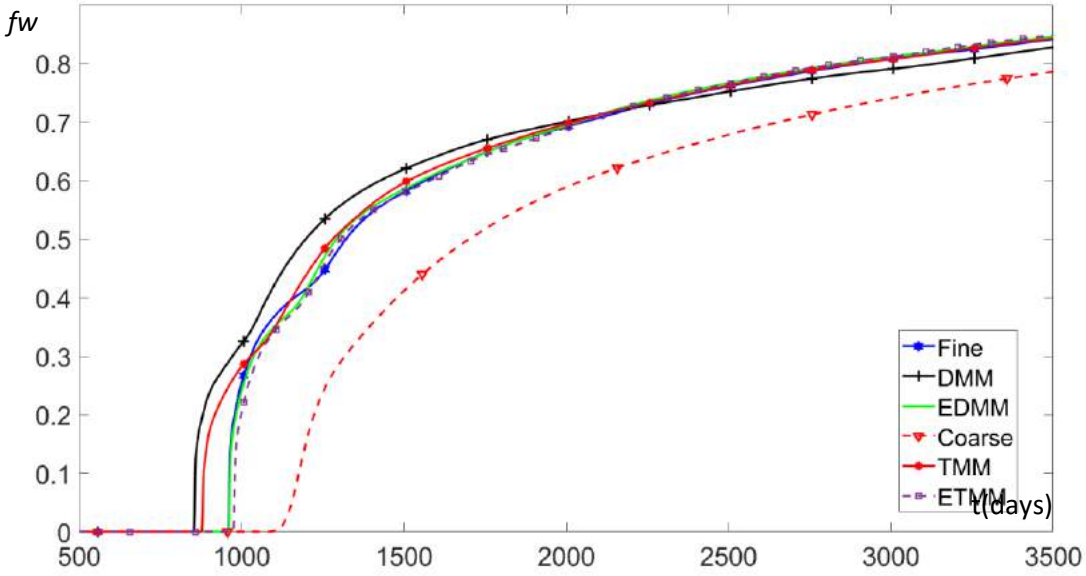

Figure 27: Water cut (fw) vs time (in days) plots for model 2 two producers using the different solution methods i.e. Coarse scale, EDMM, DMM, ETMM, TMM and Fine scale

(a)

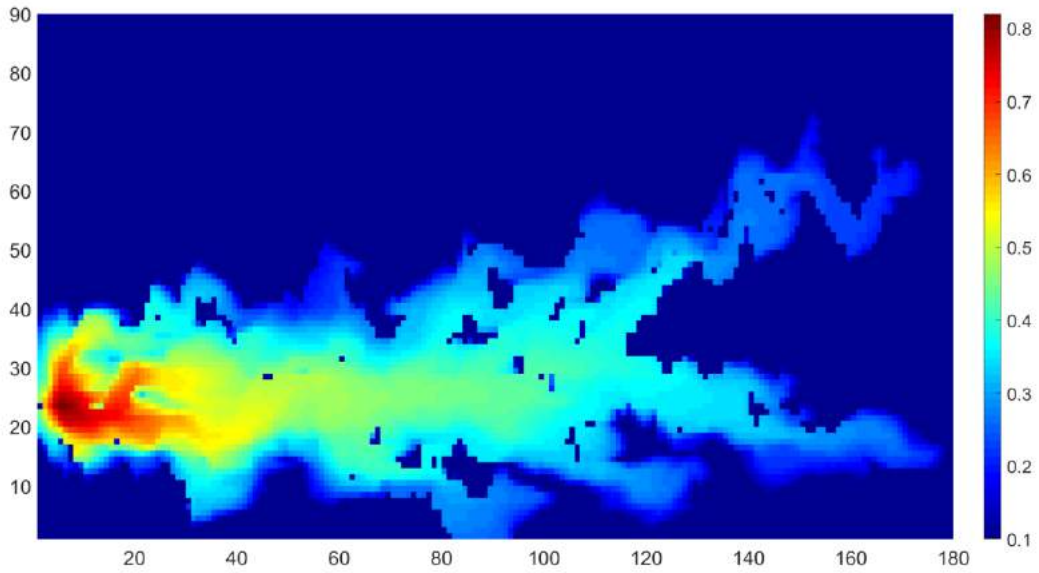

(b)

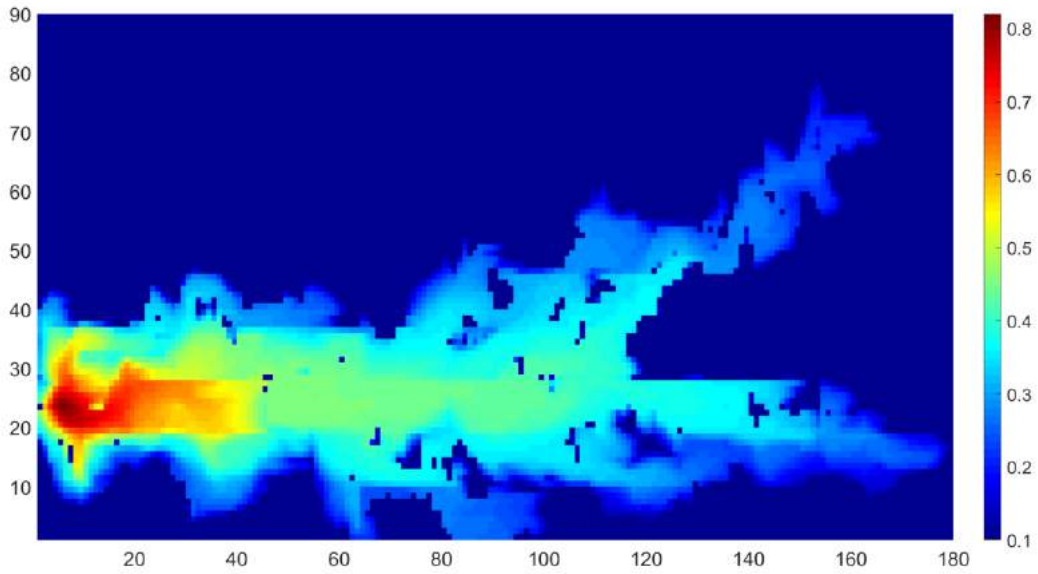
90
80
70
60
50
40
30
20
10
20
40
60
80
100
120
140
160
180
0.8
0.7
0.6
0.5
0.4
0.3
0.2
0.1

c)

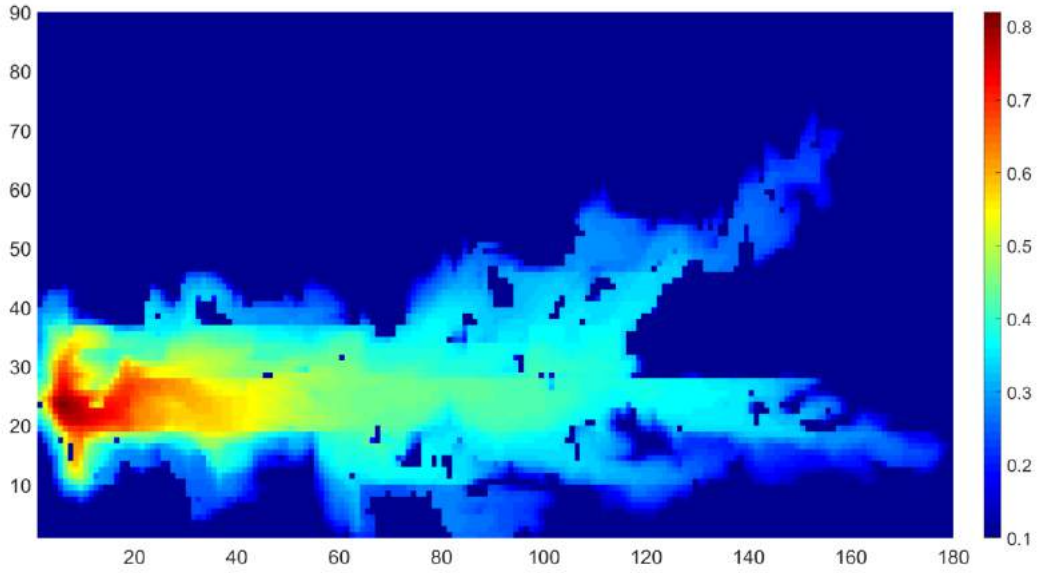
90
80
70
60
50
40
30
20
10
20
40
60
80
100
120
140
160
180
0.8
0.7
0.6
0.5
0.4
0.3
0.2
0.1

(d)

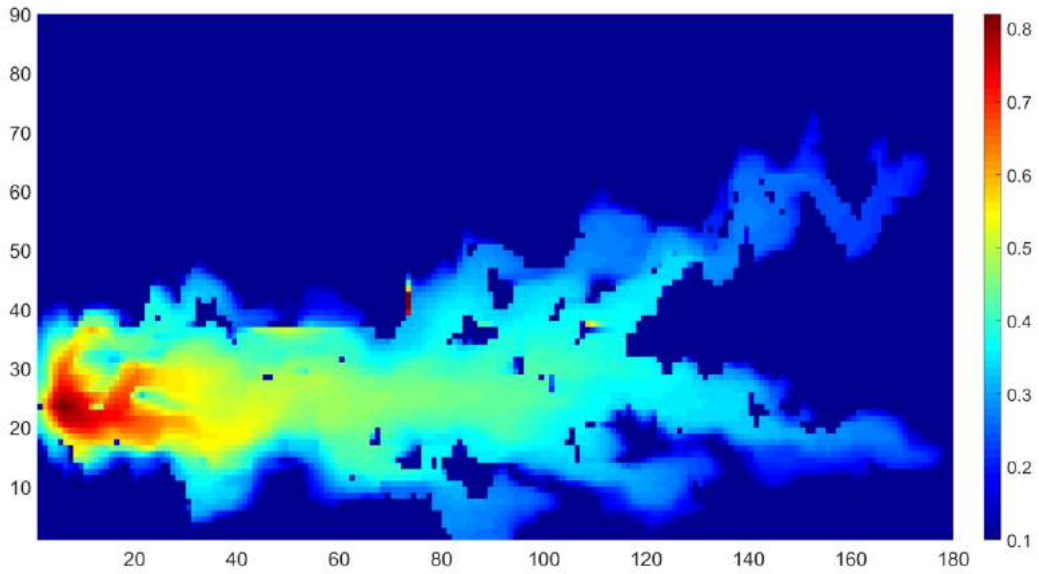

(e)

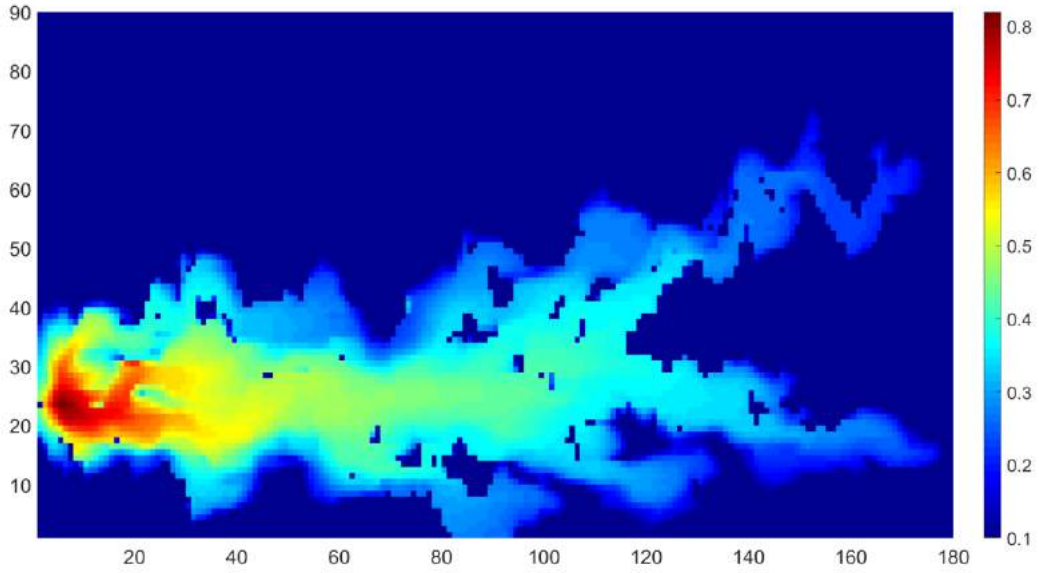

Figure 28: Model 3 Saturation field after 1000 days. *(a)* Fine Scale, *(b)* DMM, *(c)* TMM, *(d)* EDMM, *(e)* ETMM

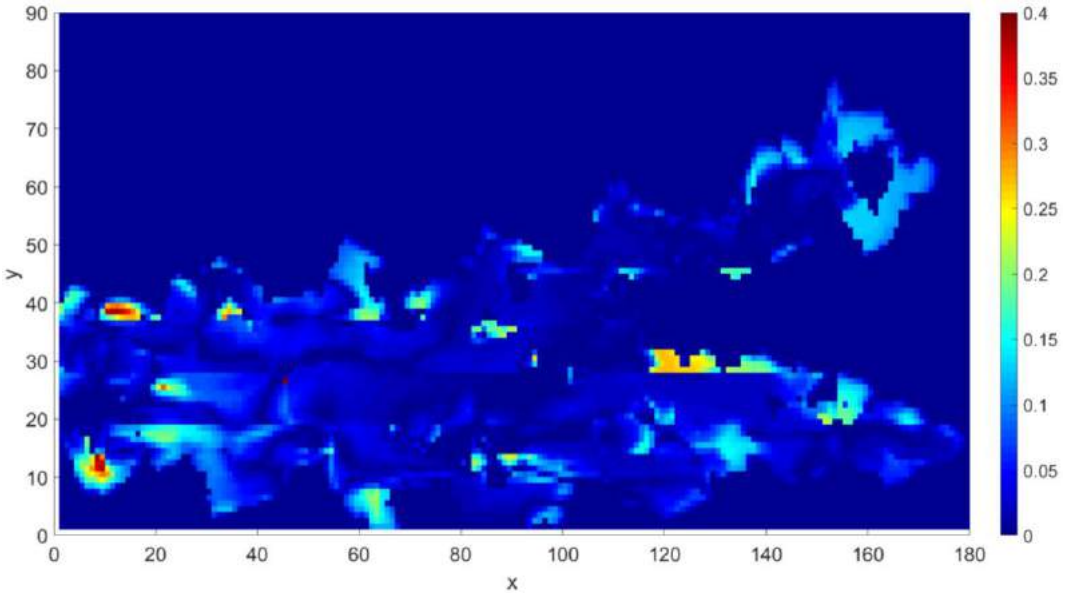
y
x
0
10
20
30
40
50
60
70
80
90
0
20
40
60
80
100
120
140
160
180
0
0.05
0.1
0.15
0.2
0.25
0.3
0.35
0.4

(a)

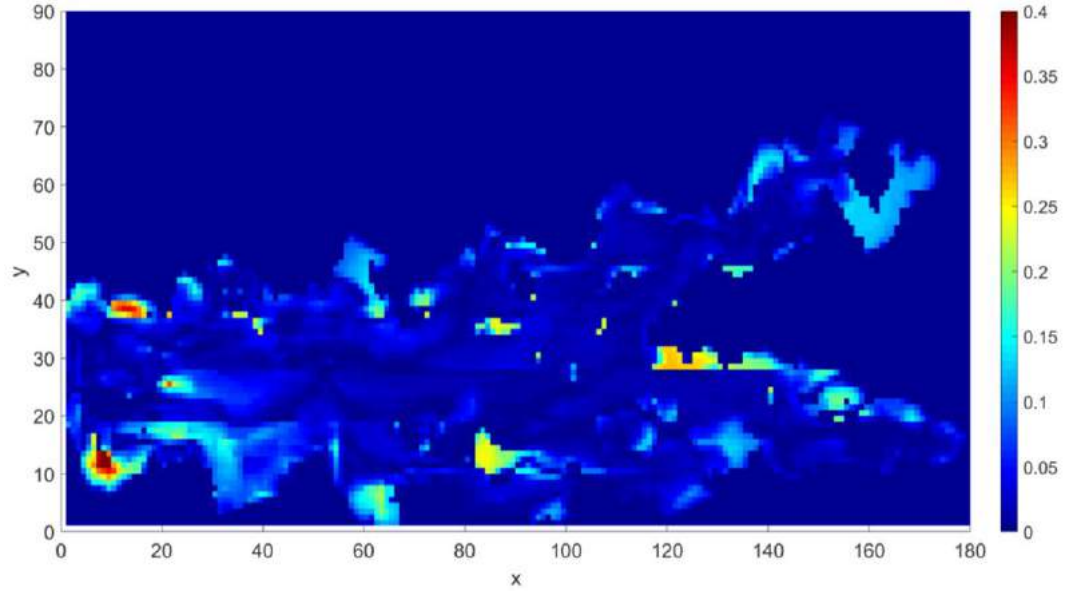
y
x
0
10
20
30
40
50
60
70
80
90
0
20
40
60
80
100
120
140
160
180
0
0.05
0.1
0.15
0.2
0.25
0.3
0.35
0.4

(b)

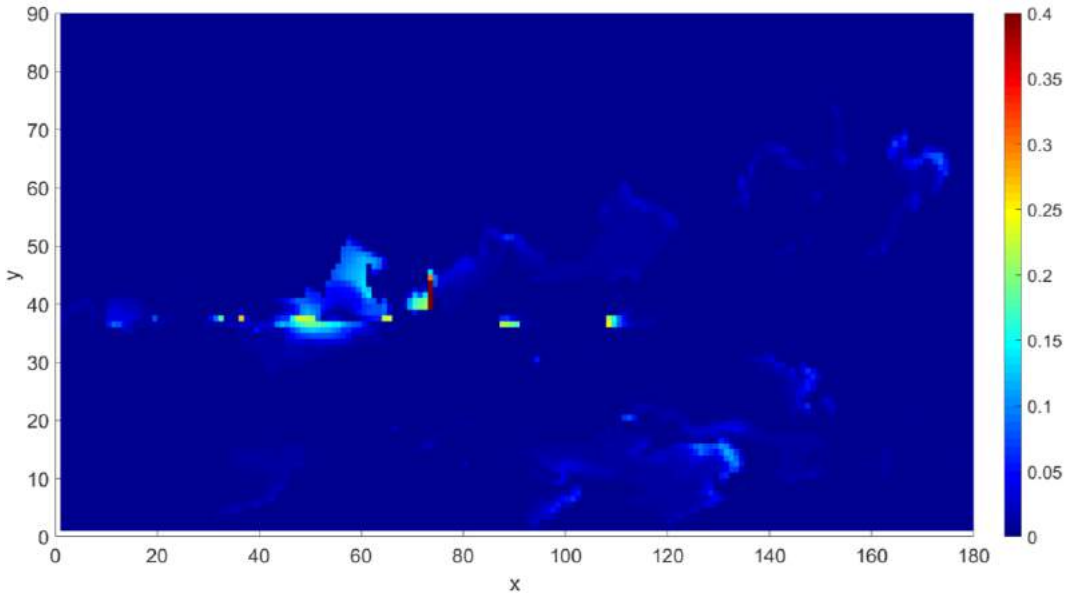

(c)

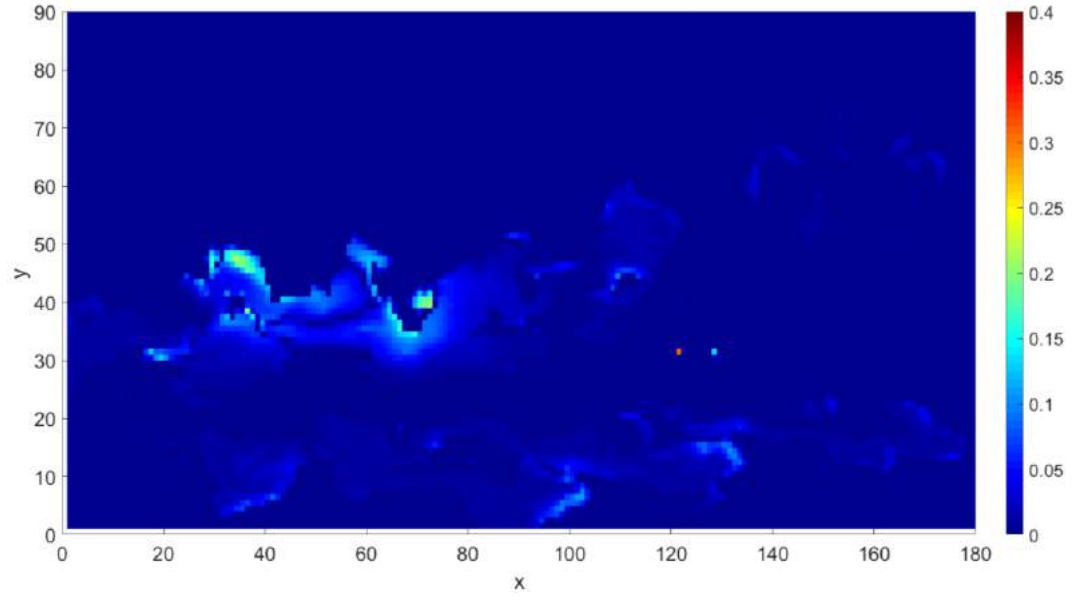

(d)

Figure 29: Model 3 Saturation error E_{SD} field after 1000 days. *(a)* DMM, *(b)* TMM, *(c)* EDMM, *(d)* ETMM

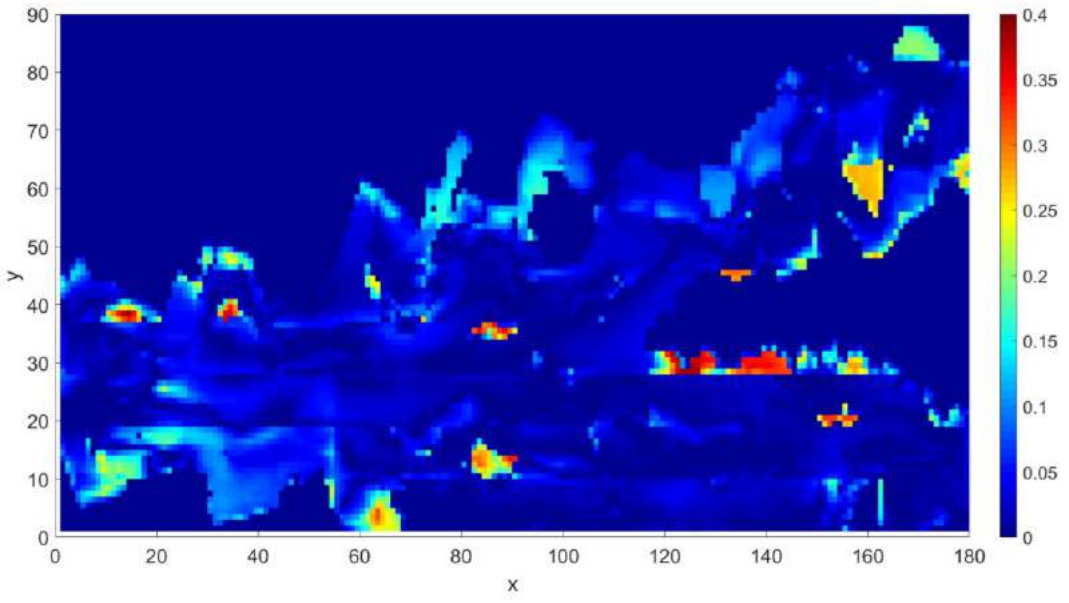
90
80
70
60
50
40
30
20
10
0
y
0
20
40
60
80
100
120
140
160
180
x
0.4
0.35
0.3
0.25
0.2
0.15
0.1
0.05
0

(a)

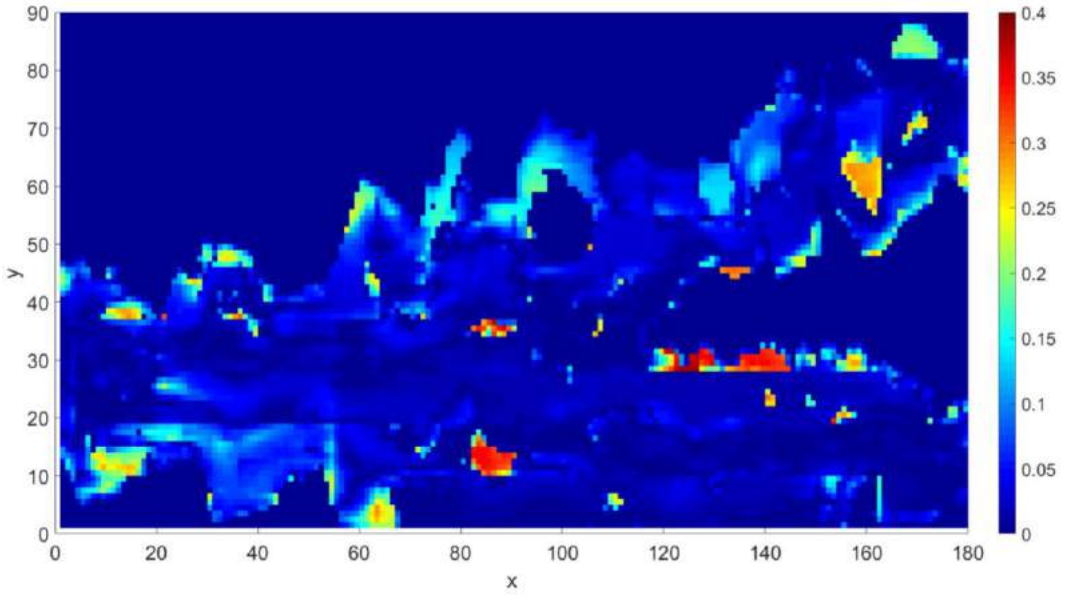
90
80
70
60
50
40
30
20
10
0
y
0
20
40
60
80
100
120
140
160
180
x
0.4
0.35
0.3
0.25
0.2
0.15
0.1
0.05
0

(b)

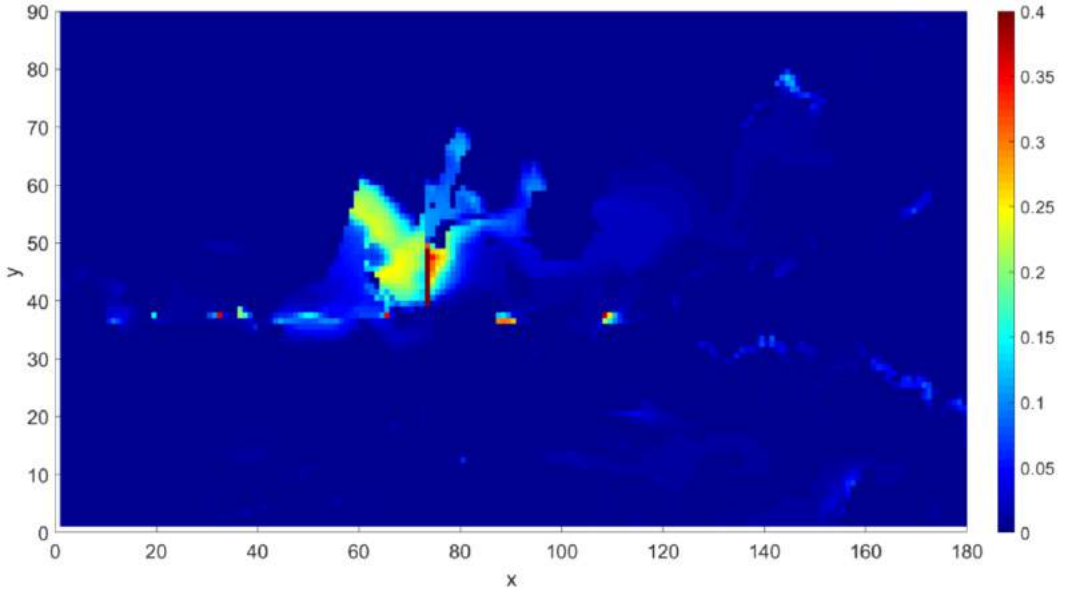

c)

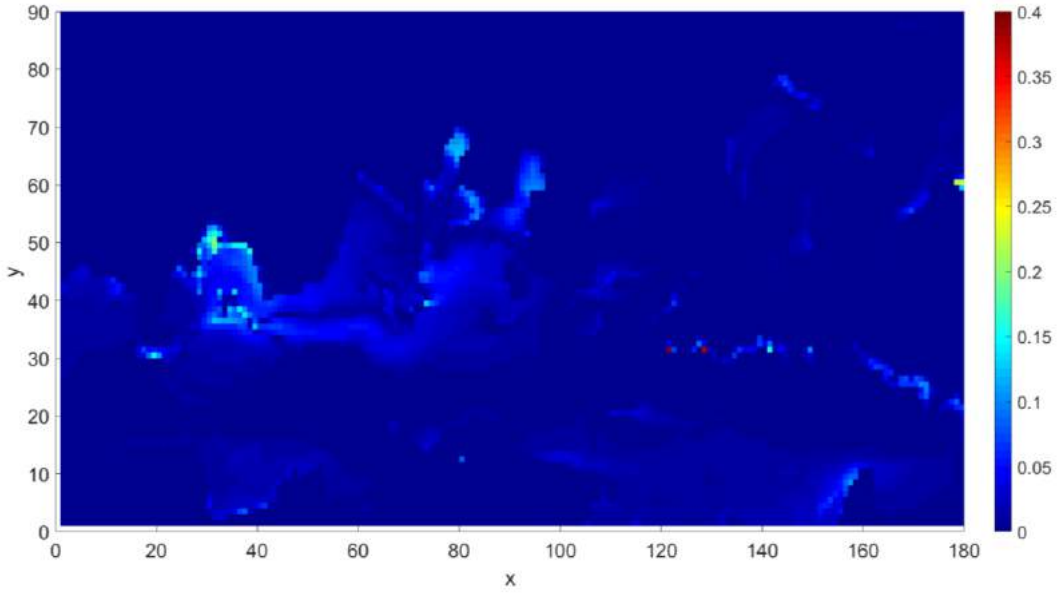

(d)

Figure 30: Model 3 Saturation error E_{SD} field after 3000 days. *(a)* DMM, *(b)* TMM, *(c)* EDMM, *(d)* ETMM

5.7 Discussion

From the examples, we have seen the effectiveness of the proposed ETMM and TMM methods and confirmed the effectiveness of EDMM and DMM in improving accuracy of water flooding problems. A general pattern is discernible when a comparison is made between the accuracies of the different methods. This pattern is consistent across the three examples and across all

error indices. The TMM and DMM both of which have similar approaches to downscaling also have accuracies that are similar across the different examples. The ETMM and EDMM both of which also have similar approaches to downscaling have accuracies that are similar across the different examples. DMM and TMM schemes are also generally less accurate than the EDMM and ETMM. The fact that EDMM was developed as an improvement on DMM makes this trend unsurprising. In this way, extending the EDMM to three levels by using the same directional oversampling method should also increase the accuracy over TMM. The negligible deterioration in accuracy is of more importance though when moving from more expensive two levels to three levels.

Quantifying the saved cost in multiscale methods can be quite challenging (Arbogast and Bryant, 2002) as different factors can affect the speed of simulation e.g. code efficiency and efficiency of solver used. As used in Figure 32 (a), pressure solution speed up factor is defined as the ratio of the time spent solving for the global fine-scale pressure compared to time spent solving for pressure using the other different methods. From Figure 32 (a), it can be seen that there is a reduction in the cost of both ETMM and TMM in comparison to EDMM and DMM methods respectively when an intermediate level is introduced between the coarse scale and the fine scale. This is not unexpected as the size of every local problem (or extended local problem) to be solved in the downscaling is reduced significantly when an intermediate level is introduced. Reduction in problem size means a reduced size of the matrix system solved for pressure and that is the most important solution step in terms of cost. This shows that there can be a significant reduction in cost without necessarily seriously impacting the accuracy by introducing an intermediate step. In Figure 32 (b), the speed up in total simulation time is shown for the different methods in comparison to the fine-scale solution. The saturation solution being solved on the global fine scale for all the methods means that the overall speed up factor in all

the tested methods is less significant than the pressure solution speed up factor. An Intel Xeon CPU with 3.5GHz paired with 16 GB of installed RAM was used for all the solution methods.

There are two forms that the application of ETMM and TMM can take with regards to the goal of implementation. The application of these methods can either be to further improve the accuracy through the introduction of a refined (instead of intermediate) third level like in model 1 or to facilitate cost reduction in comparison to their two-mesh equivalents. Thus, the first application of the methods, given a fine-scaled model and an upscaled model, entails reduction of cost of ETMM or DMM methods through the introduction of an intermediate scale. This therefore eventually causes the reduction in cost by reducing the size of each local problem solved. In the second application, accuracy is increased by downscaling further. Like before, given an upscaled model and a fine-scale model, there can be an introduction of a refinement of the fine-scale model i.e. a third finer model, and this then makes the initial fine-scale model the intermediated-scale model. Solving for transport on this finer scale improves accuracy without seriously causing an increase in the cost. TMM and ETMM may also be combined with other methods involving the downscaling of the geological models (Torrealba et.al. 2017). The downscaled geo-model, fine-scale geo-model and upscaled model can be combined by the TMM and the ETMM in order to increase accuracy without needing to solve the full field downscaled problem.

(a)

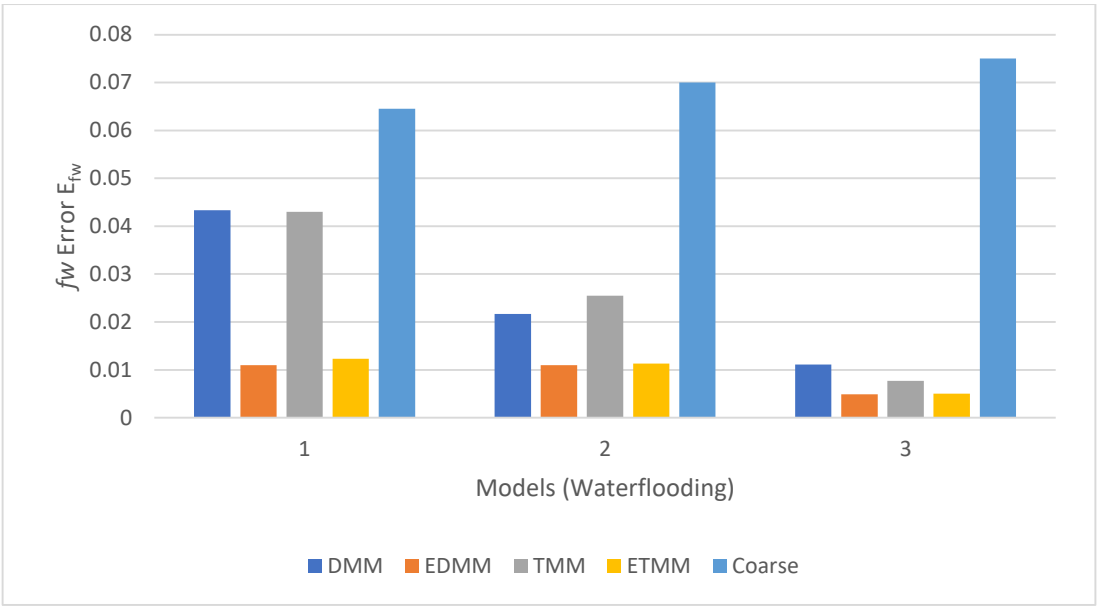

(b)

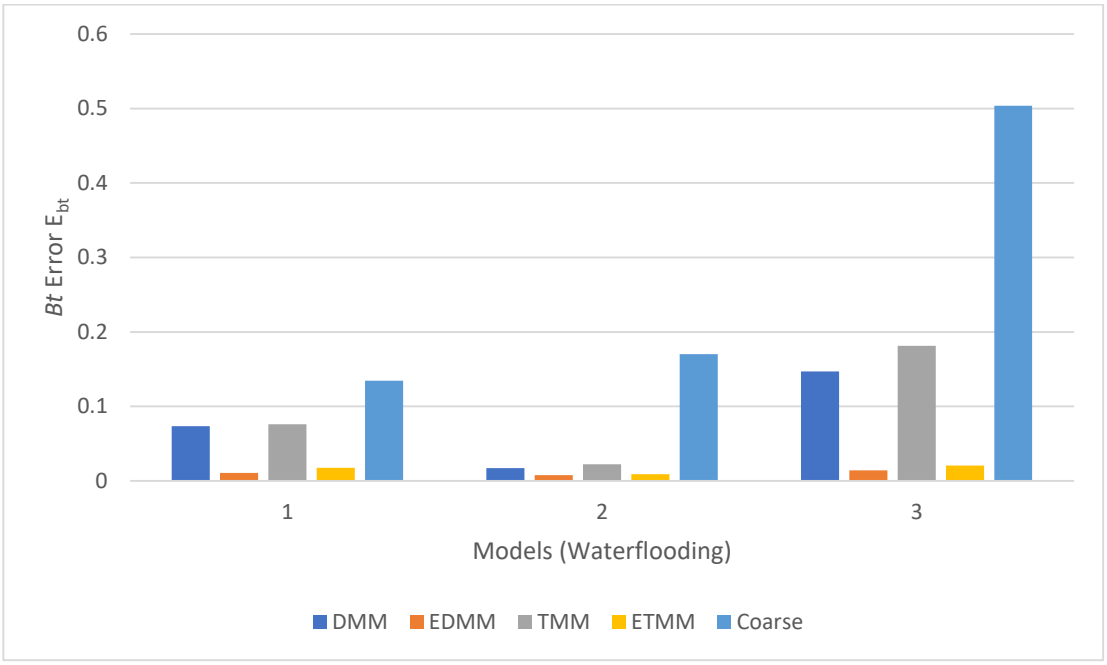

Figure 31: Error values of the different cases tested relative to fine-scale simulation *(a)* E_{fw} , *(b)* E_{bt}

(a)

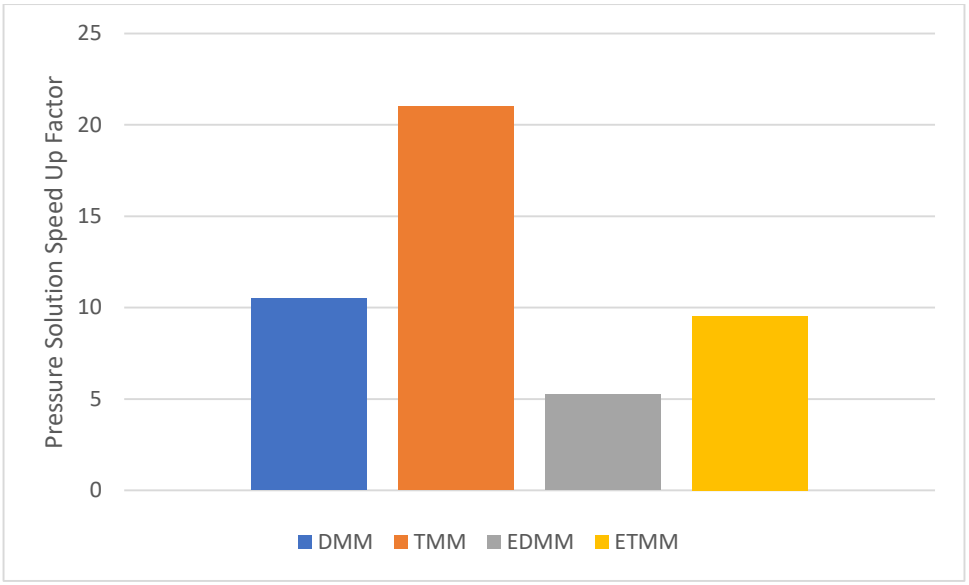

(b)

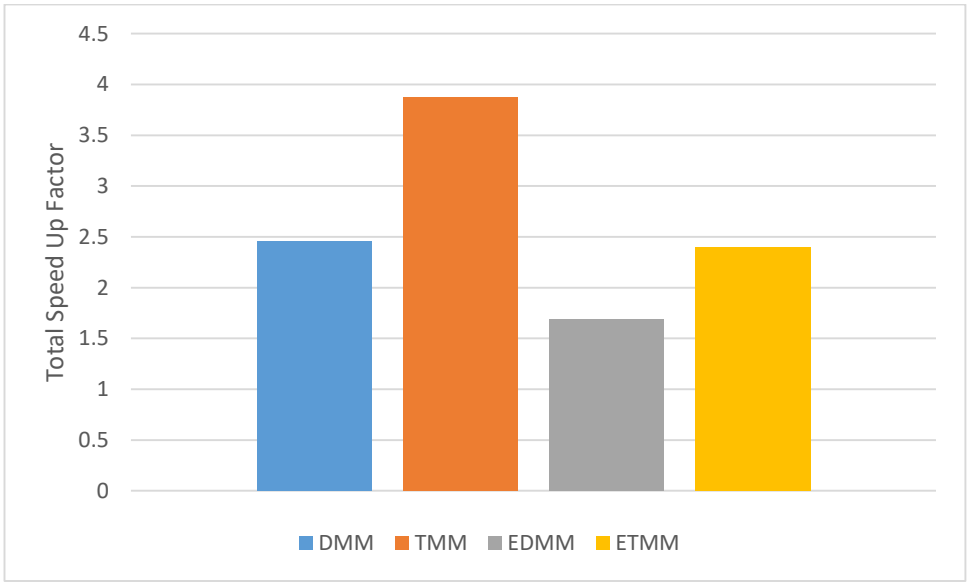

Figure 32: Speed-up factor of the different methods relative to fine-scale simulation. (a) shows the speed-up factor in the pressure solution while (b) shows the speed-up in the total simulation.

5.8 Conclusion

Two three-mesh methods TMM and ETMM have been successfully developed. They have been tested on water-flooding problems with different complexity levels. The two methods have been shown to be effective in increasing accuracy. ETMM and TMM have also both been

shown to have similar accuracy levels to EDMM and DMM respectively, given the same fine-scale and coarse-scale models, whilst also being a lot cheaper. In all examples tested, the purely local TMM and DMM methods proved to have consistently been less accurate than the extended local methods EDMM and ETMM. With an upscaled model and a fine-scaled model, TMM and ETMM can incorporate a third finer-scale model to increase accuracy or a third intermediate-scale model to improve speed. These methods provide advantages that can be extended to more complex examples of multiphase flow including introduction of compressibility and also EOR problems.

6 CHEMICAL EOR MODELLING

6.1 Introduction

Modelling EOR processes is generally more computationally intensive than simple two-phase flow modelling owing to the extra sets of equations and more complexities in the physics introduced by the injected chemicals. This means that the application of cost computation reduction methods are of significant importance in EOR modelling. Conversely, EOR processes may require high resolution modelling to accurately capture the complexities in the associated fluid displacement fronts (Babaei and King, 2013; Haajizadeh et al., 1999; Van Batenburg et al., 2011). Also, accurate simulation of EOR processes are of particular importance as they are used to show the improvements in recovery and thus justify the typically huge investments that EOR processes require. Despite this, the high computation cost typically means that EOR processes are simulated at the coarse scale which significantly impacts accuracy.

EOR modelling needs multiscale-multimesh methods. However, only a limited number of these methods have been presented, bespoke for, or adapted to EOR modelling compared to water-flooding (Babaei and King, 2013; Kumar et al., 2014; Li et al., 2016; Muggeridge and Hongtong, 2014). This chapter presents four multimesh methods for Chemical EOR, CEOR problems. These methods include the Dual Mesh Method, DMM, the Extended Dual Mesh Method, EDMM, the Triple Mesh Method, TMM, and the Extended Triple Mesh Method, ETMM. First the proposed methods are described, then they tested on three different CEOR problems. The results are compared with each other and with fine scale and coarse scale simulation results. These results were then discussed before conclusions were reached and recommendations given.

6.2 Governing Equations

Consider an incompressible, heterogeneous two-phase (oil and water) porous system with chemical component in the aqueous phase, the conservation equations for the phases can be written as

$$\phi \frac{\partial S_w}{\partial t} + \nabla \cdot \vec{u}_w = -q_w$$

$$\phi \frac{\partial S_o}{\partial t} + \nabla \cdot \vec{u}_o = -q_o \qquad (34)$$

where, ϕ, $\vec{u_i}$, q_i and S_i are the porosity, velocity vector, sink/source term and the saturation for phase i respectively with the subscripts 'w' and 'o' representing the water and oil phases respectively. This work assumes negligible capillary. The conservation equation of the chemical component is given by (Babaei and King, 2013)

$$\phi \frac{\partial [C(S_w + Ad)]}{\partial t} + u \cdot \nabla (f_w C) + C_{s/s} = 0 \qquad (35)$$

where C is concentration and $C_{s/s}$ represents the chemical sink source term. The adsorption term Ad is defined as

$$Ad = \rho_r k_d \frac{(1-\varphi)}{\varphi} \qquad (36)$$

here, the ρ_r is the rock density while the term k_d models the adoption such that $k_d C = Ca$ and Ca is the adsorption per unit rock mass. For the two phases, the Darcy velocities can be expressed as

$$\vec{u}_w = -\lambda_w \bar{\bar{k}} \cdot (\nabla p + \gamma_w i_z),$$

$$\vec{u}_o = -\lambda_o \bar{\bar{k}} \cdot (\nabla p + \gamma_o i_z) \qquad (37)$$

where p is pressure, $\bar{\bar{k}}$ is the diagonal permeability tensor of the porous medium while γ_w and γ_0 represents water and oil gravities respectively. λ_w and λ_o are the water and oil mobilities respectively and are expressed as

$$\lambda_w = \frac{k_{r_w}(S_w, C)}{\mu_w(C)},$$

$$\lambda_o = \frac{k_{r_o}(S_w, C)}{\mu_o} \qquad (38)$$

μ_i and k_{r_i} are viscosity and relative permeability of the phase i respectively.

Given that the sum $S_w + S_o = 1$ and $\dot{u} = \dot{u}_w + \dot{u}_o$, then the system of equations Eq. (34) can expressed as

$$\nabla \cdot \vec{u} = -q \qquad (39)$$

$$\phi \frac{\partial S_w}{\partial t} + \nabla \cdot f_w \left(\vec{u} + \lambda_o (\gamma_w - \gamma_o) \bar{\bar{k}} \cdot i_z \right) = -q_w \qquad (40)$$

where, $q = q_w + q_o$ and f_w represents fractional flow of water such that $\vec{u}_w = f_w \left(\vec{u} + \lambda_o (\gamma_w - \gamma_o) \bar{\bar{k}} \cdot i_z \right)$

$\vec{u}$ can be expressed as:

$$\vec{u} = \bar{\bar{k}} \cdot \left(\lambda_t \nabla p + (\lambda_w \gamma_w + \lambda_o \gamma_o) i_z \right) \qquad (41)$$

where, $\lambda_t = \lambda_w + \lambda_o$. Substituting for Eq. (41) in Eq. (39) gives the flow equation (or pressure equation) and is given by:

$$\nabla \cdot \left(\bar{\bar{k}} \cdot \left(\lambda_t \nabla p + (\lambda_w \gamma_w + \lambda_o \gamma_o) i_z \right) \right) = q \qquad (42)$$

The flow equation along with transport equation (Eq. (40)) are the main equations to be solved. These are none linear equations and can be solved using a variety of solution schemes. Here, Implicit Pressure Explicit Saturation (IMPES) scheme is employed. As the name suggests, this entails solving the pressure equation implicitly and the transport equation explicitly.

6.2.1 Flow equation discretization

The flow equation using cell-centred finite volume method can be discretized as follows:

$$\int_{V_i} \nabla \cdot \left(\bar{\bar{k}} \cdot \left(\lambda_t \nabla p + (\lambda_w \gamma_w + \lambda_o \gamma_o) i_z \right) \right) = \int_{V_i} q dV \tag{43}$$

Eq. (11) in discrete form can be approximated to:

$$\sum_{j \in N(i)} T_{ij} (p_j^{n+1} - p_i^{n+1}) = q_i^{n+1} + G^n \tag{44}$$

where j represents grid cells sharing faces with grid cell i, p_i^{n+1} is cell at pressure *i* and time-index n+1, and q_i^{n+1} represents the source term in cell i while G^n represents the gravity term. T_{ij} is transmissibility and can be expressed as:

$$T_{ij} = \frac{\lambda_{t_{ij}} k_{ij} A_{ij}}{\left\| d_{i\Gamma j} \right\| + \left\| d_{j\Gamma i} \right\|} \tag{45}$$

where A_{ij} represents area of the interface, $d_{i\Gamma j}$ represents the vector joining cell i centre to the interface.

$$k_{ij} = \left(\frac{1}{k_i} + \frac{1}{k_j} \right)^{-1} \tag{46}$$

and $\lambda_{t_{ij}}$ represents the total mobility at the interface evaluated using upstream weighting such that

$$\lambda_{t_{ij}} = \begin{cases} \lambda_{t_i} \text{ if } p_i^n > p_j^n \\ \lambda_{t_j} \text{ if } p_j^n > p_i^n \end{cases} \tag{47}$$

Eq. (12) yields the matrix system:

$$\bar{\bar{T}} \vec{P}^{n+1} = \vec{q} + G \tag{48}$$

where $\overline{\overline{T}}$ represents inter-block transmissibility matrix, $\vec{P}^{n+1}$ represents the unknown pressure vector and the RHS vector contains the gravity and source terms. The coefficients of the matrix $\overline{\overline{T}}$ are given by:

$$\overline{\overline{T}}[i,i] = \sum_{j \in N(i)} T_{ij} \text{ and}$$

$$\overline{\overline{T}}[i,j] = T_{ij} \tag{49}$$

Eq. (48) is solved implicitly and is unconditionally stable.

6.2.2 Saturation equation discretization

The saturation equation can be discretized as follows:

$$\phi \int_{V_i} \frac{\partial S_w}{\partial t} dV + \int_{V_i} \nabla \cdot (\vec{u}_w) dV = \int_{V_i} q_w dV \tag{50}$$

$$\frac{V_i \phi}{\Delta t}(S_{w_i}^{n+1} - S_{w_i}^{n}) + \sum_{j \in N(i)} \vec{u}_{w_{ij}} = q_{w_i}^{n+1} \tag{51}$$

After solving Eq. (48), $S_{w_i}^{n+1}$ are the only unknowns and can be evaluated directly from Eq. 51.

6.2.3 Concentration equation discretization

Discretising equation 3 for grid cell concentration, we have:

$$\frac{V_i \phi}{\Delta t}\left(C^{n+1}(S_{w_i}^{n+1} + Ad) - C^{n}(S_{w_i}^{n} + Ad)\right) + \sum_{j \in N(i)} \vec{u}_{w_{ij}} C = c_{s/sw_i}{}^{n+1} \tag{52}$$

Eq. (52) can be solved implicitly or explicitly for concentration.

6.3 Dual Mesh Method

The Dual Mesh Methods was adapted to incorporate chemical concentration as to be able to model surfactant and polymer flooding. The implementation was done in the steps below.

1. First, fine scale properties like saturation, concentration, and permeability are defined along with the source and sink terms.

2. Coarse scale properties like concentration saturation, porosity and transmissibility or permeability (depending on upscaling method) are updated along with the source and sink terms.
3. Coarse scale flow equation Eq. 48 is solved for pressure and the coarse fluxes are computed.
4. This step involves the computation of the approximated local fine-scale boundary fluxes from the transmissibility weighting of coarse fluxes.
5. In this step, the computed fine scale fluxes (in step 4) are applied as Neumann BC and used to solve local fine-scale flow problem to compute fine scale pressure and ultimately fine scale velocities.
6. Finally, the computed fine scale velocities are used to solve the saturation equation Eq. 51 for fine scale saturation and the concentration equation Eq. 52 for fine scale concentration.

DMM has been previously applied to both polymer flooding and surfactant EOR problems by different authors. DMM will therefore also be applied here and its results will be compared with that of the newly developed methods.

6.4 Extended DMM

EDMM was developed as an improvement on and extension to DMM. EDMM introduced extended local downscaling step using the novel concept of directional oversampling DO. EDMM, as adapted to CEOR modelling was implemented as follows:

1. First, fine scale properties like saturation, concentration, and permeability are defined along with the source and sink terms.
2. Coarse scale properties like concentration saturation, porosity and transmissibility or permeability (depending on upscaling method) are updated along with the source and sink terms.

3. Coarse scale flow equation Eq. 48 is solved for pressure and the coarse fluxes are computed.
4. This step involves the computation of the approximated local fine-scale boundary fluxes from the transmissibility weighting of coarse fluxes.
5. In this step, the computed fine scale fluxes (in step 4) are applied as Neumann BC with directional oversampling and used to solve extended local fine-scale flow problem to compute fine scale pressure and ultimately fine scale velocities.
6. Finally, the computed fine scale velocities are used to solve the saturation equation Eq. 51 for fine scale saturation and the concentration equation Eq. 52 for fine scale concentration.

EDMM has been shown to give better results than DMM in water-flooding problems. In this chapter, this will be tested to see if the improvement in results extends to CEOR problems.

6.5 Triple Mesh Method

In triple mesh method, TMM, three levels of upscaling-downscaling is involved as introduced in chapter 5. In this chapter, TMM is adapted for and extended to CEOR problems and implemented as follows.

1. First, fine scale properties like saturation, concentration, and permeability are defined along with the source and sink terms.
2. Coarse scale properties like concentration saturation, porosity and transmissibility or permeability (depending on upscaling method) are updated along with the source and sink terms.
3. Coarse scale flow equation Eq. 48 is solved for pressure and the coarse fluxes are computed.
4. Successive local downscaling: Here, the flow solution is successively downscaled to the fine-scale from the coarse-scale. First, the CSG solution is downscaled to the ISG

by solving local flow problems on the ISG with transmissibility weighted flux boundary condition using the computed CSG fluxes. This is then further downscaled to the FSG by again solving local flow problems on the FSG using transmissibility weighted flux boundary condition using the ISG fluxes. This step yields a conservative flux field on both the ISG and the FSG.

5. Finally, the computed fine scale velocities are used to solve the saturation equation Eq. 51 for fine scale saturation and the concentration equation Eq. 52 for fine scale concentration.

6.6 Extended Triple Mesh Method ETMM

In extended triple mesh method, ETMM, three levels of upscaling-downscaling is involved as also introduced in chapter 5. In this chapter, ETMM is adapted for and extended to CEOR problems and implemented as follows.

1. First, fine scale properties like saturation, concentration, and permeability are defined along with the source and sink terms.
2. Coarse scale properties like concentration saturation, porosity and transmissibility or permeability (depending on upscaling method) are updated along with the source and sink terms.
3. Coarse scale flow equation Eq. 48 is solved for pressure and the coarse fluxes are computed.
4. Successive extended local downscaling: This involves the successive extended local downscaling of the flow solution from the coarse scale ultimately to the fine scale. First, the CSG solution is downscaled to the ISG by solving extended local flow problems on the ISG with the application of directional oversampling. This is then further downscaled to the FSG by again solving extended local flow problems on the FSG

again applying directional oversampling. This step yields a conservative flux field on both the ISG and the FSG.

5. Transport Solution: In this final step, the already computed conservative fine-scale flux field is used to solve the transport equation on the FSG

The above steps are illustrated in Figure 33.

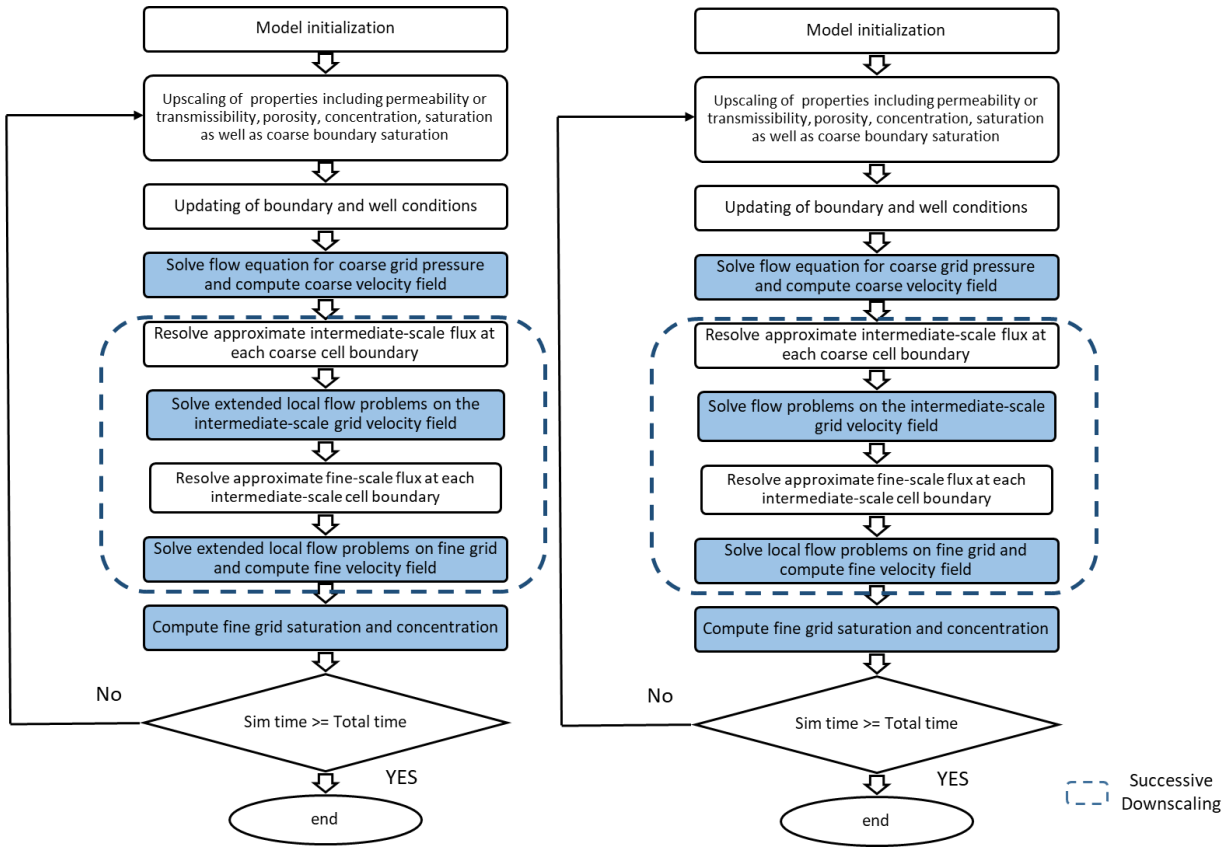

Figure 33: Flowcharts for ETMM (left) and TMM (right) algorithms

Table 5 – Comparison between the approaches to TMM and ETMM method

TMM	**ETMM**
Both involve two levels of downscaling of the flow solution and solves saturation at the fine scale	
Errors inherent in the coarse-scale and intermediate-scale solutions are passed down to the fine-scale through the BC	Effects of the BC condition on the accuracy is reduced through the application of directional oversampling
Limited coupling between the fine-scale, intermediate-scale and coarse-scale models	Improved coupling between the three scales
Highly dependent on the accuracy of the upscaling method	ETMM focuses on reducing the impact of upscaling method and BC of choice on the accuracy

6.7 Implementation and Results

For the effectiveness and efficiency of the proposed methods to be evaluated, they were tested on polymer flooding and surfactant flooding problems. The methods, DMM, TMM, ETMM and EDMM as well as fine scale and coarse scale solutions were all implemented in every example problem. Quantitative and qualitative comparison were made between the results. Comparisons were made between performances using error indicators with the fractional water flow error E_{fw} which is expressed by

$$E_{fw} = \frac{1}{t_{total}} \sum_{i=1}^{nt} \left| \frac{\left[f_w^f(i) - f_w^c(i) \right] \Delta t_i}{f_w^f(i)} \right| \qquad (53)$$

where, $t_{total} = \sum_{i=1}^{n_t} \Delta t_i$ is the total simulation time, nt is the number of time-steps and f_w^f and f_w^c respectively represent the fine-scale model water-cut and the water-cut of the evaluated model.

Error in water breakthrough time E_{bt} is another error indicator that is employed and it is expressed as

$$E_{bt} = \frac{1}{n_w} \sum_{j=1}^{nw} \left| \frac{t_{bt}^f(j) - t_{bt}^c(j)}{t_{bt}^f(j)} \right| \qquad (54)$$

where n_w represents the number of producer wells, t_{bt}^f and t_{bt}^c is the breakthrough time in the reference fine-scale model and the breakthrough time in the evaluated model respectively. Together, the indicators evaluate the ability of the model to predict recovery as well as the breakthrough time of the flood front (which is one of the most significant event in the life of a well)

The model for polymer flooding that was used is similar to the one employed by Babaei and King, 2013 and first presented in Green Willhite, G. Paul., 1998. Miscibility is assumed between the polymer and the injected water with negligible adsorption on the rock. The polymer and the resident connate water are assumed to not mix. Therefore, there is a lagging polymer front and a leading resident water front. The model also assumes negligible adsorption. The effective fractional flow of the aqueous phase was modelled according to equation 55 (Alsofi and Blunt, 2012). Table 6 show the properties used for the polymer examples.

$$\tilde{f}_w = (1-C) f_w + C f_p = (1-C) \frac{1}{1 + \frac{\mu_w k_{ro}}{k_{rw} \mu_o}} + C \frac{1}{1 + \frac{\mu_p k_{ro}}{k_{rp} \mu_o}} \qquad 55$$

Table 6: Model properties for the polymer flooding problems

Parameter	
Porosity	0.25
Permeability	Specified heterogeneous distribution
Oil Viscosity (cP)	5.0
Water Viscosity (cP)	1.0
Polymer Viscosity (cP)	4.0
Well primary control (Producers)	Total liquid rates
Well primary control (Injectors)	Injectors (Total voidage replacement)
Kro_{max}	1
Sor	0.18
No (Corey)	2
Krw_{max}	0.6
Swc	0.1
Nw (Corey)	2

In the surfactant flooding examples, the model for surfactant flooding that was used is similar to the one employed by Babaei and King, 2013. IFT reduction manifests in two modelled effects. The change in curvature of the relative permeability curve and the reduction of the residual saturations. Again, the SEG scheme is used. Two relative permeability curves are specified representing the normal IFT regime and the ultra-low IFT regime. The fraction flow computed is similar to Equation 56 i.e. aqueous phase mobility are concentration scaled between ultra-low IFT properties and normal IFT properties.

$$\tilde{f}_w = (1-C)\,f_w + Cf_s = (1-C)\frac{1}{1+\left(\frac{\mu_w k_{ro}}{k_{rw}\mu_o}\right)_{nomal-IFT}} + C\frac{1}{1+\left(\frac{\mu_s k_{ro}}{k_{rs}\mu_o}\right)_{ultralow-IFT}} \quad 56$$

Table 7: Saturation properties used for the surfactant flooding example

	n	Swc	1-Sor	K^0_{rw}	K^0_{ro}
Normal IFT	2	0.1	0.82	1	0.6
Ultra-Low IFT	1	0.05	0.98	1	1

6.8 Model 1: SPE 10 Layer 1.

Model 1 which is the layer 1 from the 10th SPE comparative project model (Christie and Blunt, 2001) is the first model that the methods were tested on. It is a highly heterogeneous 2D model with log permeability distribution and well distribution shown in Figure 34. The reservoir has a dimension of 1200ft by 2200ft. The FSG has 90 cells by 180 cells i.e. it contains 16200 cells, ISG has 30 cells by 60 cells i.e. contains 1800 cells while the CSG has 20 cells by 10 cells i.e. contains 200 cells. The PSM method was used to upscale the FSG to the ISG and the ISG to the CSG. Both Polymer flooding and Surfactant flooding problems were tested on the model.

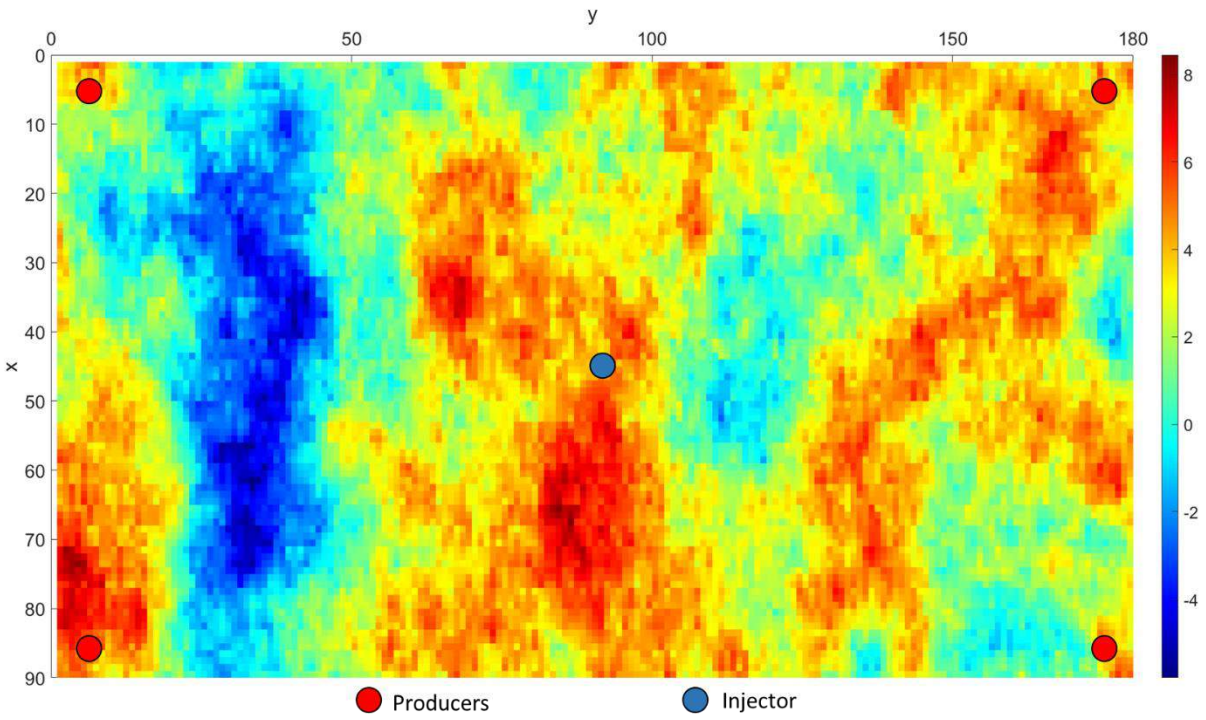

Figure 34 Model 1 permeability field and well locations

In the polymer flooding problem, Figure 35 shows the 10,000-day water-cut at the four producers. The CSG model has the highest errors just as expected. The accuracy of all the tested schemes as shown in the plot is higher than the CSG both in predicting breakthrough time as well as water-cut. The DMM, EDMM, TMM, ETMM methods have significantly higher accuracy compared to the CSG results and this is clearly shown by the error values. There is a pattern when these four schemes are compared. The accuracies of EDMM and ETMM are similar and clearly more than that of the DMM and TMM also with their similar accuracies. This is consistent with results from two phase flow (Adeyemi et al., 2022, 2021)

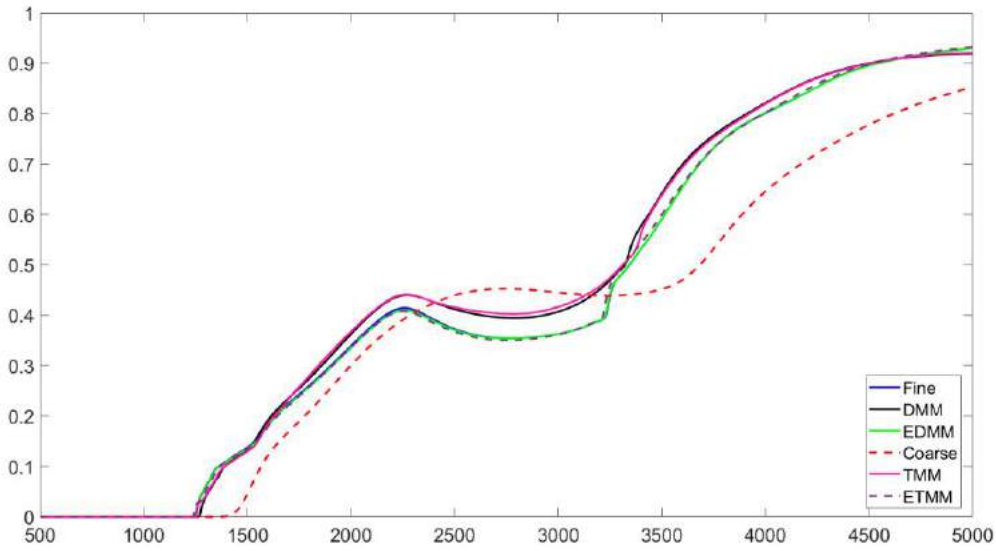
Fine
DMM
EDMM
Coarse
TMM
ETMM

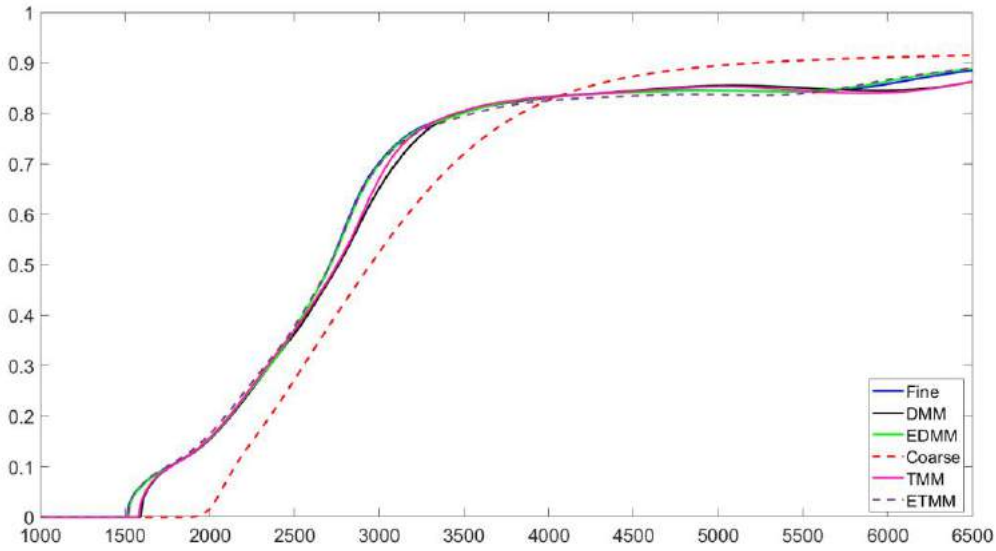
Fine
DMM
EDMM
Coarse
TMM
ETMM

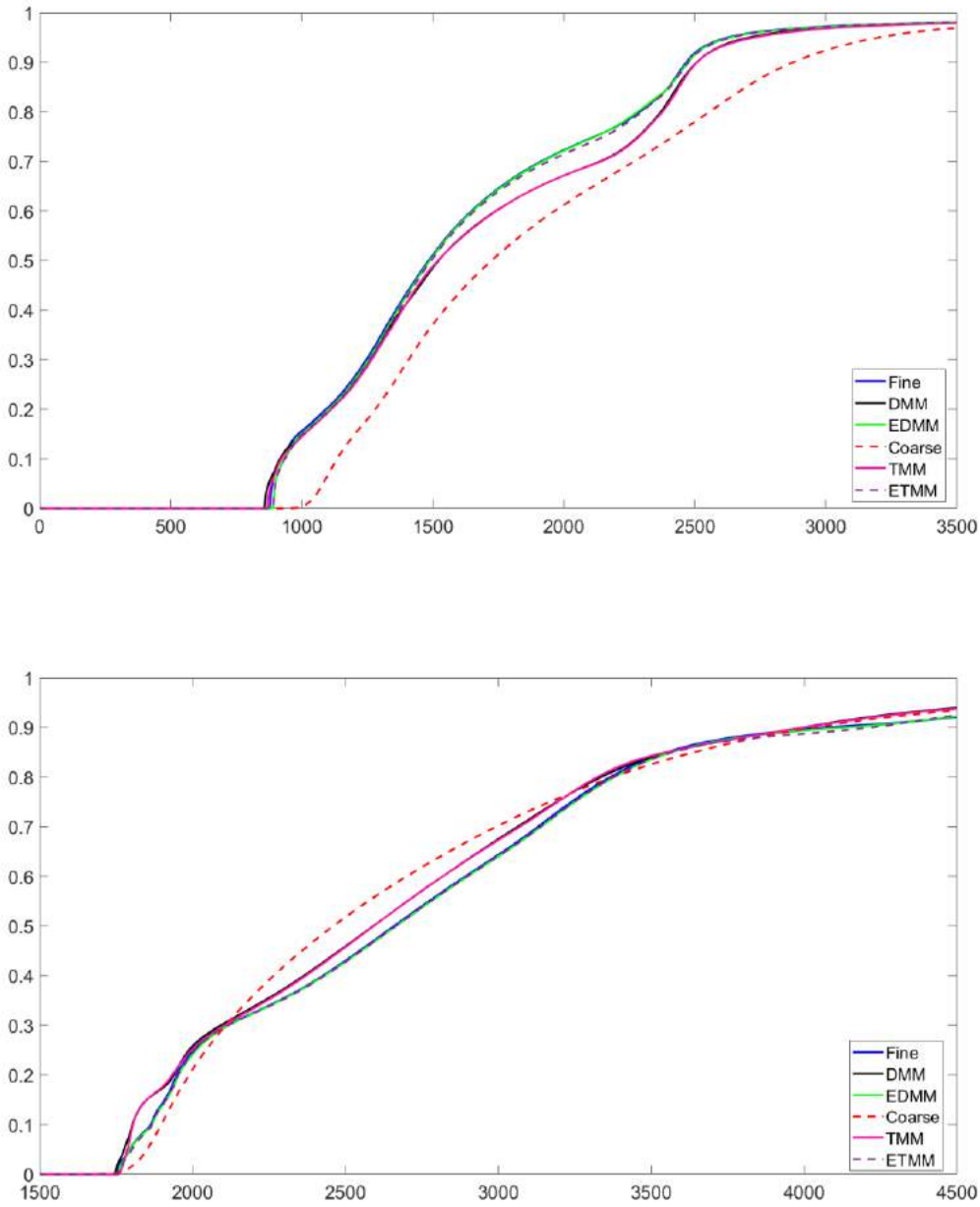

Figure 35: Water cut (fw) vs time (in days) plots for model 1 *polymer flooding*

In the surfactant flooding problem, Figure 36 shows the 10,000-day water-cut at the four producers. Like before, the coarse solution is less accurate than all the tested methods in the recovery prediction as well as the prediction of surfactant breakthrough. And like before, the DMM and TMM are less accurate than EDMM and ETMM. DMM has been shown to be effective with surfactant flooding problems (Babaei and King, 2013), however, this example shows that despite the fact that EDMM, ETMM and TMM were originally developed for two-

phase flow problems, they can also be effective and compatible with surfactant flooding problems. It also shows that the EDMM and DMM methods respectively have similar accuracy levels compared to that of the triple mesh methods ETMM and TMM.

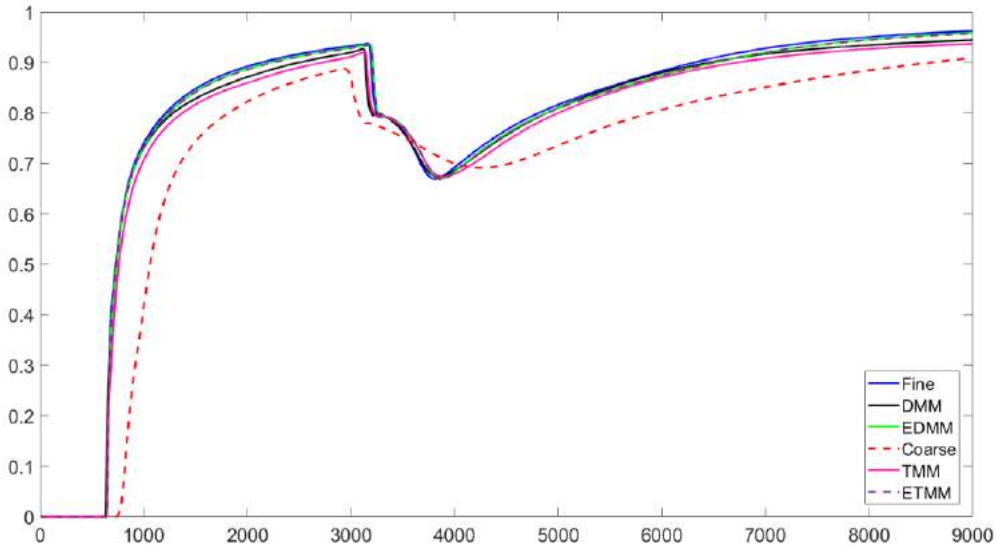

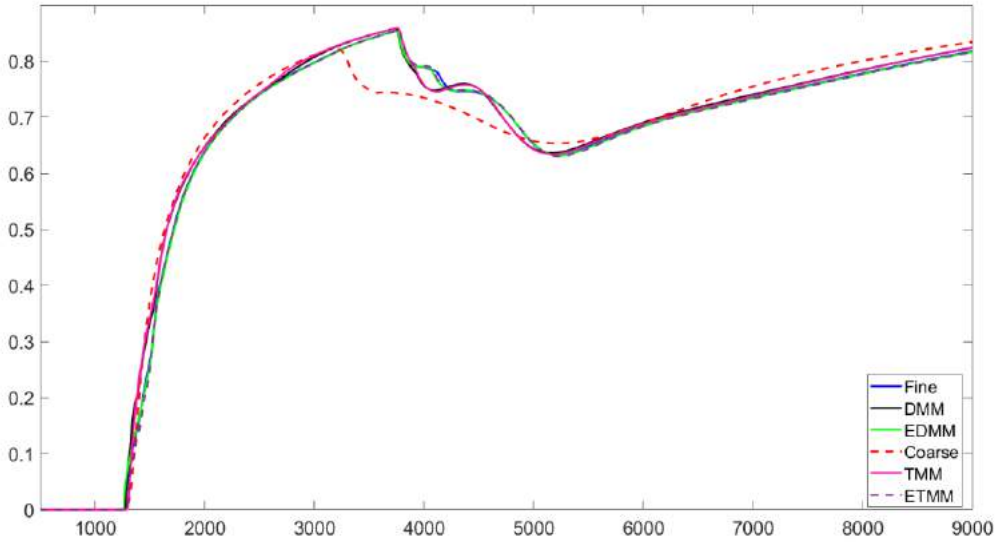

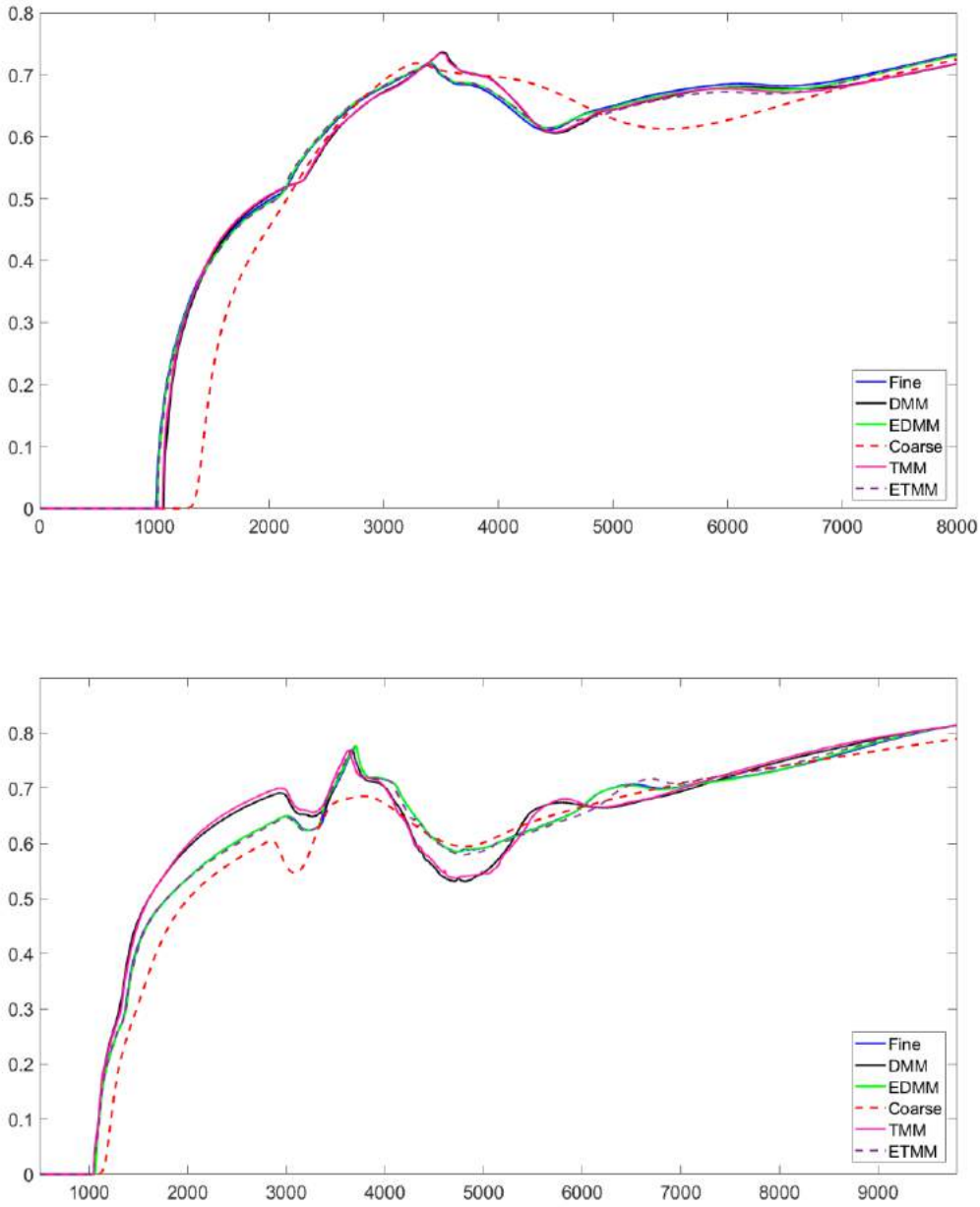

Figure 36: Water cut (fw) vs time (in days) plots for model 1 *for surfactant flooding*

6.9 Model 2: SPE 10 Layer 59

Model 2 which is the layer 59 from the 10th SPE comparative project model (Christie and Blunt, 2001) is the second model that the methods were tested on. It is an even more complex highly heterogeneous 2D model with log permeability distribution and well distribution shown in Figure 37. The reservoir has a dimension of 1200ft by 2200ft. The FSG has 90 cells by 180cells

i.e. it contains 16200 cells, ISG has 30 cells by 60 cells i.e. contains 1800 cells while the CSG has 20 cells by 10 cells i.e. contains 200 cells. The upscaling was also done using PSM.

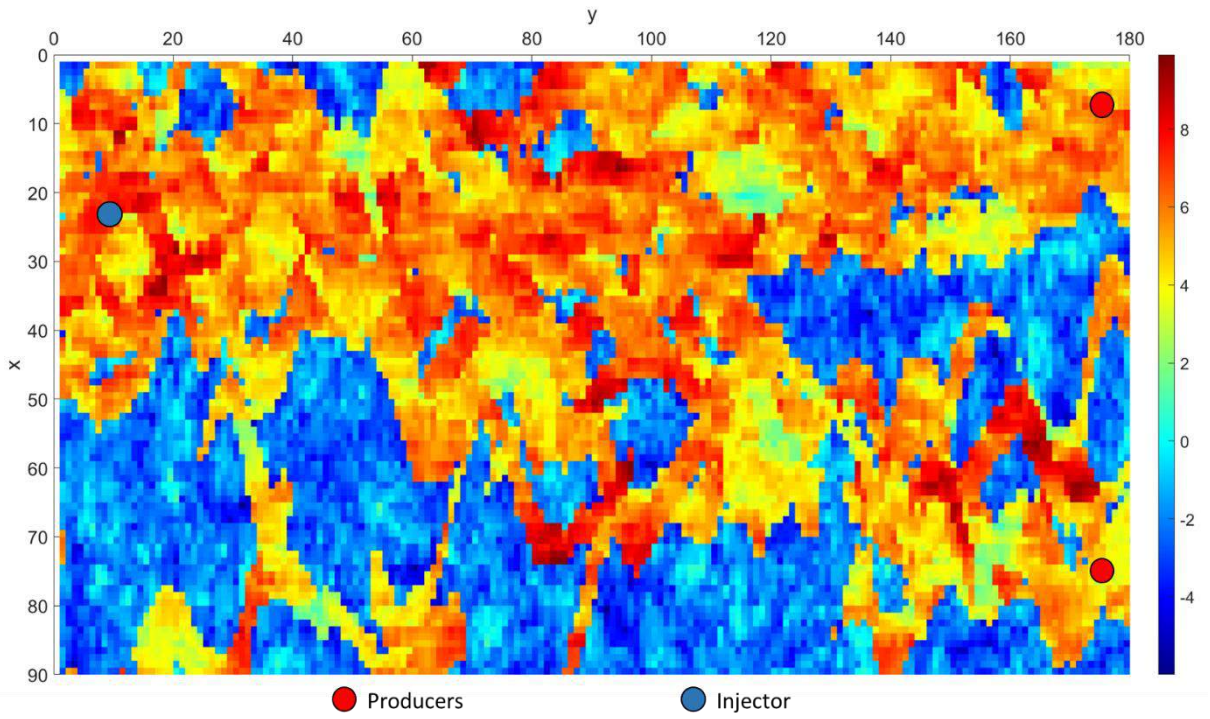

Figure 37: Model 2 permeability field with well locations superimposed

Two polymer flooding schemes were tested. In the first scheme (Figure 38), polymer was injected from the start of production. In the second scheme (Figure 39), polymer was injected after 2000 days of water-flooding. In the two schemes, the established accuracy pattern continues with DMM, EDMM, TMM and ETMM methods significantly better compared to the CSG results. The EDMM and ETMM also display superior accuracy over TMM and DMM. This is consistent with results from two-phase flow.

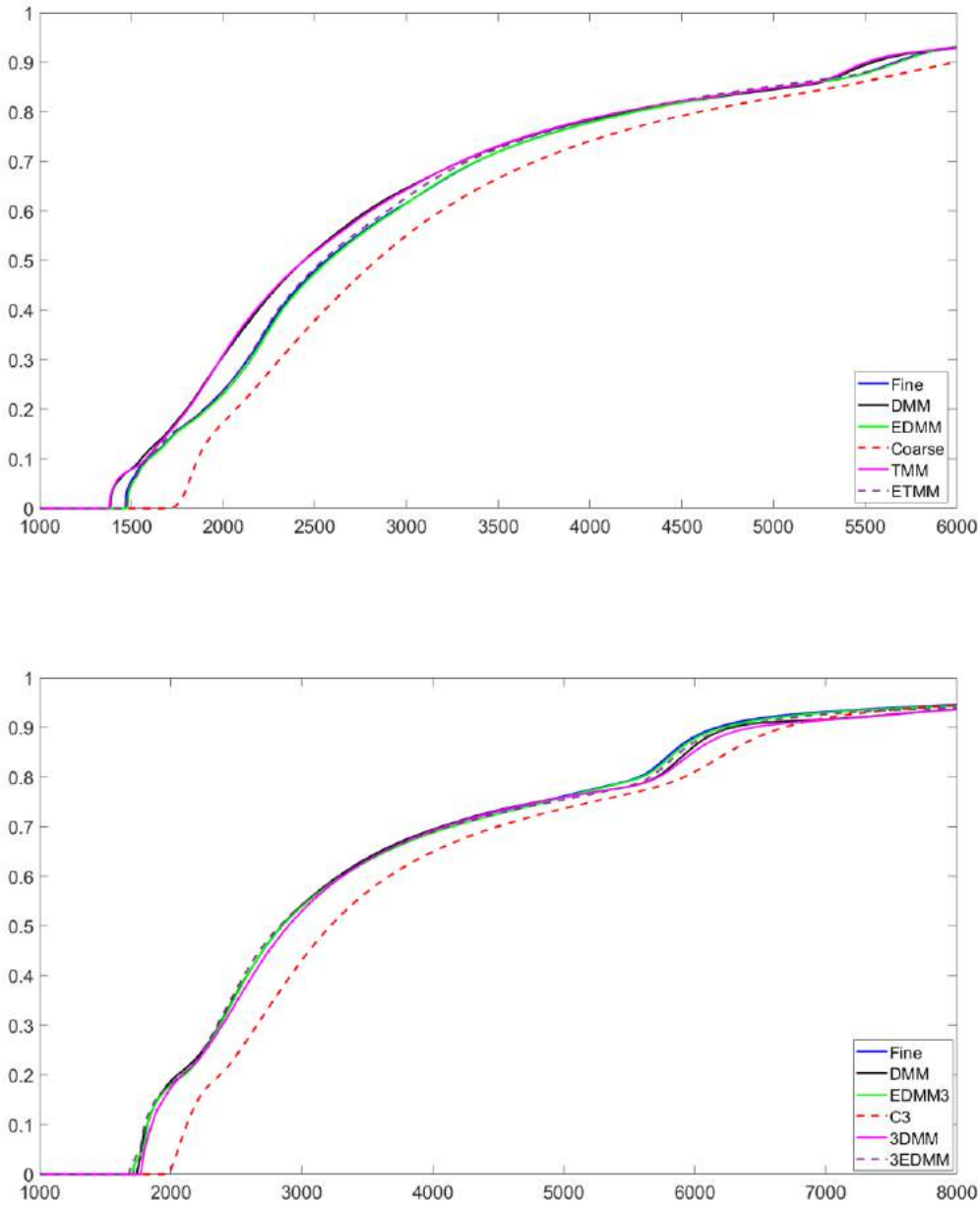

Figure 38: Water cut (fw) vs time (in days) plots for model 2 *for polymer flooding from day 1*

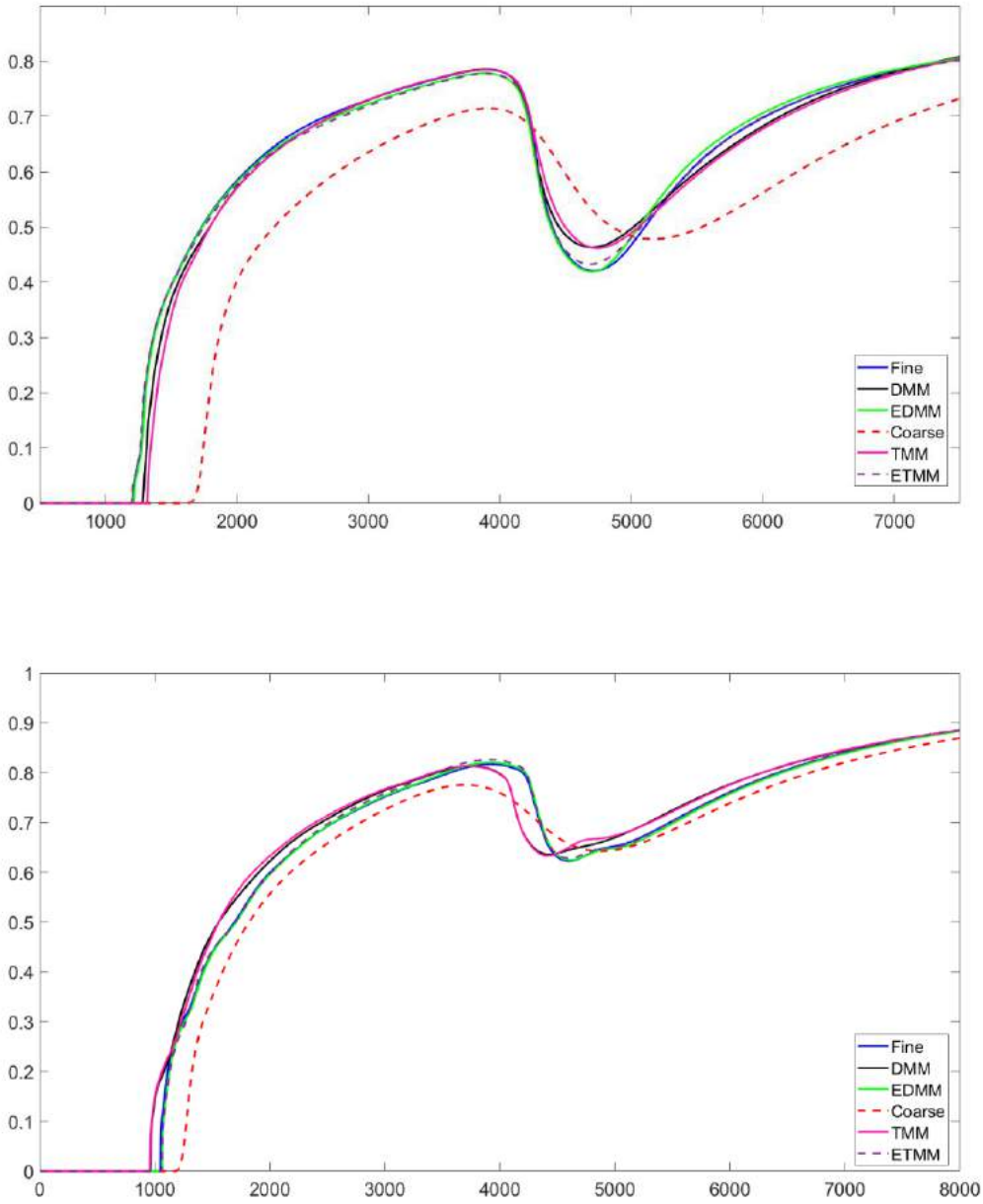

Figure 39: Water cut (fw) vs time (in days) plots for model 2 *for polymer flooding after 2000 days*

In the surfactant flooding problem, the water-cut at the two producers (Figure 40) follow the same pattern as previous examples. Figure 41 and Figure 43 show the accuracy of the different method in the spacial saturation and concentration distributions respectively, of the surfactant flooding example. Figure 41 and Figure 43 show the saturation distribution error E_{SD} and

concentration distribution error E_{CD} of the different solution methods after 5000 days respectively. $E_{SD} = \left| Sw_x^f - Sw_x \right|$ where Sw_x^f is the reference fine-scale water saturation and Sw_x is the water saturation using the solution method employed. $E_{CD} = \left| C_x^f - C_x \right|$ where C_x^f is the reference fine-scale water concentration and C_x is the concentration using the solution method employed. They clearly show the superiority of the extended local methods over the local methods consistent with all the other examples.

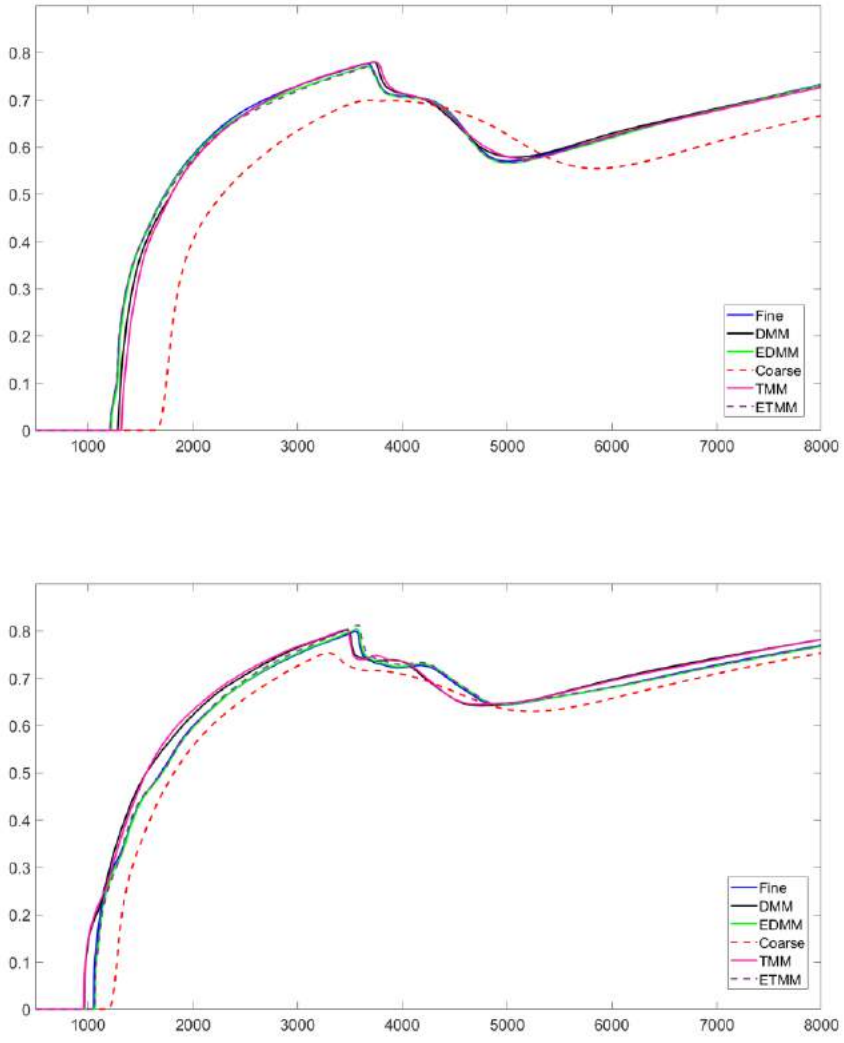

Figure 40: Water cut (fw) vs time (in days) plots for model 2 two producers using the different solution methods i.e. Coarse-scale, EDMM, DMM, ETMM, TMM and Fine scale (Surfactant Flooding Case)

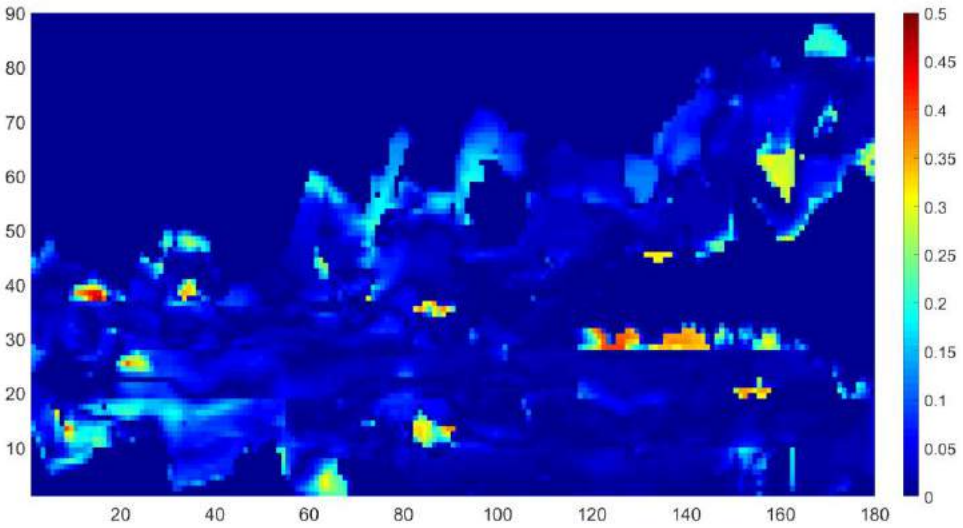
90
80
70
60
50
40
30
20
10
20
40
60
80
100
120
140
160
180
0.5
0.45
0.4
0.35
0.3
0.25
0.2
0.15
0.1
0.05
0

a)

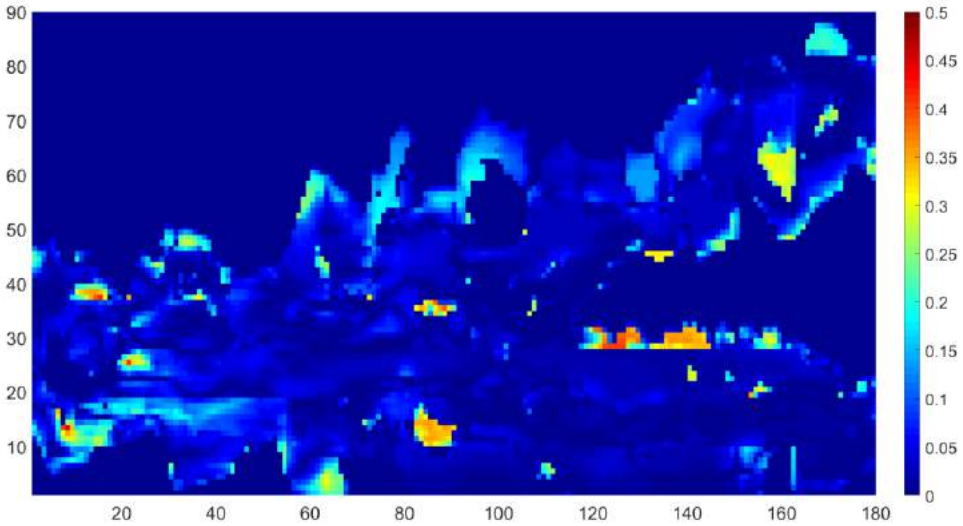
90
80
70
60
50
40
30
20
10
20
40
60
80
100
120
140
160
180
0.5
0.45
0.4
0.35
0.3
0.25
0.2
0.15
0.1
0.05
0

b)

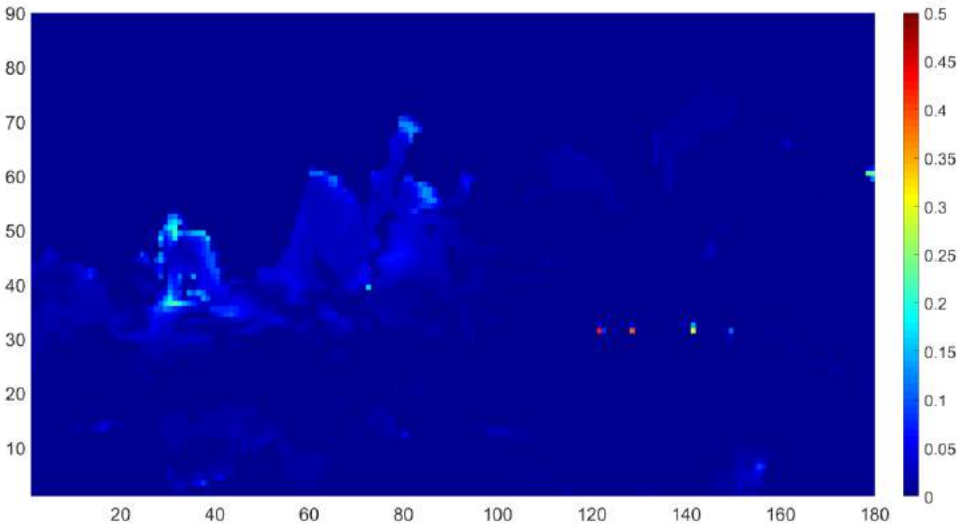

c)

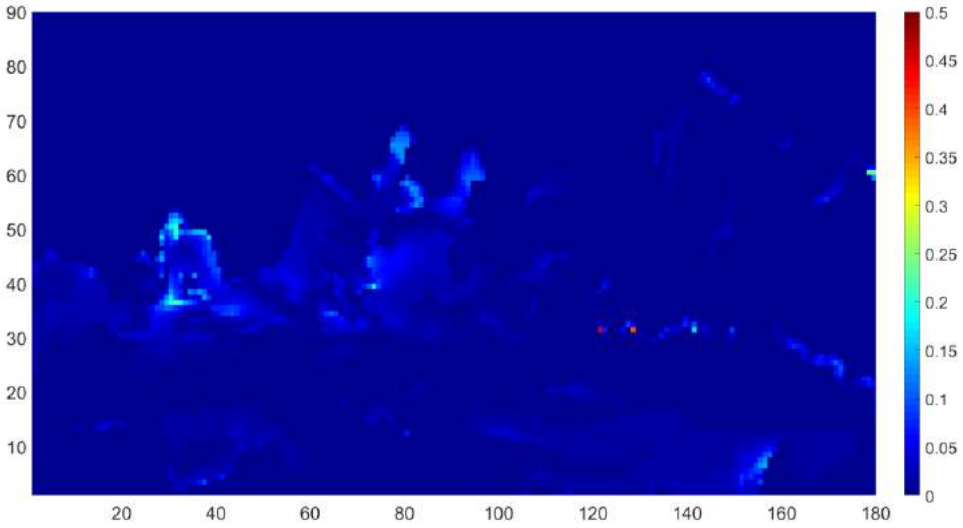

d)

Figure 41: Saturation distribution error E_{SD} for a) DMM, b) TMM, c) EDMM, d) ETMM for the surfactant flooding example

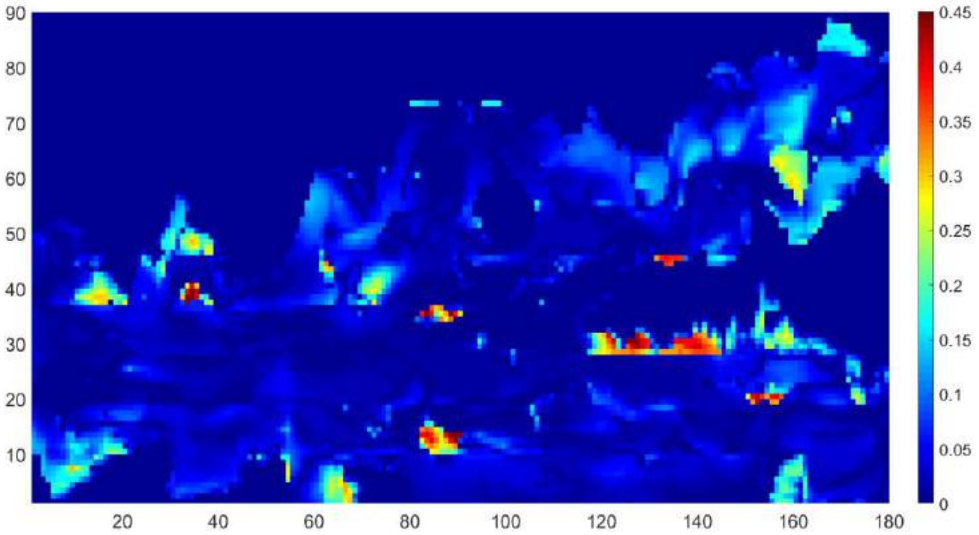
90
80
70
60
50
40
30
20
10
20
40
60
80
100
120
140
160
180
0.45
0.4
0.35
0.3
0.25
0.2
0.15
0.1
0.05
0

a)

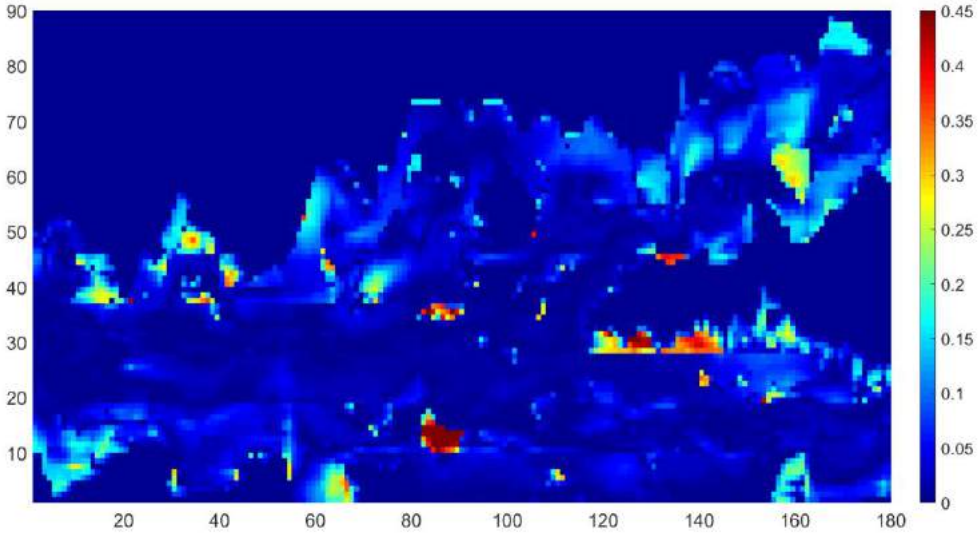
90
80
70
60
50
40
30
20
10
20
40
60
80
100
120
140
160
180
0.45
0.4
0.35
0.3
0.25
0.2
0.15
0.1
0.05
0

b)

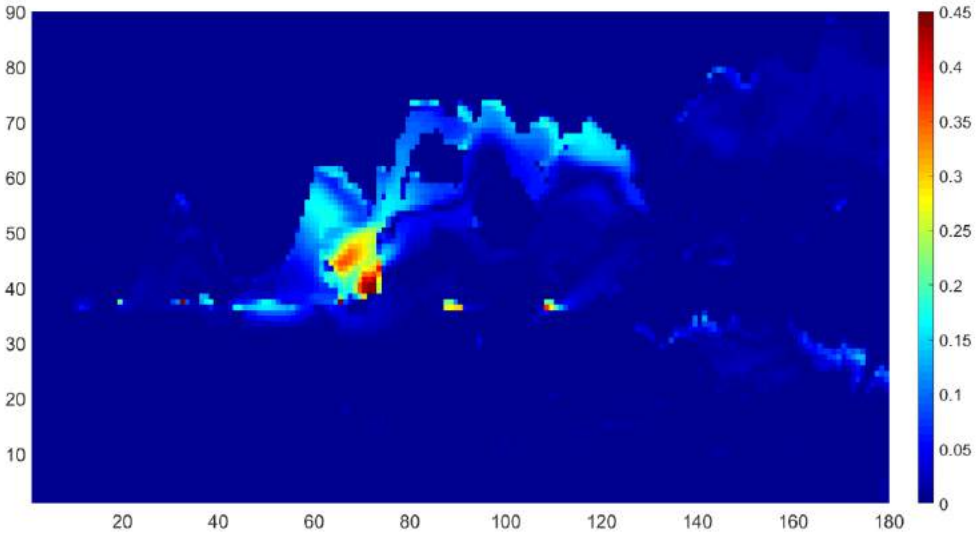

c)

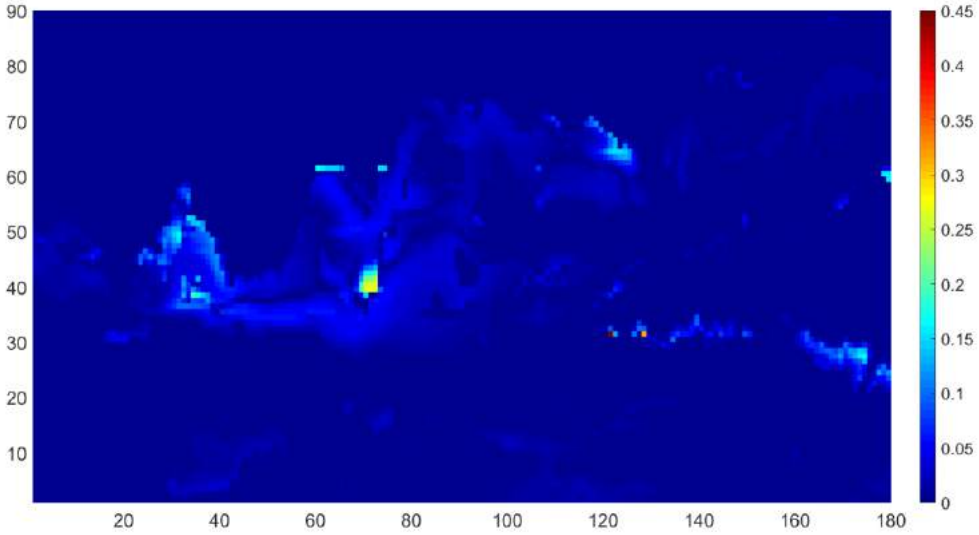

d)

Figure 42: Saturation distribution error E_{SD} for a) DMM, b) TMM, c) EDMM, d) ETMM for the polymer flooding example

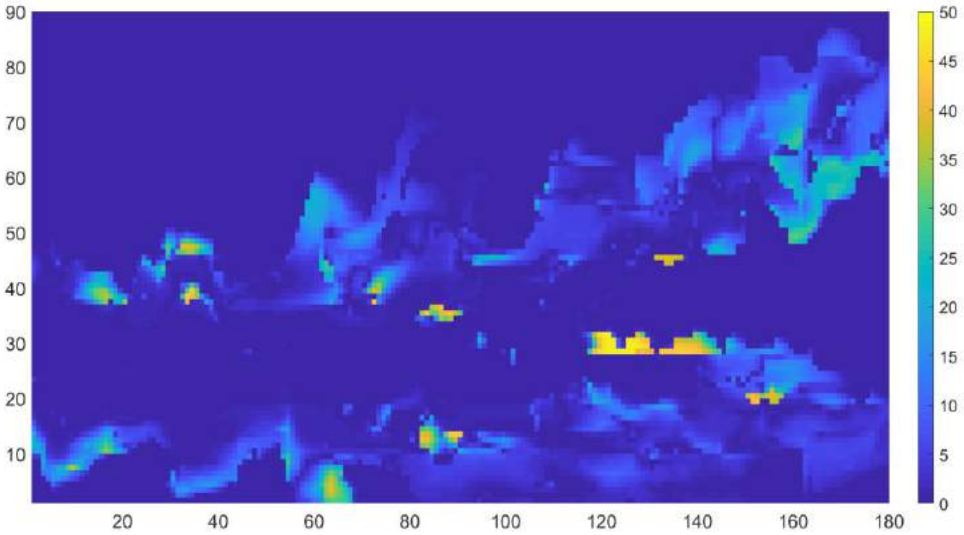
90
80
70
60
50
40
30
20
10
20
40
60
80
100
120
140
160
180
50
45
40
35
30
25
20
15
10
5
0

a)

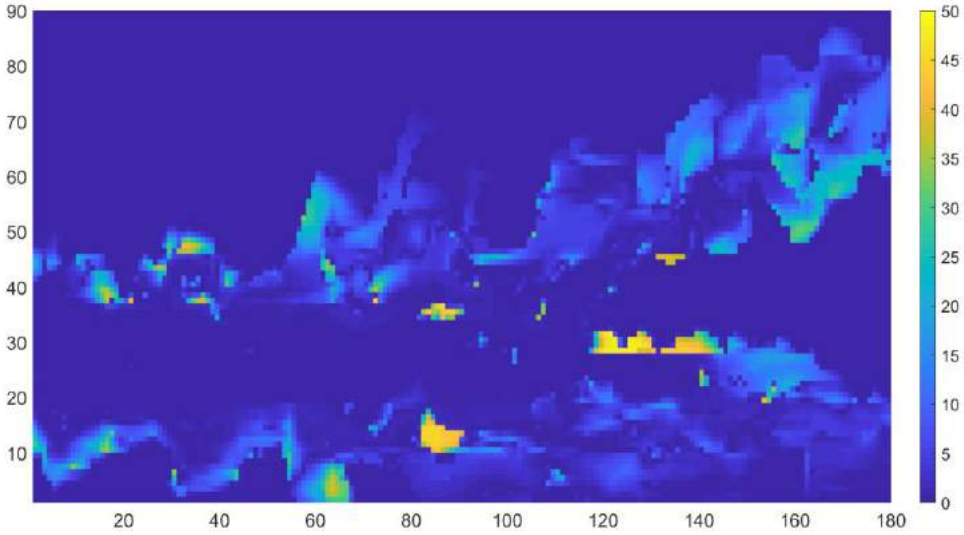
90
80
70
60
50
40
30
20
10
20
40
60
80
100
120
140
160
180
50
45
40
35
30
25
20
15
10
5
0

b)

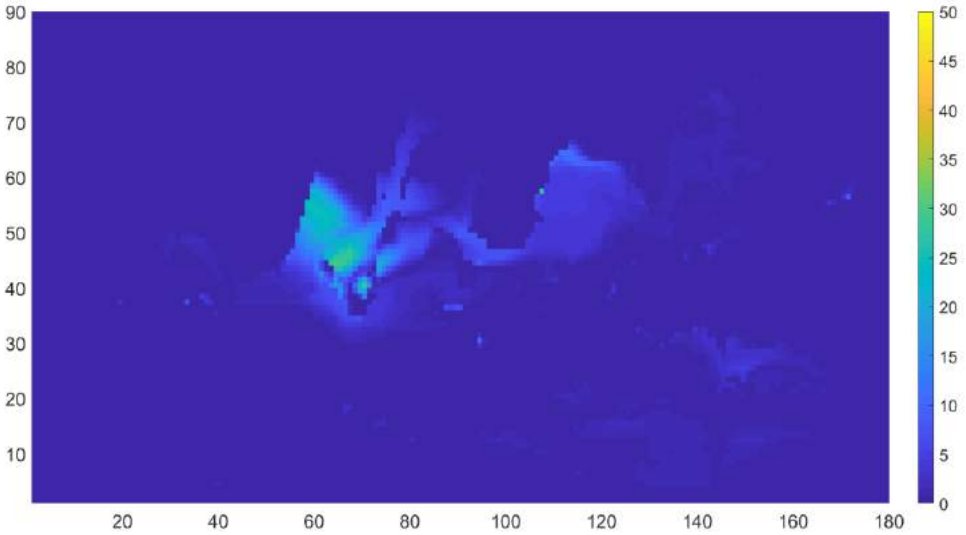

c)

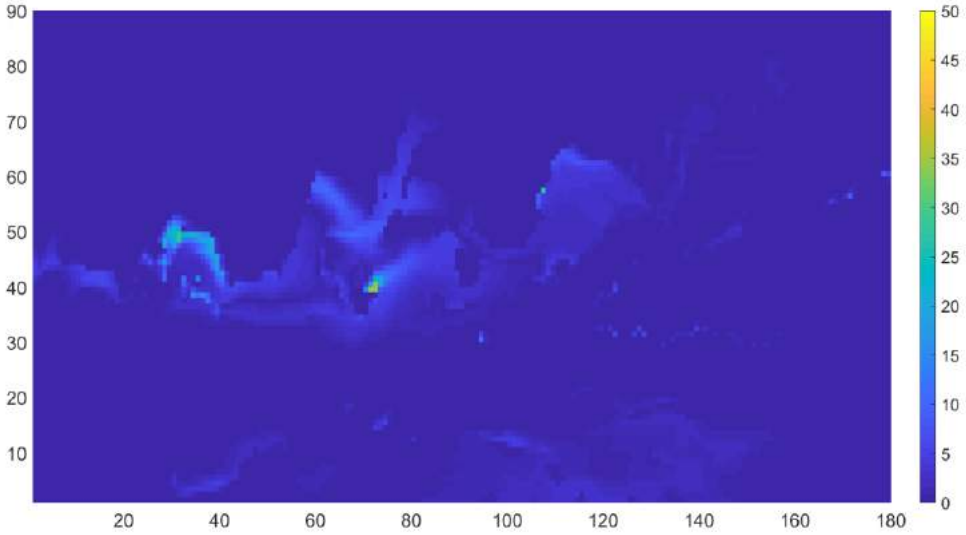

d)

Figure 43: Concentration distribution error E_{CD} for a) DMM, b) TMM, c) EDMM, d) ETMM for the surfactant flooding

6.10 Discussion

From all the results, the different methods have been shown to be effective in modelling CEOR problems. A general pattern is discovered when the accuracies of the different methods are compared that is consistent across all examples and in both the polymer flooding and surfactant flooding problems. The TMM and DMM have close approaches to downscaling and they also

have accuracies that are similar across the different examples. EDMM and ETMM also have similar approaches to the downscaling and are also similar in accuracy across the examples in both surfactant flooding and water flooding problems. DMM and TMM schemes are also generally less accurate than the EDMM and ETMM. As, EDMM was developed to improve the DMM, this is an expected result.

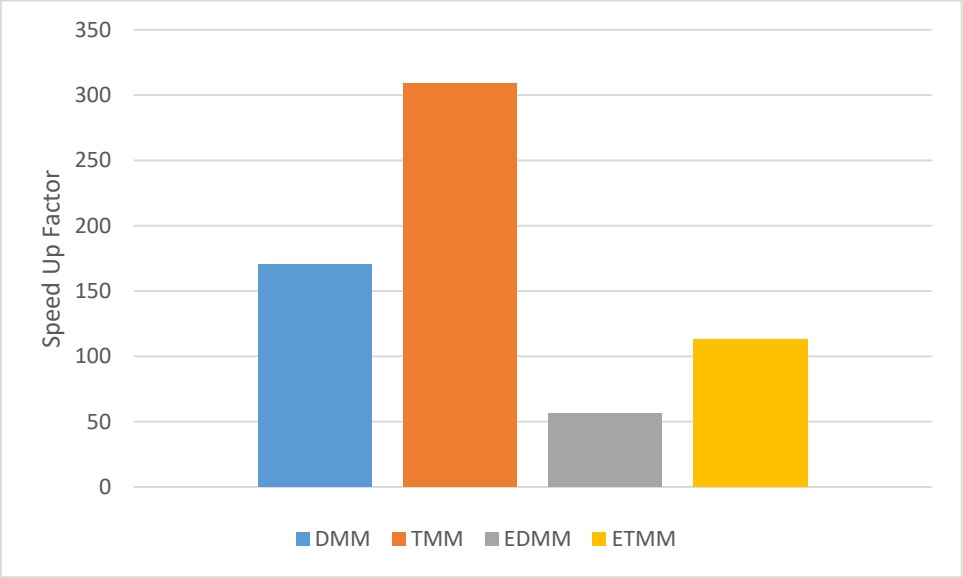

Figure 44: Speed up factor of the different methods relative to fine scale simulation

In terms of cost, Figure 44 shows that there is a reduction in cost of both ETMM and TMM in comparison to EDMM and DMM methods respectively when an intermediate level is introduced between the coarse scale and the fine scale. This is not unexpected as the size of every local problem (or extended local problem) to be solved in the downscaling is reduced significantly when an intermediate level is introduced. Reduction in problem size means a reduced size of the matrix system solved for pressure and that is the most important solution step in terms of cost. This therefore shows that there can be a significant reduction in cost without necessarily seriously impacting the accuracy by introducing an intermediate step.

6.11 Conclusion

TMM and ETMM are two triple mesh methods that have been developed for two-phase flow but now adapted to handle CEOR problems. They have been tested on complex surfactant flooding and polymer flooding examples. An extension of the existing EDMM and DMM to the surfactant flooding and polymer flooding problems has also been developed. ETMM and TMM have also both been proven to have similar accuracy to EDMM and DMM respectively, given the same fine-scale and coarse-scale models, whilst being a lot cheaper. The accuracy of the two extended methods ETMM and EDMM have also proven to be higher than that of DMM and TMM methods in both polymer flooding and surfactant flooding examples, consistent with the surfactant flooding results.

7 CONCLUSIONS AND RECOMMENDATION

The main outcomes of this work can be summarized as follows

- Dual Mesh Method is an efficient method in improving cost relative to fine scale simulation. This method is also effective in error reduction relative to the coarse scale simulation. This advantages are present both in water flooding as well as CEOR problems. However, this method has a poor accuracy relative to fine scale simulation. This accuracy gets even worse in highly heterogeneous problems
- Extended Dual Mesh method was developed to improve on the accuracy of DMM whilst not compromising efficiency too significantly. EDMM with the application of directional oversampling displayed a significant improvement in accuracy relative to DMM. While EDMM is significantly less costly that fine scale simulation, it is a more expensive method than DMM.
- TMM and ETMM were developed as triple mesh methods requiring two levels of upscaling-downscaling unlike DMM and ETMM which are just two level. They both differ in their approach to downscaling as TMM utilizes the local downscaling similar to DMM while ETMM employs the extended local downscaling similar to EDMM. Both triple mesh methods are significantly less costly than their two-mesh analogues whiles maintaining similar levels of accuracy.
- All four methods were extended to CEOR problems of polymer flooding and surfactant flooding. The results are consistent with water-flooding results in terms of cost and relative accuracy.
- A lot of simplifying assumptions were made in the development of each model. This methods can therefore be further developed by incorporating more physics into the formulation including compressibility and capillary pressure.

REFERENCES

1. Aarnes, Jørg E. “On the Use of a Mixed Multiscale Finite Element Method for Greater Flexibility and Increased Speed or Improved Accuracy in Reservoir Simulation.” *Multiscale Modeling and Simulation* 2, no. 3 (2004): 421–39. https://doi.org/10.1137/030600655.
2. Aarnes, Jørg E., and Yalchin Efendiev. “An Adaptive Multiscale Method for Simulation of Fluid Flow in Heterogeneous Porous Media.” *Multiscale Modeling and Simulation* 5, no. 3 (September 2006): 918–39. https://doi.org/10.1137/050645117.
3. Adak, A., Bandyopadhyay, M., Pal, A.: Adsorption of Anionic Surfactant on Alumina and Reuse of the Surfactant-Modified Alumina for the Removal of Crystal Violet from Aquatic Environment. Journal of Environmental Science and Health, Part A. 40, 167–182 (2005).
4. Adeyemi, Adedimeji A., Abeeb A. Awotunde, Qinzhuo Liao, Kishore Mohanty, and Shirish Patil. “Extended Dual Mesh Method with Applications in Two-Phase Flow in Heterogeneous Porous Media.” *Journal of Petroleum Science and Engineering* 204 (September 1, 2021): 108729. https://doi.org/10.1016/j.petrol.2021.108729.
5. Adeyemi, Adedimeji A, Abeeb A Awotunde, Shirish Patil, Mohamed N Mahmoud, Abdullah S Sultan, and Kishore Mohanty. “Triple Mesh Methods and Their Application to Two-Phase Flow in Porous Media.” *Journal of Petroleum Science and Engineering* 212 (2022): 110252. https://doi.org/https://doi.org/10.1016/j.petrol.2022.110252.
6. Arbogast, Todd, and Steven L. Bryant. “A Two-Scale Numerical Subgrid Technique for Waterflood Simulations.” *SPE Journal* 7, no. 4 (2002): 446–57. https://doi.org/10.2118/81909-PA.

7. Audigane, P., Blunt, M.: Dual Mesh Method in Upscaling. Proceedings of SPE Reservoir Simulation Symposium. (2003).
8. Audigane, Pascal, and Martin J. Blunt. “Dual Mesh Method for Upscaling in Waterflood Simulation.” *Transport in Porous Media* 55, no. 1 (April 2004): 71–89. https://doi.org/10.1023/B:TIPM.0000007309.48913.d2.
9. Babaei, Masoud, and Peter R. King. “A Modified Nested-Gridding for Upscaling-Downscaling in Reservoir Simulation.” *Transport in Porous Media* 93, no. 3 (July 5, 2012): 753–75. https://doi.org/10.1007/s11242-012-9981-4.
10. ———. “An Upscaling-Static-Downscaling Scheme for Simulation of Enhanced Oil Recovery Processes.” *Transport in Porous Media* 98, no. 2 (June 29, 2013): 465–84. https://doi.org/10.1007/s11242-013-0154-x.
11. Bachu, Stefan, and David Cuthiell. “Effects of Core-scale Heterogeneity on Steady State and Transient Fluid Flow in Porous Media: Numerical Analysis.” *Water Resources Research* 26, no. 5 (1990): 863–74. https://doi.org/10.1029/WR026i005p00863.
12. Barker, John W., and Sylvain Thibeau. “A Critical Review of the Use of Pseudorelative Permeabilities for Upscaling.” *SPE Reservoir Engineering (Society of Petroleum Engineers)* 12, no. 2 (May 1, 1997): 138–43. https://doi.org/10.2118/35491-PA.
13. Batenburg, D. W. Van, A. H. De Zwart, P. M. Boerrigter, M. Bosch, and J. C. Vink. “Application of Dynamic Gridding Techniques to IOR/EOR Processes.” In *16th European Symposium on Improved Oil Recovery 2011*, 1–15. Society of Petroleum Engineers, 2011. https://doi.org/10.2118/141711-ms.
14. Begg, S H, R R Carter, and P Dranfield. “Assigning Effective Values to Simulator Gridblock Parameters for Heterogeneous Reservoirs.” *SPE Reservoir Engineering* 4,

no. 04 (1989): 455–63. https://doi.org/10.2118/16754-PA.

15. Chang, Y. C., and K. K. Mohanty. “Scale-up of Two-Phase Flow in Heterogeneous Porous Media.” *Journal of Petroleum Science and Engineering* 18, no. 1–2 (July 1, 1997): 21–34. https://doi.org/10.1016/S0920-4105(97)00002-8.
16. Chen, Y., L. J. Durlofsky, M. Gerritsen, and X. H. Wen. “A Coupled Local-Global Upscaling Approach for Simulating Flow in Highly Heterogeneous Formations.” *Advances in Water Resources* 26, no. 10 (October 1, 2003): 1041–60. https://doi.org/10.1016/S0309-1708(03)00101-5.
17. Chen, Yuguang. “Upscaling and Subgrid Modeling of Flow and Transport in Heterogeneous Reservoirs.” Stanford University, 2005.
18. Chen, Yuguang, and Louis J. Durlofsky. “Adaptive Local-Global Upscaling for General Flow Scenarios in Heterogeneous Formations.” *Transport in Porous Media* 62, no. 2 (February 2006): 157–85. https://doi.org/10.1007/s11242-005-0619-7.
19. Chen, Zhiming, and Thomas Y Hou. “A Mixed Multiscale Finite Element Method for Elliptic Problems with Oscillating Coefficients.” *Mathematics of Computation*. Vol. 72, 2002. https://www.ams.org/journal-terms-of-use.
20. Christie, M A, and M J Blunt. “Tenth SPE Comparative Solution Project: A Comparison of Upscaling Techniques.” *SPE Reservoir Evaluation & Engineering* 4, no. 04 (2001): 308–17. https://doi.org/10.2118/72469-PA.
21. Cusini, Matteo, Barnaby Fryer, Cor van Kruijsdijk, and Hadi Hajibeygi. “Algebraic Dynamic Multilevel Method for Compositional Flow in Heterogeneous Porous Media.” *Journal of Computational Physics* 354 (February 1, 2018): 593–612. https://doi.org/10.1016/j.jcp.2017.10.052.
22. Cusini, Matteo, Cor van Kruijsdijk, and Hadi Hajibeygi. “Algebraic Dynamic Multilevel (ADM) Method for Fully Implicit Simulations of Multiphase Flow in

Porous Media." *Journal of Computational Physics* 314 (June 1, 2016): 60–79. https://doi.org/10.1016/j.jcp.2016.03.007.

23. Cusini, Matteo, Alexander A. Lukyanov, Jostein Natvig, and Hadi Hajibeygi. "Constrained Pressure Residual Multiscale (CPR-MS) Method for Fully Implicit Simulation of Multiphase Flow in Porous Media." *Journal of Computational Physics* 299 (October 5, 2015): 472–86. https://doi.org/10.1016/j.jcp.2015.07.019.
24. Das, S., Butler, R.: Extraction Of Heavy Oil And Bitumen Using Solvents At Reservoir Pressure. Technical Meeting / Petroleum Conference of The South Saskatchewan Section. (1995).
25. Durlofsky, L J, R A Behrens, R C Jones, and A Bernath. "Scale Up of Heterogeneous Three Dimensional Reservoir Descriptions." *SPE Journal* 1, no. 03 (1996): 313–26. https://doi.org/10.2118/30709-PA.
26. Durlofsky, Louis J. "Numerical Calculation of Equivalent Grid Block Permeability Tensors for Heterogeneous Porous Media." *Water Resources Research* 27, no. 5 (1991): 699–708. https://doi.org/10.1029/91WR00107.
27. Durlofsky, Louis J, Richard C Jones, and William J Milliken. "A Nonuniform Coarsening Approach for the Scale-up of Displacement Processes in Heterogeneous Porous Media." *Advances in Water Resources* 20, no. 5 (1997): 335–47. https://doi.org/https://doi.org/10.1016/S0309-1708(96)00053-X.
28. Durlofsky, L.J.: Upscaling of Geocellular Models for Flow Simulation. 66th EAGE Conference and Exhibition - Workshops. (2004).
29. Durlofsky, J. L. "Upscaling of Geocellular Models for Flow Simulation." In *66th EAGE Conference and Exhibition - Workshops*. EAGE Publications BV, 2014. https://doi.org/10.3997/2214-4609.201405607.
30. E. Pickup, G., J. L. Jensen, P. S. Ringrose, and K. S. Sorbie. "A Method for

Calculating Permeability Tensors Using Perturbed Boundary Conditions," cp-232-00019. EAGE Publications, 1992. https://doi.org/10.3997/2214-4609.201411077.

31. Efendiev, Yalchin, Seong Lee, Guanglian Li, Jun Yao, and Na Zhang. "Hierarchical Multiscale Modeling for Flows in Fractured Media Using Generalized Multiscale Finite Element Method." *GEM - International Journal on Geomathematics* 6, no. 2 (November 1, 2015): 141–62. https://doi.org/10.1007/s13137-015-0075-7.
32. Farmer, C. L. "Upscaling: A Review." *International Journal for Numerical Methods in Fluids* 40, no. 1–2 (September 10, 2002): 63–78. https://doi.org/10.1002/fld.267.
33. Firoozabadi, B., H. Mahani, M. A. Ashjari, and P. Audigane. "Improved Upscaling of Reservoir Flow Using Combination of Dual Mesh Method and Vorticity-Based Gridding." *Computational Geosciences* 13, no. 1 (2009): 57–78. https://doi.org/10.1007/s10596-008-9105-y.
34. Firoozabadi, B, and M A Ashjari. "Performance of Combined Vorticity-Based Gridding and Dual Mesh Method for Gravity Dominated Reservoir Flows." *Journal of Petroleum Science and Engineering* 67, no. 3 (2009): 127–39. https://doi.org/https://doi.org/10.1016/j.petrol.2009.05.010.
35. Froning, H., Leach, R.: Determination of Chemical Requirements and Applicability Of Wettability Alteration Flooding. Journal of Petroleum Technology. 19, 839–843 (1967).
36. Fu, Shubin, and Eric T. Chung. "A Local-Global Multiscale Mortar Mixed Finite Element Method for Multiphase Transport in Heterogeneous Media." *Journal of Computational Physics* 399 (December 15, 2019): 108906. https://doi.org/10.1016/j.jcp.2019.108906.
37. Gautier, Yann, Martin J. Blunt, and Michael A. Christie. "Nested Gridding and Streamline-Based Simulation for Fast Reservoir Performance Prediction."

Computational Geosciences 3, no. 3/4 (1999): 295–320. https://doi.org/10.1023/A:1011535210857.

38. Gomez-Hernandez, J Jaime, and Andre G Journel. “Stochastic Characterization of Gridblock Permeabilities.” *SPE Formation Evaluation* 9, no. 02 (1994): 93–99. https://doi.org/10.2118/22187-PA.
39. Gogarty, W., Tosch, W.: Miscible-Type Waterflooding: Oil Recovery with Micellar Solutions. Journal of Petroleum Technology. 20, 1407–1414 (1968).
40. Green, D.W., Willhite, G.P.: Enhanced oil recovery. Society of Petroleum Engineers, Richardson, TX, USA (1998).
41. Green Willhite, G. Paul., Don W. *Enhanced Oil Recovery*. Richardson, TX: Henry L. Doherty Memorial Fund of AIME, Society of Petroleum Engineers, 1998.
42. Guérillot, Dominique, and Jérémie Bruyelle. “Compositional Dual Mesh Method for Single Phase Flow in Heterogeneous Porous Media—Application to CO2 Storage.” *Computational Geosciences* 21, no. 5–6 (December 1, 2017): 949–61. https://doi.org/10.1007/s10596-017-9645-0.
43. Guérillot, Dominique, and Sophie Verdiere. “Different Pressure Grids for Reservoir Simulation in Heterogeneous Reservoirs,” February 1, 1995. https://doi.org/10.2118/29148-MS.
44. Haajizadeh, M., F.J. Fayers, A.P. Cockin, M. Roffey, and D.J. Bond. “On the Importance of Dispersion and Heterogeneity in the Compositional Simulation of Miscible Gas Processes.” Society of Petroleum Engineers (SPE), 1999. https://doi.org/10.2118/57264-ms.
45. Hajibeygi, H., and H. A. Tchelepi. “Compositional Multiscale Finite-Volume Formulation.” *SPE Journal* 19, no. 2 (2014): 316–26. https://doi.org/10.2118/163664-PA.

46. Healy, R., Reed, R., Stenmark, D.: Multiphase Microemulsion Systems. Society of Petroleum Engineers Journal. 16, 147–160 (1976).
47. Hitzman, D., Sperl, G.: A New Microbial Technology for Enhanced Oil Recovery and Sulfide Prevention and Reduction. Proceedings of SPE/DOE Improved Oil Recovery Symposium. (1994).
48. Holden, L., and B. F. Nielsen. "Global Upscaling of Permeability in Heterogeneous Reservoirs; the Output Least Squares (OLS) Method." *Transport in Porous Media* 40, no. 2 (2000): 115–43. https://doi.org/10.1023/A:1006657515753.
49. Holden, Lars, and Oddvar Lia. "A Tensor Estimator for the Homogenization of Absolute Permeability." *Transport in Porous Media* 8, no. 1 (May 1992): 37–46. https://doi.org/10.1007/BF00616891.
50. Hou, Thomas Y, and Xiao-Hui Wu. "A Multiscale Finite Element Method for Elliptic Problems in Composite Materials and Porous Media." *Journal of Computational Physics* 134, no. 1 (1997): 169–89. https://doi.org/https://doi.org/10.1006/jcph.1997.5682.
51. Hou, Thomas Y, Xiao-Hui Wu, and Zhiqiang Cai. "CONVERGENCE OF A MULTISCALE FINITE ELEMENT METHOD FOR ELLIPTIC PROBLEMS WITH RAPIDLY OSCILLATING COEFFICIENTS." *MATHEMATICS OF COMPUTATION*. Vol. 68, 1999. https://www.ams.org/journal-terms-of-use.
52. Hui, M., and Lou J. Durlofsky. "Accurate Coarse Modeling of Well-Driven, High-Mobility-Ratio Displacements in Heterogeneous Reservoirs." *Journal of Petroleum Science and Engineering* 49, no. 1–2 (October 30, 2005): 37–56. https://doi.org/10.1016/j.petrol.2005.07.004.
53. Jenny, P, S H Lee, and H A Tchelepi. "Multi-Scale Finite-Volume Method for Elliptic Problems in Subsurface Flow Simulation." *Journal of Computational Physics* 187, no.

1 (2003): 47–67. https://doi.org/https://doi.org/10.1016/S0021-9991(03)00075-5.

54. Johansson Ingegärd, Somasundaran, P.: Handbook for cleaning/decontamination of surfaces. Elsevier Science, Amsterdam (2007).
55. Jones, A, J Doyle, T Jacobsen, and Dagrun Kjoensvik. "Which Sub-Seismic Heterogeneities Influence Waterflood Performance? A Case Study of a Low Net-to-Gross Fluvial Reservoir." *Geological Society, London, Special Publications* 84 (January 1, 1995): 5–18. https://doi.org/10.1144/GSL.SP.1995.084.01.02.
56. Khoozan, D, B Firoozabadi, D Rashtchian, and M A Ashjari. "Analytical Dual Mesh Method for Two-Phase Flow through Highly Heterogeneous Porous Media." *Journal of Hydrology* 400, no. 1 (2011): 195–205. https://doi.org/https://doi.org/10.1016/j.jhydrol.2011.01.042.
57. King, M J, and Mark Mansfield. "Flow Simulation of Geologic Models." *SPE Reservoir Evaluation & Engineering* 2, no. 04 (1999): 351–67. https://doi.org/10.2118/57469-PA.
58. Kippe, Vegard, Jørg E. Aarnes, and Knut Andreas Lie. "A Comparison of Multiscale Methods for Elliptic Problems in Porous Media Flow." In *Computational Geosciences*, 12:377–98, 2008. https://doi.org/10.1007/s10596-007-9074-6.
59. Kumar, D., M. Murugesu, and S. Srinivasan. "Modeling Effect of Permeability Heterogeneities on SAGD Performance Using Improved Upscaling Schemes." In *Society of Petroleum Engineers - SPE Heavy Oil Conference Canada 2014*, 2:1318–35. Society of Petroleum Engineers, 2014. https://doi.org/10.2118/170115-ms.
60. Künze, Rouven, Ivan Lunati, and Seong H. Lee. "A Multilevel Multiscale Finite-Volume Method." *Journal of Computational Physics* 255 (December 15, 2013): 502–20. https://doi.org/10.1016/j.jcp.2013.08.042.
61. Kyte, J. R., and D. W. Berry. "NEW PSEUDO FUNCTIONS TO CONTROL

NUMERICAL DISPERSION." *Soc Pet Eng AIME J* 15, no. 4 (August 1, 1975): 269–76. https://doi.org/10.2118/5105-pa.

62. Lake, L.W.: Enhanced oil recovery. University Co-op, Austin, TX (1989).
63. Li, Hangyu, Jeroen C. Vink, and Faruk O. Alpak. "A Dual-Grid Method for the Upscaling of Solid-Based Thermal Reactive Flow, with Application to the in-Situ Conversion Process." In *SPE Journal*, 21:2097–2111. Society of Petroleum Engineers, 2016. https://doi.org/10.2118/173248-PA.
64. Mehmood, Saad, and Abeeb A. Awotunde. "Sensitivity-Based Upscaling for History Matching of Reservoir Models." *Petroleum Science* 13, no. 3 (August 1, 2016): 517–31. https://doi.org/10.1007/s12182-016-0107-4.
65. Muggeridge, A. H., and P. Hongtong. "An Upscaling Methodology for EOR." In *14th European Conference on the Mathematics of Oil Recovery 2014, ECMOR 2014*, 2014:1–21. European Association of Geoscientists and Engineers, EAGE, 2014. https://doi.org/10.3997/2214-4609.20141862.
66. Nielsen, Bjørn Fredrik, and Aslak Tveito. "An Upscaling Method for One-Phase Flow in Heterogeneous Reservoirs. A Weighted Output Least Squares (WOLS) Approach." *Computational Geosciences* 2, no. 2 (1998): 93–123. https://doi.org/10.1023/A:1011541917701.
67. Pope, G., Wu, W., Narayanaswamy, G., Delshad, M., Sharma, M., Wang, P.: Modeling Relative Permeability Effects in Gas-Condensate Reservoirs With a New Trapping Model. SPE Reservoir Evaluation & Engineering. 3, 171–178 (2000).
68. Rame, M., Killough, J.: A New Approach to Flow Simulation in Highly Heterogeneous Porous Media. SPE Formation Evaluation. 7, 247–254 (1992).
69. Rame, Marcelo, and J E Killough. "A New Approach to Flow Simulation in Highly Heterogeneous Porous Media." *SPE Formation Evaluation* 7, no. 03 (1992): 247–54.

https://doi.org/10.2118/21247-PA.

70. Renard, Ph, and G. De Marsily. “Calculating Equivalent Permeability: A Review.” *Advances in Water Resources*. Elsevier Ltd, October 1, 1997. https://doi.org/10.1016/s0309-1708(96)00050-4.
71. Selley, R.C.: J. O. Aasen, E. Berg, A. T. Buller, O. Hjelmeland, R. M. Holt, J. Kleppe, & O. Torsaeter (eds) 1994. North Sea Oil & Gas Reservoirs III. Proceedings of the 3rd North Sea Oil and Gas Reservoirs Conference held in Trondheim, Norway, 30 November–2 December 1992. ix 388 pp. Dordrecht, Boston, London: Kluwer for the Norwegian Institute of Technology. Price Dfl. 440.00, US $249.00, £176.00 (hard covers). ISBN 0 7923 2304 1. Geological Magazine. 132, 359–360 (1995).
72. Schramm, L.L.: Suspensions: fundamentals and applications in the petroleum industry. American Chemical Soc., Washington, DC (2000).
73. Shah, Swej, Olav Møyner, Matei Tene, Knut-Andreas Lie, and Hadi Hajibeygi. “The Multiscale Restriction Smoothed Basis Method for Fractured Porous Media (F-MsRSB).” *Elsevier*. Accessed March 9, 2020. https://www.sciencedirect.com/science/article/pii/S0021999116301267.
74. Somasundaran, P., Fuerstenau, D.W.: Mechanisms of Alkyl Sulfonate Adsorption at the Alumina-Water Interface1. The Journal of Physical Chemistry. 70, 90–96 (1966).
75. Stone, H.L. “Rigorous Black Oil Pseudo Functions.” Society of Petroleum Engineers (SPE), 1991. https://doi.org/10.2118/21207-ms.
76. Thomas, S., Ali, S.F., Daharu, R.: Tertiary Recovery Of Two Alberta Oils By Micellar Flooding. Annual Technical Meeting. (1986).
77. Thomas, S.: Enhanced Oil Recovery - An Overview. Oil & Gas Science and Technology - Revue de lIFP. 63, 9–19 (2007).
78. Verdière, S., and M. H. Vignal. “Numerical and Theoretical Study of a Dual Mesh

Method Using Finite Volume Schemes for Two Phase Flow Problems in Porous Media." *Numerische Mathematik* 80, no. 4 (1998): 601–39. https://doi.org/10.1007/s002110050380.

79. Wen, X. H., L. J. Durlofsky, and M. G. Edwards. "Upscaling of Channel Systems in Two Dimensions Using Flow-Based Grids." *Transport in Porous Media* 51, no. 3 (June 2003): 343–66. https://doi.org/10.1023/A:1022318926559.
80. ———. "Use of Border Regions for Improved Permeability Upscaling." *Mathematical Geology* 35, no. 5 (July 2003): 521–47. https://doi.org/10.1023/A:1026230617943.
81. Wen, Xian Huan, and J. Jaime Gómez-Hernández. "Upscaling Hydraulic Conductivities in Heterogeneous Media: An Overview." *Journal of Hydrology*. Elsevier, August 1, 1996. https://doi.org/10.1016/s0022-1694(96)80030-8.
82. White, C.D., and R.N. Horne. "Computing Absolute Transmissibility in the Presence of Fine-Scale Heterogeneity." In *Ninth SPE Symposium on Reservoir Simulation*. Society of Petroleum Engineers (SPE), 1987. https://doi.org/10.2118/16011-ms.
83. Wu, X. H., Y. Efendiev, and T. Y. Hou. "Analysis of Upscaling Absolute Permeability." *Discrete and Continuous Dynamical Systems - Series B* 2, no. 2 (2002): 185–204. https://doi.org/10.3934/dcdsb.2002.2.185.
84. Yang, Yanfang, Eric T. Chung, and Shubin Fu. "An Enriched Multiscale Mortar Space for High Contrast Flow Problems." *Communications in Computational Physics* 23, no. 2 (2018). https://doi.org/10.4208/cicp.oa-2016-0147.
85. Zhang, P., Pickup, G., Christie, M.: A New Upscaling Approach for Highly Heterogeneous Reservoirs. SPE Reservoir Simulation Symposium. (2005).
86. Zhang, Qingfu, Zhaoqin Huang, Jun Yao, Yueying Wang, and Yang Li. "Two-Phase Numerical Simulation of Discrete Fracture Model Based on Multiscale Mixed Finite

Element Method." *Kexue Tongbao/Chinese Science Bulletin* 62, no. 13 (May 1, 2017): 1392–1401. https://doi.org/10.1360/N972016-00584.

87. Zhang, Qingfu, Jun Yao, Zhaoqin Huang, Yang Li, and Kai Zhang. "Hybrid Multiscale Method for Numerical Modeling of Coupled Flow and Geomechanics." *Journal of Petroleum Science and Engineering* 176 (May 1, 2019): 943–51. https://doi.org/10.1016/j.petrol.2019.02.009.
88. Zijl, W., and A. Trykozko. "Numerical Homogenization of the Absolute Permeability Using the Conformal-Nodal and Mixed-Hybrid Finite Element Method." *Transport in Porous Media* 44, no. 1 (July 2001): 33–62. https://doi.org/10.1023/A:1010776124186.

VITAE

Name: Adedimeji Abdulsalam Adeyemi

Nationality: Nigerian

Email: adeyemiadedimeji@gmail.com

Address: 11, Selesi Street, 102216, Lagos Nigeria

King Fahd University of Petroleum and Minerals, Saudi Arabia **2017 - 2022**

PhD. in Petroleum Engineering

Institute Francais du Petrole, IFP School, Rueil Malmaison, France **2013 - 2015**

MSc in Reservoir Geosciences and Engineering

University of Ibadan, Ibadan, Nigeria **2006 - 2011**

BSc in Petroleum Engineering

Journal Publications during Ph.D:

Adedimeji A. Adeyemi, Abeeb A. Awotunde, Shirish Patil, Mohamed N. Mahmoud, Abdullah S. Sultan, Kishore Mohanty, Triple mesh methods and their application to two-phase flow in porous media, Journal of Petroleum Science and Engineering, Volume 212, 2022, 110252, ISSN 0920-4105, https://doi.org/10.1016/j.petrol.2022.110252.

Adedimeji A. Adeyemi, Abeeb A. Awotunde, Qinzhuo Liao, Kishore Mohanty, Shirish Patil,

Extended Dual Mesh Method with applications in two-phase flow in heterogeneous porous media, Journal of Petroleum Science and Engineering, Volume 204, 2021,

108729, ISSN 0920-4105, https://doi.org/10.1016/j.petrol.2021.108729.